The role of the MTG family and BVES in intestinal biology and tumorigenesis

By

Bobak Parang

Dissertation

Submitted to the Faculty of the
Graduate School of Vanderbilt University
in partial fulfillment of the requirements
for the degree of
DOCTOR OF PHILOSOPHY
In

Cancer Biology

August, 2015

Nashville, TN

Approved:
Barbara Fingleton, PhD
R. Daniel Beauchamp, MD
Keith T. Wilson, MD
David Bader, PhD
Christopher Williams, MD PhD

To my loving father, who has been a limitless source of wisdom

and

To my late mother, whose love has been the anchor of my life

Acknowledgements

My experience in graduate school has been challenging but also endlessly stimulating and satisfying. I have grown professionally, intellectually, and personally over the last four years. And I have had a wonderful time doing so. This would not have been possible without countless individuals who have graciously provided support, time, and resources.

First and foremost, I must acknowledge my mentor, Dr. Christopher Williams. I could not have asked for a more dedicated and helpful advisor. Chris has generously invested his time, energy, and patience into my development. As his mentee, it often felt like Chris had a limitless amount of time allotted to me. Whether it was early mornings or late nights, he was always willing to review manuscripts, applications, or personal statements. It also felt like Chris had a limitless amount of confidence in me—this was a powerful motivating force throughout the last four years. Leaving the lab is bittersweet in large part because I will no longer be his formal mentee. But from observing his continued interactions with his own mentors, it's clear to me that the mentor-mentee relationship never ends. And I'm grateful for that because it's been a wonderful relationship. The only way I can truly return the favor and honor his commitment is to show the same level of mentorship, if I'm lucky enough to have the opportunity, to students of mine in the future.

My deepest thanks to the members of my thesis committee: Drs. Barbara Fingleton, Keith Wilson, David Bader, and Daniel Beauchamp. They provided key advice that led to experimental breakthroughs as well as publications. They expanded my understanding of how to design experiments as well as present data in the most impactful

way. It has been a real honor to have their guidance, and it's not lost on me how fortunate I am to have had the help of such a distinguished group.

Throughout my time at Vanderbilt, the Vanderbilt Medical Scientist Training Program has been a source of endless support. Terence Dermody has been a mentor and friend. His leadership has inspired and motivated me to better myself and to take advantage of the opportunities I have been given. Melissa Krasnove and Jim Bills have also been tremendous sources of support. I entered the program looking up to them, and while I still certainly look up to them, I also consider them good friends. Larry Swift and Michelle Grundy have also been helpful both in providing advice on navigating graduate school as well as how an MSTP program functions administratively.

I would like to thank the various core facilities throughout Vanderbilt. They have all been exceedingly kind and helpful. In particular, I would like to thank Dr. Joseph Roland of the Epithelial Biology Core, who went above and beyond answering any question I had.

Thank you to the former members of the Williams lab. Caitlyn Barret, in particular, taught me how to get 12 hours worth of data from 8 hours of experiments. Her approach to planning her day had a profound influence on my work ethic. I am also grateful for having the opportunity to work with Beth McDounough, Yash Choksi, and Shenika Poindexter, who all volunteered their time to teach and mentor me.

My sincere thank you to Sarah Short, Cody Keating, and Mukul Mittal, who joined the lab recently and have infused a new energy into our group. They have been noting short of a supportive family.

I would also like to acknowledge my undergraduate mentor, Paul Sniegowski, who cultivated my interest in biology and was more than generous with his time. I enjoyed every minute I spent in his lab and under his guidance. The experience was formative in that it cemented my desire to pursue a PhD. It was also under his mentorship that I gained a deep appreciation for the rich history of science. I am indebted to him for promoting my personal and professional development.

Lastly, on a personal note, I want to thank my family. My two older brothers, Zhubin Parang and Farzin Parang, are two of the most intelligent, creative, and hard-working individuals I know. They set a benchmark that I have been aspiring to my entire life. My father, Masood Parang, who has supported and encouraged any and all of my educational and personal endeavors. When I expressed interest in biology, he reinforced it. And whenever I expressed self-doubt, he removed it. To my late mother, Safura Parang, whose love and confidence in me has been an anchor throughout my life. Any success, professionally or personally, in my life is due to her influence.

The work in this dissertation could not have been conducted without the financial assistance. This work was supported by the National Institutes of Health grants DK080221, 1F30DK096718-01A1, T32 GM07347, VA Merit Review Grants from the Office of Medical Research, Department of Veterans Affairs 1I01BX001426, and ACS-RSG 116552.

Table of contents

List of tables

Table

List of figures

Figure

List of abbreviations

AOM	azoxymethane
AML	acute myeloid leukemia
APC	adenomatous polyposis coli
ATOH1	atonal homologue 1
β-catenin	beta-catenin
BCL-2	B-cell lymphoma 2
BVES	blood vessel epicardial substance
CAC	colitis-associated cancer
ChIP	chromatin immunoprecipitation
c-Myc	v-myc avian myelocytomatosis viral oncogene homolog
CRC	colorectal cancer
CSL	suppressor of hairless
DSS	dextran sodium sulfate
E-cadherin	epithelial-cadherin
EMT	epithelial-to-mesenchymal transition
GEF	guanine nucleotide exchange factor
GFI1	growth factor independent 1
GI	gastrointestinal
GSI	gamma-secretase inhibitor
Hes1	hes family BHLH transcription factor
HEK293T	human embryonic kidney 293T
IBD	inflammatory bowel disease

IF	immunofluorescence
IHC	immunohistochemistry
IP	immunoprecipitate
LCM	laser capture microdissection
LGR5	leucine-rich repeating-containing G-protein coupled receptor 5
MTG8	myeloid translocation gene 8
MTG16	myeloid translocation gene 16
MTGR1	myeloid translocation gene related 1
NICD	Notch intracellular domain
PAS	periodic acid Schiff
PLA	proximity ligation assay
PR61α	protein phosphatase 2, regulatory subunit B', alpha
PP2A	protein phosphatase 2
RHOA	ras homolog gene family, member a
TCF4	transcription factor 4
TCGA	the cancer genome atlas
UC	ulcerative colitis
WT	wildtype
ZO1	zonula occludens protein-1

Chapter 1

Introduction

Introduction to the intestinal epithelium

The intestine is divided into two anatomical compartments: the small intestine, where food is absorbed and digested, and the large intestine, or colon, where water and electrolytes are absorbed. At the histological level, the small intestine consists of villi, or finger-like projections (**Figure 1.1**), which protrude into the lumen providing maximal surface area to absorb food. At the base of each villus is a crypt, or invagination, where cells divide and migrate upward to repopulate the structure. Whereas the small intestine contains "crypt-villus units," the colon consists of only crypts. A single layer of cells lines these crypts and villi and is collectively referred to as the "intestinal epithelium." As the intestine is constantly enduring mechanical and chemical stress, this epithelium regenerates entirely every 7 days. The source of this regeneration is rapidly dividing stem cells that reside at the base each crypt. These cells give rise to progenitors that differentiate into absorptive cells (**enterocytes**) or secretory cells (**goblet**, **enteroendocrine**, or **Paneth** cells). As cell differentiate, they migrate up the crypt base to the villus where they ultimately undergo apoptosis and slough off into the lumen. Understanding this dynamic—stem cells giving rise to various lineages along the crypt-villus axis—has been the subject of intense investigation over the last decade.

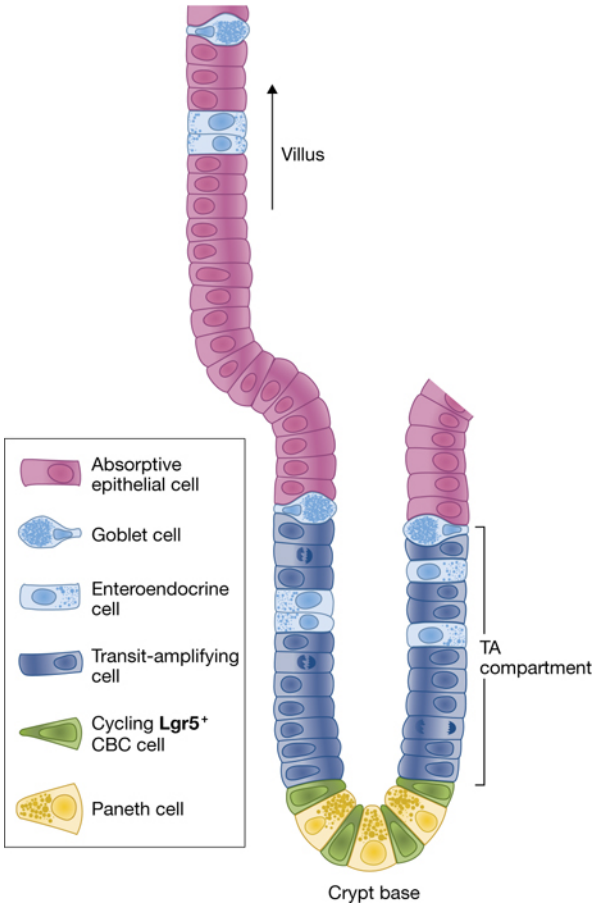

Figure 1.1 Schematic of small intestinal villus and crypt. Intestinal stem cells (green) reside at the base of the crypt interspersed between Paneth cells (yellow). Wnt signaling is critical in maintaining and propagating intestinal stem cells. A stem cell progenitor migrates up the crypt and either differentiates into an enterocyte (pink) or into one of secretory cells goblet (blue), enteroendocrine (blue), or Paneth cells. High Notch signaling drives the stem cell progenitor into an enterocyte while low Notch signaling triggers secretory cell differentiation. Enterocytes, goblet cells, and enteroendocrine cells continue to migrate up the crypt-villus until they ultimately slough off into the lumen. In contrast, the Paneth cell migrates back down to the bottom of the crypt where it takes its place intermingled between stem cells. This figure was adapted[1].

Wnt signaling and intestinal stem cells

While Rudolf Virchow made the observation that *omnis cellula e cellula* ("every cell stems from another cell") in 1835, our insight into this fundamental biological principle of self-renewal has been limited until recently. With the advent of powerful genetic mouse models, our knowledge of intestinal stem cells has rapidly expanded. What has emerged over the last ten years is the principle that the two most important signaling pathways that regulate the intestinal epithelium are the Wnt and Notch pathways. Broadly, Wnt signaling primarily drives stem cell regeneration, while Notch signaling controls cellular differentiation as cells migrate up the crypt.

The Wnt signaling pathway is initiated when Wnt ligands bind to a family of extracellular receptors, Frizzled (Fz), and co-receptors including Lrp-5/6[2] (**Figure 1.2A**). Activation of Fz induces the stabilization of the transcription factor, β-catenin. This stabilization is due to the inactivation of the β-catenin destruction complex, which includes the protein APC. Once β-catenin is stabilized, it translocates to the nucleus where it couples with the TCF4 family of transcriptional factors to activate expression of target genes, such as *c-Myc, c-jun,* and *cyclin d1*[3–5], that promote proliferation and stem cell-like phenotypes. Initial studies in the 1980's and 1990's uncovered that key components of the Wnt signaling pathway were mutated in colorectal cancer (CRC). For example, *APC* mutations, rendering APC unable to destabilize β-catenin, were identified in CRC[6,7]. Moreover, mice carrying mutant *Apc* alleles developed intestinal adenomas featuring nuclear β-catenin[8]. Likewise, mutations stabilizing β-catenin were shown to promote adenoma formation and growth[9].

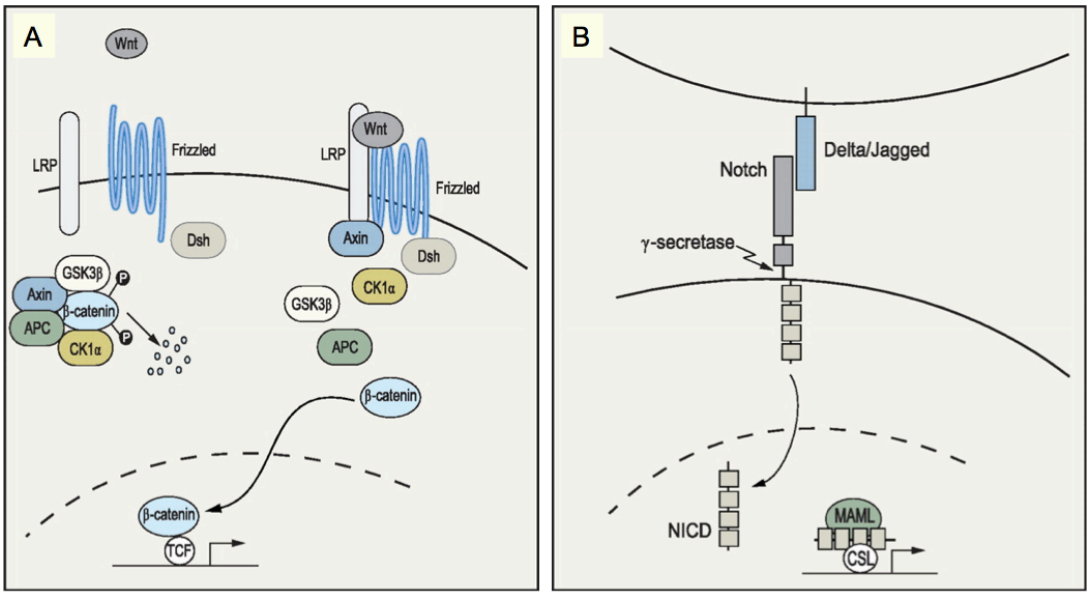

Figure 1.2. Wnt and Notch signaling cascades. (**A**) Wnt ligands bind to extracellular Wnt receptors, Frizzled (Fz) and Lrp-5/6, to inhibit formation of the APC-GSK3β complex that degrades β-catenin. Free β-catenin then translocates to the nucleus where it couples with TCF4 to initiate transcription of Wnt target genes. (**B**) Notch ligands (Delta-like 1-4 or Jagged 1-4) bind to Notch receptors (Notch 1-4). This binding induces intracellular cleavage of Notch receptors by gamma-secretase, releasing the Notch intracellular domain (NICD) to interact with MAML and CSL to drive Notch target genes. This figure has been adapted[158].

As it became increasingly clear that dysregulation of the Wnt pathway drives malignancy, the field began to ask how the Wnt pathway operates in non-pathological settings. This pivot from studying Wnt signaling in malignant epithelium to studying Wnt signaling in the normal epithelium was in large part led by Hans Clevers' group and enabled by a battery of new genetic mouse models. Clevers' groups first generated a *Tcf4*-deficient mouse in 1998, which resulted in death shortly after birth[10]. Studying the tissue, Clevers noticed that *Tcf4*$^{-/-}$ mice lacked intestinal crypt proliferation. This observation highlighted the fundamental requirement of Wnt signaling to *maintain* a healthy intestinal epithelium. In support of this, it was shown in 2004 that adenoviral-mediated expression of the Wnt antagonist Dickkopf-1 inhibited intestinal proliferation and induced substantial architectural degeneration[11]. In 2007, Wnt/*Tcf4* target genes were shown primarily to be confined to the intestinal crypt, strongly suggesting that the source of the intestinal epithelium's Wnt-driven self-renewal was operating within the crypt. The notion of crypt-based stem cells dates back to 1975[12], but identification of a putative stem cell marker had remained elusive because of limited molecular and genetic tools. Once the Wnt pathway was shown to be essential in maintaining the intestinal crypt, the framework was in place to identify the cellular source of intestinal self-renewal.

The search for an intestinal cell "marker" came to fruition when Barker *et al.* identified *Leucine-rich-repeat-containing- G-protein coupled protein receptor 5* (*Lgr5*), a *Tcf4* target, marked rapidly dividing crypt-based cells that had the capability of generating all epithelial lineages[13]. Moreover, a single *Lgr5*$^{+}$ cell had the potential to recapitulate intestinal cultures *in vivo*[14]. *Lgr5*, a seven-pass transmembrane protein consisting of large extracellular domain with leucine-rich repeats[15], associates with

Frizzled/Lrp5/6 receptors and binds the Wnt agonist R-spondin to stimulate Wnt signaling. Thus, *Lgr5* is not only a target of Wnt signaling but also enhances Wnt tone. *Lgr5*$^{+}$ cells are interspersed at the crypt between Paneth cells (**Figure 1.1**). The molecular underpinnings of how *Lgr5*$^{+}$ cells divide and repopulate the intestinal crypt remains incompletely characterized, but it is an area of intense investigation.

Notch signaling and intestinal cell fate

Whereas as Wnt signaling is critical in maintaining stem cell self-renewal, Notch signaling plays a critical role in specifying intestinal epithelial cell fate[16]. Notch signaling consists of Notch ligands (Delta-like 1-4 or Jagged 1-4) binding to Notch receptors (Notch 1-4) (**Figure 1.2B**). The binding induces intracellular cleavage of Notch receptors by gamma-secretase, releasing the Notch intracellular domain (NICD) to translocate to the nucleus where it complexes with CSL to induce transcription of Notch targets genes like *Hes1*. Studies over the last decade have revealed that Notch signaling regulates whether cells differentiate into absorptive enterocytes or secretory cells (goblet, enteroendocrine, or Paneth cells). Ectopic expression of Notch1[17] or NICD[18] was shown to drive cells into enterocytes at the expense of secretory cells. Conversely inhibiting Notch signaling through pharmacologic[19] or genetic[20] mechanisms resulted in increased goblet, enteroendocrine, and Paneth cells at the expense of enterocytes. These complementary studies revealed that hyperactive Notch signaling augments enterocyte production while low Notch activity releases cells to differentiate into secretory cells.

Genetic studies have teased out specific downstream effectors essential for this absorptive versus secretory cell decision. *Hes1,* for example, is a critical Notch effector. Constitutive expression of NICD expression upregulates *Hes1*[18], and in the absence of

Hes1, mice have more secretory cells and less absorptive enteroctyes[21]. In contrast to *Hes1*, *Atoh1* (*Math1*) was shown to be essential for *secretory* cell differentiation. Indeed, *Atoh1*$^{-/-}$ mice lack secretory cells[22] while mice overexpressing ATOH1 had crypts and villi populated with secretory cells at the expense of enterocytes[23]. Mice lacking *Atoh1* are even resistant to gamma secretase inhibitor (GSI)-induced secretory cell differentiation[24]. As increased *Atoh1* expression was observed in the setting of Notch inhibition[19], it was postulated that *Atoh1* and Notch share an epistatic relationship. This was strongly supported by an elegant genetic model showing that while knocking out *CSL*, an important component of the Notch transcription activation complex, led to a loss of enterocytes and an increase in secretory cells, knocking out both *CSL* and *Atoh1* completely rescued the phenotype and resulted in complete loss of intestinal secretory cells[25]. Thus, Notch signaling determines whether stem cell progenitors give rise to absorptive versus secretory cells largely through its effects on *Hes1* and *Atoh1*.

While Atoh1 is required for any secretory cell lineage, there are other lineage specification factors that operate downstream of Atoh1 to ensure proper differentiation. Knocking out *Gfi1* prevented differentiation of goblet and Paneth cells yet increased enteroendocrine production[26,27], suggesting a branch point in intestinal lineage differentiation is enteroendocrine versus goblet/Paneth. Indeed, transgenic expression of *Neurogenin3* resulted in increased embryonic enteroendocrine cells at the expense of goblet cells[28]. There have been increasing reports that support the hypothesis of a goblet/Paneth progenitor. Genetic deletion of *Sox9*[29] or *Spedf*[30], for example, result in decreased goblet and Paneth cells but normal enteroendocrine numbers. Understanding

the genetic factors that dictate these lineage branch points is important to further clarify how intestinal stem cells give rise to differentiated cells.

Paneth cells and their unique role

Amongst the three main secretory cell types, the Paneth cells are unique. While goblet and enteroendocrine cells migrate up the intestinal crypt-villus, the Paneth cell migrates down into the crypt where it nestles between *Lgr5*$^{+}$ cells (**Figure 1.1**). Moreover, as opposed to enteroendocrine and goblet lineages, Paneth cells do not differentiate until after birth when crypts emerge. Paneth cells were once thought primarily to generate and secrete anti-microbial peptides, but recent studies have shown that they cells also produce Notch and Wnt ligands[31]. Because Paneth cells express Wnt and Notch ligands and are located interspersed between *Lgr5*$^{+}$ cells, they have been suggested as key stem-cell niche regulators. But their role in maintaining the intestinal stem cell crypt is controversial. Sato *et al.* proposed that Paneth cells were essential for maintenance of stem cells by showing that *Gfi1*$^{-/-}$ and *Sox9*$^{-/-}$ mice lacking Paneth cells have diminished stem cell function[31]. An important caveat to these findings, however, was that *Gfi1*$^{-/-}$ and *Sox9*$^{-/-}$ mice have incomplete or temporary loss of Paneth cells. Moreover, Sato *et al.* used immunohistochemistry for the stem cell marker OLMF4 as the only readout for stem cell function. In contrast, Kim *et al.* conditionally deleted *Atoh1* from the intestinal epithelium, thus permanently ablating Paneth cells, in a *Lgr5*^{GFP} reporter mouse[32]. They found that despite the loss of Paneth cells, *Lgr5* positive cells were intact and functioning. In fact, *Lgr5*+ cells populated the entire crypt. Kimi *et al.*'s findings were inconsistent with Sato et al.'s conclusions that Paneth cells are required for

stem cell maintenance. Thus, the role of Paneth cells remains incompletely understood, especially with respect to maintaining a stem cell niche.

Overall, the intestinal epithelium–stretching from the small intestine to the colon—is a complex and dynamic regenerating tissue. Intestinal homeostasis relies on complex interactions between the intestinal epithelium, microbiota, and host immune system, all of which cooperate to maintain homeostasis in an environment colonized and challenged by an estimated 100 trillion bacteria. It is the disruption and dysregulation of these interactions that is currently thought to underlie intestinal pathologies. When normal processes are disrupted, the epithelium becomes dysregulated. Given their prominent role in the intestinal epithelium, it is not surprising then that Wnt and Notch signaling are often dysregulated in intestinal pathologies like colorectal cancer (CRC) and inflammatory bowel disease (IBD).

The genetics of colon cancer

Colorectal cancer is one of the leading causes of cancer mortality in the United States[33]. Work in the 1980's and 1990's conducted by Bert Vogelstein led to a breakthrough in understanding CRC. Through analysis of colonic tumors from various stages of development, Vogelstein proposed a model in which CRC develops through serial acquisition of specific mutations (**Figure 1.3**). Importantly, these mutations were both in oncogenes *and* in tumor suppressor genes, underscoring the still nascent concept that tumor promoters and suppressors must be dysregulated for most cancers to develop[34]. Vogelstein's landmark work was eventually supported and expanded by future sequencing analyses and functional studies. With the advent of large scale genomic

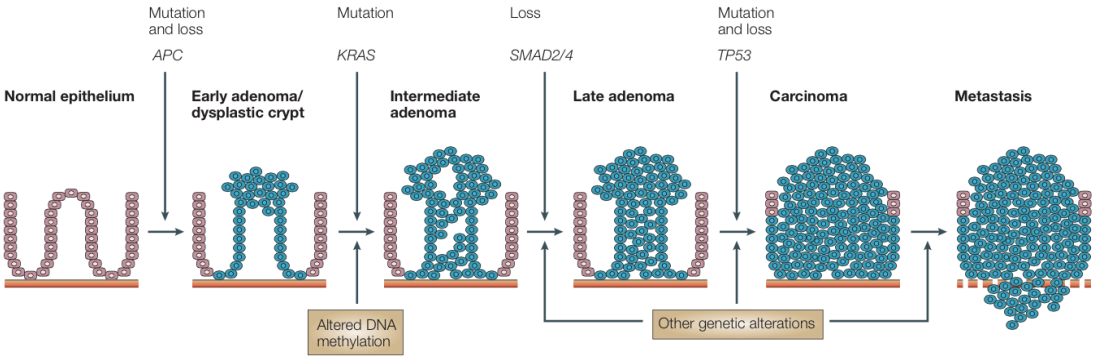

Figure 1.3. The genetic progression of colorectal cancer. "Vogelgram" of sequential mutations that transform a normal colonic crypt into a pre-malignant neoplasm and ultimately into a colorectal carcinoma. This figure has been adapted [159].

sequencing and generation of mouse tumor models, the mutations that were required for CRC came into focus.

More than 80% of CRCs feature a mutation inactivating *adenomatous polyposis coli* (APC), a tumor suppressor that acts as a regulator of the Wnt/β-catenin signaling pathway[6,35]. Inactive APC allows β–catenin to accumulate and shift to the nucleus where it couples with TCF4 to initiate transcriptional programming, promoting tumor development[2,6]. The role of constitutive Wnt signaling is well-established in intestinal carcinogenesis. Familial Adenomatous Polyposis (FAP), a disease marked by the development of hundreds of colonic tumors, often features APC loss of function[36]. Similarly, mice carrying inactive APC mutations, such as the $Apc^{1638/+}$allele, are predisposed to developing intestinal tumors[8,37]. In both human and mouse tumors Wnt target genes such as *Lgr5, Myc,* and *Ccnd1* are overexpressed[3,38,39]. Similarly, dysregulated Notch signaling contributes to CRC. Inhibiting Notch pharmacologically inhibits intestinal tumorigenesis[19,24]. Moreover, Notch signaling is required to maintain the intestinal proliferative compartment[20]. Indeed, recent studies show that Notch and Wnt cooperatively induce tumorigenesis[40,41]. How the Wnt and Notch networks escape regulation and become dysregulated is incompletely understood.

Inflammatory bowel disease and colitis-associated cancer

Ulcerative colitis and Crohn's disease are the two primary forms of inflammatory bowel disease (IBD). IBD is one of the most common intestinal diseases in the United States with an estimated 1.4 million suffering from the disease[42]. The medical complications of IBD are serious and numerous: stricture and fistula formation, infection, severe pain, anemia, biliary disease, malnutrition, and an elevated risk of developing colorectal cancer[42]. Despite this devastating impact and concerted research efforts, the fundamental pathophysiology of IBD remains unclear.

Defects in mucosal integrity are thought to be important contributors to IBD. Indeed, alterations in mucosal junctional proteins, such as the Cadherin and the Claudin families, that help maintain barrier function have been documented in IBD patients[43–45]. Animal modeling has supported the notion that barrier dysfunction underlies IBD: transgenic mice expressing an active form of *Myosin light chain kinase* (MLCK), which impairs the intestinal barrier, have increased susceptibility to experimentally induced colitis[46]; mice expressing a dominant-negative form of N-cadherin, a junctional protein, develop spontaneous colitis[47]; and mice lacking the tight-junction protein, JAM-A, have worse colitis after dextran sodium sulfate (DSS) administration[48]. Dysfunction of differentiation programs can also compromise the intestinal barrier. *Muc2*$^{-/-}$ mice, who lack intestinal goblet cells, develop colitis spontaneously and have significant barrier defects[49,50]. Similarly, intestinal specific deletion of the Notch transcription factor, *CSL*, allows bacterial translocation into the intestinal barrier, inducing spontaneous colitis[51]. Thus, preservation of the intestinal epithelial barrier is critical in protecting against colitis.

Given the intestinal epithelium sustains continual injury and insult, defects in mucosal repair programs are also thought to be contributing factors to IBD pathology[48,52–54]. Resealing of the epithelium after an injury requires a process termed restitution, in which epithelial cells migrate to the damaged area and subsequently proliferate and differentiate. It is currently held that in order for epithelial cells to migrate and properly heal injured mucosa, they must convert to a mesenchymal-like phenotype, a process broadly defined as epithelial-to-mesenchymal transition (EMT)[55]. A key switch in this transition is the change in junctional protein characteristics. E-cadherin, for example, an adherens junction protein distinct to epithelial cells that is a negative regulator of Wnt signaling, is abnormal in clinical samples from IBD patients where its sub-cellular localization is altered in regenerating and migrating epithelium adjacent to ulcers and appears to correlate with disease severity[52]. Cellular adhesion proteins provide not only structural support, but they also provide a means for cellular signaling. For example, ZO-1, a tight junction protein, sequesters GEF-H1 (activator of RhoA) and ZONAB (a Y-box transcription factor) at the cell membrane and initiates cytoskeletal rearrangement. Given the implications, EMT is rapidly emerging as a pivotal player in repair programs and consequently IBD. Recently, EMT defects in Crohn's disease patients were postulated to be responsible for fistula formation[56]. To date, the regulation of EMT in response to inflammatory injury remains unclear and complex. But it is an area of intense investigation because of the immense therapeutic potential.

As IBD patients experience recurrent, chronic inflammation, they are at an estimated 10-fold elevated risk of developing colon cancer[57,58]. Indeed, the longer duration and severity of disease, the higher risk IBD patients have of developing cancer[59].

This colitis-associated cancer (CAC), however, that IBD patients are prone to developing has its own set of genetic properties that make it distinct from sporadic CRC. For example, whereas inactivation of APC is a foundational, early event in sporadic CRC, inactivation of APC is thought to occur at a later stage in CAC[58]. More broadly, while sporadic CRC appears to be primarily driven by sequential genetic changes, CAC development appears to be more multifactorial and dynamic. Indeed, there appears to be a complex interplay between the epithelium, immune system, and microbiota that is ultimately dysregulated. Loss of the anti-inflammatory cytokines such as IL-10 have been shown to accelerate CAC development in mice[60,61]. Dysregulation of the myeloid-epithelial NF-κB-IL6-Stat3 signaling axis[62] contributes to CAC, as does dysregulation of the innate immune system[63]. More recently, changes in the microbiota have been shown to alter CAC development[64]. Thus, while it is well known that chronic inflammation promotes colon cancer, the precise mechanisms underlying this transformation remain unclear.

Introduction to Myeloid Translocation Genes

In 1993, it was discovered that a frequent chromosomal translocation in acute myeloid leukemia (AML) t(8;21)(q22;q22) resulted in the genetic fusion of *AML1* and *MTG8*[65]. The discovery strongly suggested that that both genes played an important role in hematopoiesis and prompted further studies. Indeed, *AML1* was shown to be an essential transcriptional regulator for appropriate hematopoiesis[66]. Based on the presence of proline-rich regions and zinc-finger like motifs, *MTG8* was postulated to be a transcriptional factor. Soon after the 1993 report, two MTG8 human homologues were identified: MTG16 and MTGR1[67]. *In vitro* experiments revealed that MTGs are transcriptional corepressors that bind to DNA binding proteins and recruit other corepressors and histone deacetylases (HDACs) to downregulate transcription of target genes[68–70] (**Figure 1.4**).

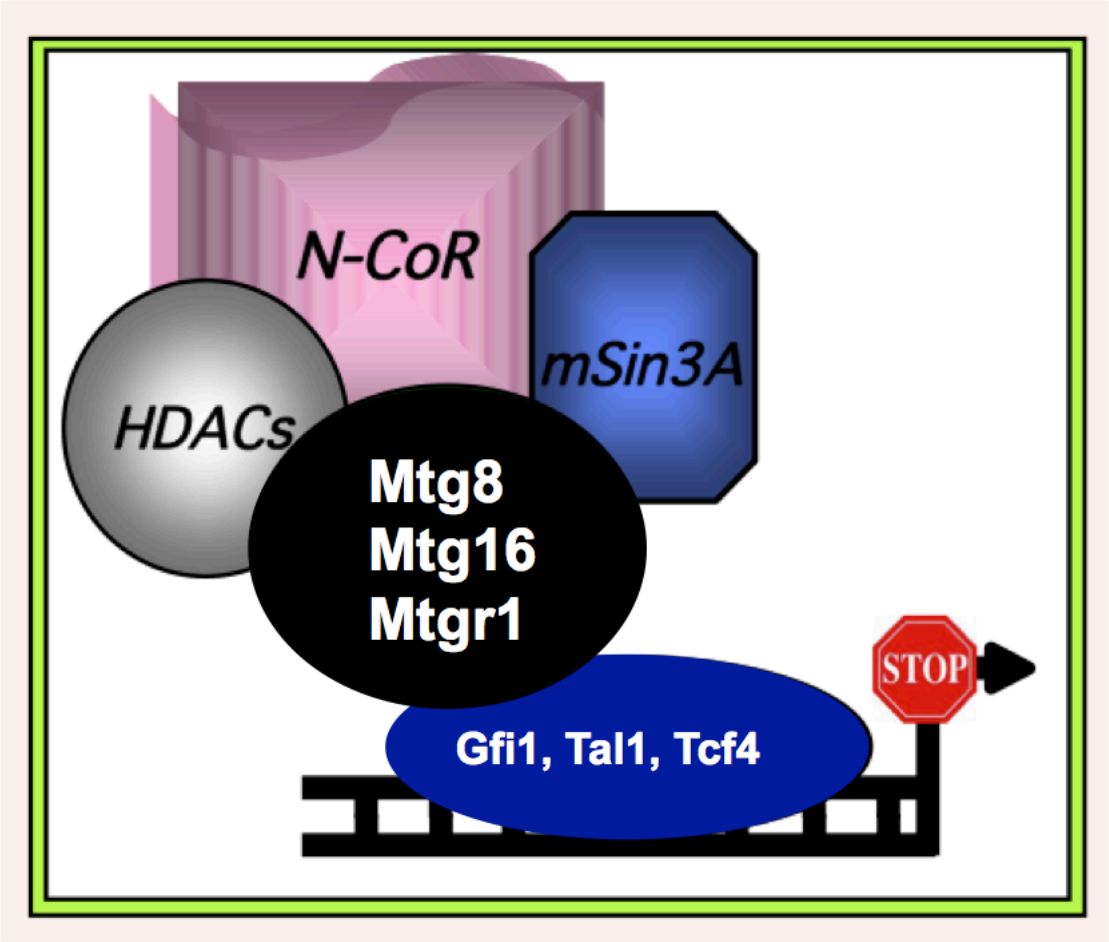

Figure 1.4 Myeloid translocation genes act as transcriptional corepressors. MTGs do not bind DNA, but interact with and recruit other transcriptional corepressors such as Histone Deacetlysates, NCoR, and mSin3A to repress transcription. MTGs can also associate with DNA binding transcription factors like Gfi1, Tal1, and Tcf4.

The scope of MTG function was substantially broadened when Calabi *et al.* generated *Mtg8* knockout mice. *Mtg8*$^{-/-}$ showed deletion of their mid-gut[71], demonstrating that the MTGs play not only a regulatory role in hematopoiesis but in the gastrointestinal system. This was further supported when Amann *et al*. deleted *Mtgr1* and observed the mutants had a dramatic reduction in intestinal secretory cells[70]. *Mtg16*$^{-/-}$ mice had a less dramatic phenotype but also had less goblet cells[72]. Moreover, both *Mtgr1*$^{-/-}$ and *Mtg16*$^{-/-}$ mice demonstrated increased intestinal proliferation[70,72–74]. The role of MTGs in the gut was not just confined to baseline physiology. Mice lacking MTGs have impaired recovery after intestinal injury. *Mtgr1*$^{-/-}$ and *Mtg16*$^{-/-}$ mice experience worse injury in response to DSS and infectious-induced colitis[73,74]. Thus, while MTGs were initially discovered because of the t(8;21)(q22;q22) in AML, genetic experiments indicated that MTGs play an essential role in maintaining intestinal homeostasis by regulating stem cell and differentiation programs.

Given that MTG-deficient mice had significant intestinal phenotypes, it was postulated that MTGs could regulate Wnt or Notch signaling. Moore *et al*. showed that all three MTG family members interact with TCF4 and compete with β-catenin for TCF4 occupancy[75]. This competition suggested a model in which loss of MTGs results in unfettered β-catenin access to TCF4 and activation of Wnt targets. In support of this model, *Mtgr1*$^{-/-}$ mice had increased intestinal Wnt targets[75]. While MTGs did not bind to ATOH1, all three associated with the Notch effector CSL and MTG16 uniquely associated with NICD[75]. This suggested a model in which MTGs serve as key upstream regulators of Wnt and Notch signaling.

Mammalian MTG family members are closely related to a Drosophila homologue, *Nervy*[76]. In particular, there are four MTG regions that are highly homologous to *Nervy*, and these are designated "Nervy Homology Region" (NHR 1-4) (F**igure 1.5A**). Each NHR domain is important for various MTG interactions (**Figure 1.5B**). For example, NHR1 can interact with DNA binding transcription factors like E2A[77] while NHR2 associates with mSin3A[78,79]. While the conservation of these NHR domains is putatively responsible for MTGs having similar binding partners, there are unique MTG interactions. MTGR1 and MTG8, for example, can interact with mSin3a, but MTG16 is unable to[69,70]. Moreover, each family member has different binding affinities. MTGR1, MTG8, and MTG16 can repress E47 mediated transcription, but MTG16 is more effective[80]. Thus, the molecular mechanisms underlying the differences in MTG binding partners and binding affinities remains unclear. Given the conservation of the NHR domains, it is likely the regions between the nervy homology domains have an important role to play.

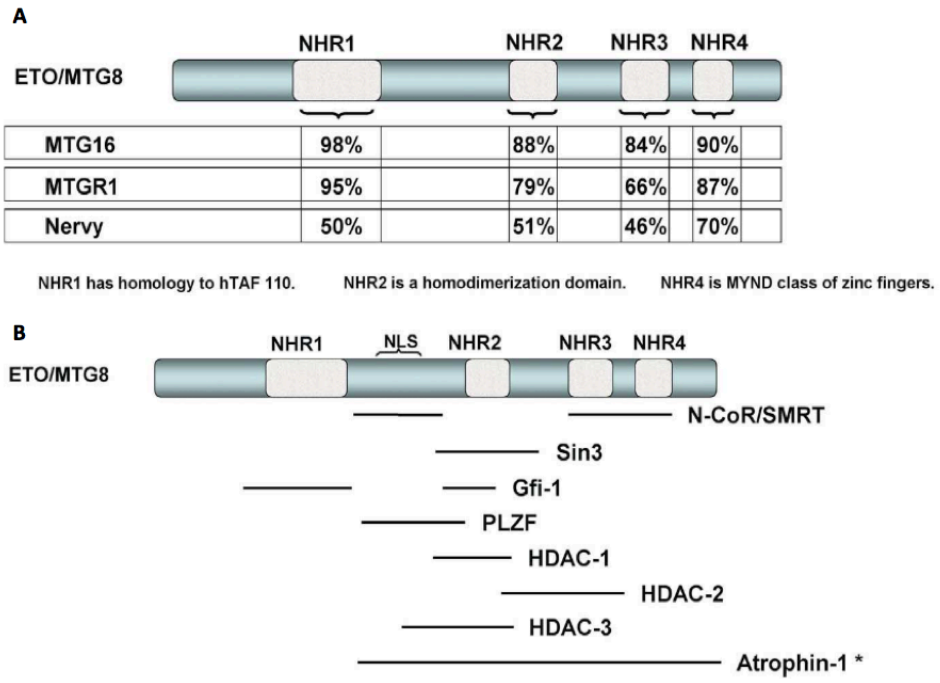

Figure 1.5 Schematic of MTG homology and binding domains. (A) Mtg8, Mtgr1, and Mtg16 are highly homologous with the drosophila protein Nervy in four regions designated the Nervy Homology Domains (NH1-4). (**B**) Map of known MTG interacting proteins. This figure has been adapted[76].

Introduction to BVES

Blood vessel epicardial substance (BVES or POPDC1) is a tight junction associated protein originally discovered from a cDNA screen of a developing heart by two independent laboratories[81,82]. BVES is the founding member of the POPDC family, which also consists of POPDC2 and POPDC3. POPDC2 and POPDC3 are 50% homologous while BVES is only 25% homologous to either family member, suggesting an evolutionary divergence[83,84]. The structure of the POPDC family members has no homology with other proteins, implicating a unique cellular function. BVES, the most well studied family member, consists of 360 residues with three hydrophobic regions, two glycosylation sites, and an intracellular domain of high intra-family homology termed the POPEYE domain (**Figure 1.6**). The POPEYE domain is highly conserved (80%) across the family throughout different vertebrates[84,85]. Interestingly, BVES does not contain any motifs or domains found in known classes of adhesion molecules. Two lysines (K272, K273) located on the carboxy end of this domain are required for homodimerization[86].

While the structure of BVES does not provide immediate clues to its function, its expression pattern does. BVES is expressed in a wide-variety of tissues: heart[81,82], smooth and skeletal muscle[87], retina[88], intestine[89,90], lung[91], and breast[89]. The common property of BVES-expressing tissue is cell adherence. Indeed, further work identified that BVES contributes to cell-cell adhesion. When cells are in a subconfluent state, BVES is primarily localized to the cytoplasm (**Figure 1.7**). But when cells make contact, BVES traffics to the cellular membrane[83] (**Figure 1.7**). Specifically, BVES localizes to

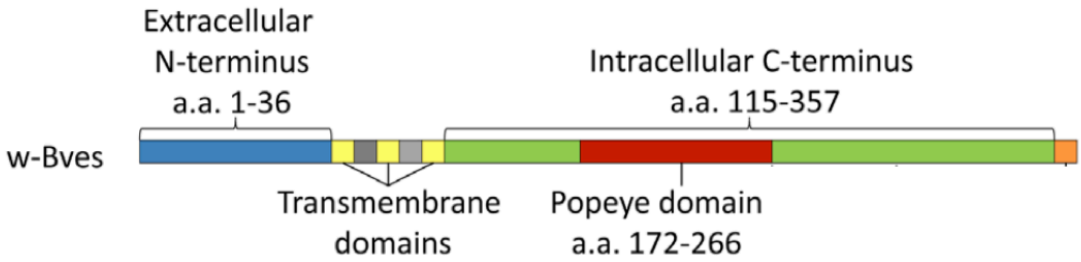

Figure 1.6 Schematic of BVES. Blood vessel epicardial substance (BVES/POPDC1) consists of a 36 residue extracellular amino terminus followed by three transmembrane domains. The cytoplasmic portion is approximately 200 residues and contains the Popeye domain which is highly conserved with POPDC2 and POPDC3. This figure has been adapted[92].

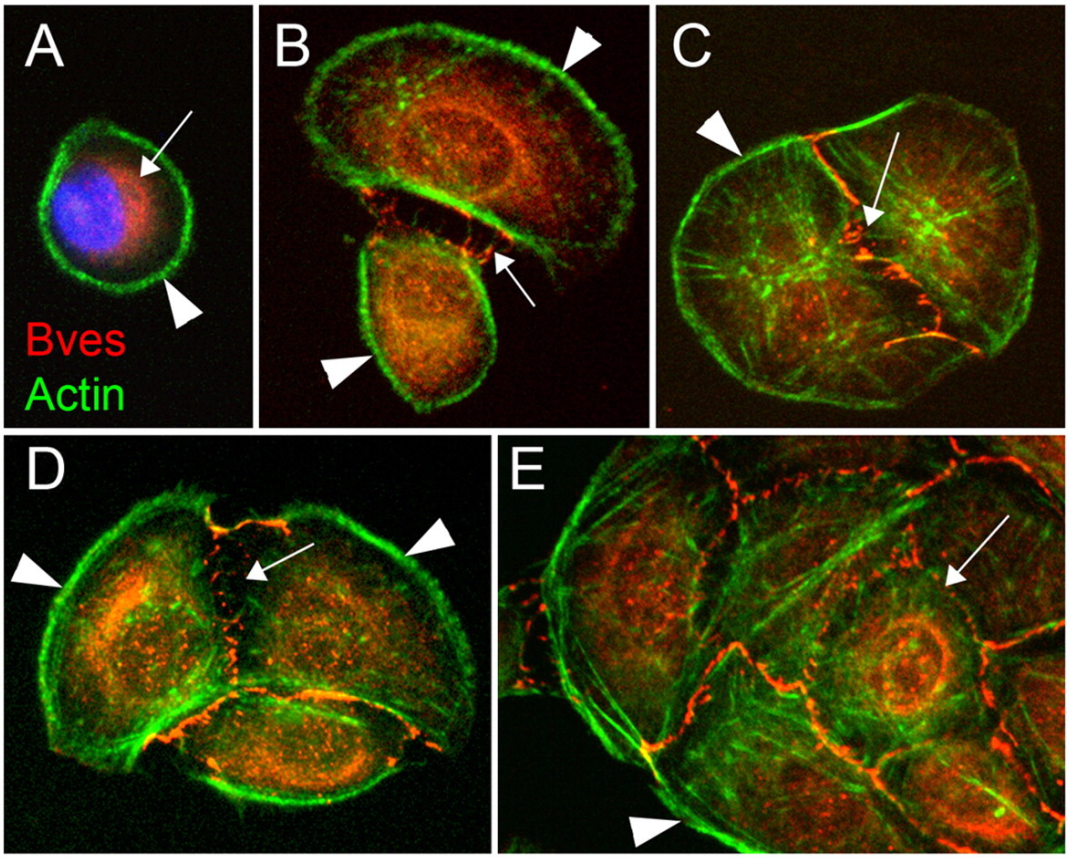

Figure 1.7. BVES localization is dynamic. BVES subcellular localization changes depending on cell-cell contact. BVES (red) is primarily confined to the cytoplasm when cells (Epicardial mesothelial cells) are subconfluent (A-B), but as cells make contact, BVES localizes to the plasma membrane (C-E). This figure has been adapted[83].

points of cell-cell contact and co-localizes at the tight junction with ZO-1 and Occludin[83].

Because of the dynamic subcellular localization of BVES, it was postulated that BVES plays an important role in epithelial-to-mesenchymal transition (**EMT**) similar to the regulatory role of E-cadherin. In support of this, overexpression of BVES increased transepithelial resistance (TER), and conversely, disruption of BVES reduced TER[83,92]. This was further supported by the *in vivo* observation that *Bves*$^{-/-}$ mice have impaired skeletal muscle recovery after injury[87]. Recovery from injury requires the orchestration of cellular migration and polarization—both of which were abnormal in *Bves*$^{-/-}$ muscle. Thus, initial reports about BVES suggested that BVES generally played a role in maintaining epithelial states.

Studies eventually began to elucidate the cellular mechanisms by which BVES regulates epithelial states. Smith *et al.* conducted a yeast-two-hybrid screen and identified that BVES interacted with Guanine nucleotide exchange factor T (GEFT)[93]. Broadly, GEFs stimulate the exchange of GDP for GTP and thereby activate Rho GTPases. GEFT activates Rac1 and Cdc42 to induce lamelipodia and filopodia formation during cellular migration. It was shown that expression of a mutant form of BVES resulted in less motile and more round cells[93]. This correlated with less active forms of Rac1 and Cdc42. However, the report was not conclusive as to how BVES regulates RhoA signaling. In a follow up study, Russ *et al.* provided evidence that BVES acts to reduce RhoA signaling as well as maintain junctional integrity in epithelial cells. They not only showed that BVES could interact with GEFH, but they also showed that overexpression of BVES reduced RhoA activity[92]. In contrast, expression of a dominant negative form of BVES increased RhoA activity. Moreover, they found that in addition to co-localizing with ZO-

1, BVES immunoprecipitated with ZO-1. When BVES was overexpressed, ZO-1 and Occludin were confined to the cellular membrane. But when a dominant negative form of BVES was expressed, ZO-1 and Occludin were primarily intracellular. This suggested that BVES was essential in maintaining junctional integrity.

More recently, Hager *et al.* identified VAMP3, a SNARE protein family member involved in vesicular transport, as a BVES interacting protein via a yeast-two-hybrid approach[94]. Hager *et al.* showed that silencing BVES disrupted β-1-integrin recycling during cellular migration. The identification of VAMP3 as a BVES binding partner placed BVES in a dual-regulatory role of cellular migration. While VAMP3 and GEF proteins function within the cell differently, both signaling pathways fundamentally govern cellular migration. That BVES is important in both suggested it acts as a broad regulator of cellular migration. The mechanism of the regulation is unclear other than the importance of the interaction. But more generally this report suggested that BVES could act as an important regulator of multiple signaling pathways.

In 2012, Froese *et al.* showed that BVES has an important regulatory role in cardiac myocytes[95]. *Bves*$^{-/-}$ mice had impaired stress-induced bradycardia, suggesting a sinus node defect. Because of the importance of cAMP in cardiac pacemaking and because a cAMP binding domain was present in the POPEYE domain, they tested whether BVES could bind to cAMP. Biochemical experiments showed that BVES directly bound to cAMP and the binding domain was mapped to a three amino acid stretch in the POPEYE domain. Moreover, BVES bound to the 2-pore domain potassium channel TREK-1, and this BVES-TREK1 interaction was sensitive to cAMP stimulation. It was postulated that BVES could recruit TREK-1 to the membrane to enhance current,

and that this recruitment was modulated by levels of cAMP[95]. This report dramatically expanded the known regulatory roles of BVES by showing its importance in cardiac pacemaking. Moreover, the report showed a firm *in vivo* functional relevance to BVES.

In addition to acting as a regulator cellular motility and cardiac packemaking, Williams *et al.* found that BVES has an important tumor-suppressive function. BVES was underexpressed in several epithelial malignancies, including breast and colorectal cancer[89]. This downregulation was putatively due to BVES promoter hypermethylation, and the report showed that treatment of CRC cell lines with demethylating agents restored BVES expression. Moreover, restoration of BVES expression in CRC cell lines induced an epithelial-like morphology and decreased cellular proliferation, invasion, and metastasis (**Figure 1.8**). In contrast, disrupting BVES in epithelial cells induced a mesenchymal-like morphology and increased cellular proliferation. In sum, BVES acted as a regulator of EMT. The study concluded that this regulation was in part due to BVES-induced regulation of RhoA signaling. But how BVES reduced cellular proliferation, migration, and invasion remained only partially explained. Given the increasing number of identified BVES interacting proteins, it was reasonable to predict that other unknown interacting proteins also explained the tumor suppressive mechanisms of BVES.

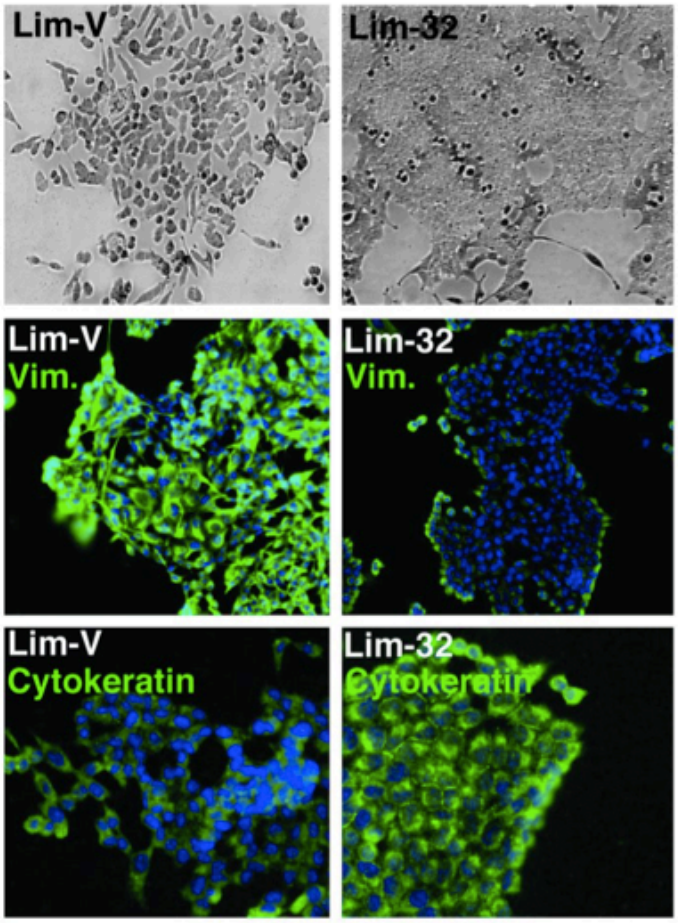

Figure 1.8. BVES expression in CRC cell lines induces epithelial-like phenotype. Bright field microscopy and immunofluorescent staining for vimentin and cytokeratin in Lim2405 cells (Lim-V) and Lim2405 cells that express BVES (Lim-32). This figure has been adapted[89].

Rationale and hypothesis for dissertation

For my thesis work, my general hypothesis was that the MTG family and BVES were important regulators of the intestinal epithelium and tumorigenesis. Specifically, I hypothesized that given the role of MTGs in regulating hematopoietic stem cells and *Mtg16*$^{-/-}$ and *Mtgr1*$^{-/-}$ intestinal phenotypes, MTGs have an important role in regulating intestinal stem cell biology and tumorigenesis. Also, because BVES is underexpressed in CRC and BVES regulates epithelial phenotypes, I hypothesized that loss of BVES would augment intestinal tumorigenesis. Moreover, other BVES interacting proteins would explain how BVES regulates epithelial phenotypes. Overall, the primary objective of my work was to further elucidate the functional role of MTGs and BVES in the intestinal epithelium and carcinogenesis.

Chapter 2

The transcriptional corepressor MTGR1 regulates intestinal secretory lineage allocation[1]

Introduction

Intestinal differentiation programs are highly complex and dynamic. Stem cells reside at the crypt base intermingled with Wnt-agonist-secreting Paneth cells. As the stem cell divides, it gives rise to daughter cells that migrate along the crypt-villus axis and differentiate into secretory cells (goblet, enteroendocrine, and Paneth) or absorptive enterocytes[16,17]. The molecular mechanisms underlying how intestinal stem cells differentiate into secretory or absorptive cells are incompletely understood, but Notch signaling plays a critical role in lineage allocation[96].

The Notch pathway is activated by ligand binding to Notch receptors, which induces intracellular proteolytic cleavage by gamma-secretase releasing the Notch Intracellular Domain (NICD) to translocate to the nucleus, where it binds to the DNA binding transcription factor Suppressor of Hairless Homolog (CSL)[96]. NICD then cooperates with Mastermind-like (MAML) to drive the expression of Hairy/Enhancer of Split 1 (HES1) and commits the intestinal progenitor to an absorptive fate[16,97]. Genetic experiments in mice show that ectopic expression of Notch receptors or NICD result in villi populated predominantly by absorptive enterocytes at the expense of secretory lineage production and concomitant downregulation of secretory transcript markers *Mucin2 (Muc2)* and *Chromogranin A (Chga)*[16–18,98]. Conversely, in the absence of Notch signaling, intestinal progenitor cells differentiate preferentially into secretory cells. Pharmacologic inhibition of Notch signaling using gamma-secretase inhibitors (GSI) or

[1] Published in The FASEB Journal (2015).

genetic ablation of Notch function causes villi to be populated by secretory cells at the expense of absorptive enterocytes[19,20,99].

Myeloid translocation gene-related 1 (MTGR1) is a member of the myeloid translocation gene (MTG) family of transcriptional corepressors. MTGs were originally discovered in acute myeloid leukemia and function as scaffolding proteins, orchestrating the formation of repression complexes[76]. *MTGR1* is widely expressed, including in the intestinal epithelium, and complexes with mSin3a, N-CoR, and histone deacetylases[70]. Experiments with knockout mice for all three family members have identified MTGs as regulating developmental, differentiation, and cancer programs. Some mice lacking *Mtg8,* a family member of *Mtgr1,* show a deletion of the midgut, suggesting an important role for MTGs in gut development[71]. *Mtg16*$^{-/-}$ mice revealed that Mtg16 was required for hematopoietic progenitor allocation and early progenitor differentiation[100]. Lastly, genetic ablation of *Mtgr1* revealed an increase in intestinal proliferation and a dramatic reduction in intestinal secretory cells, indicating *Mtgr1* is required for appropriate lineage allocation[70,75].

Given the importance of Notch signaling in determining intestinal differentiation, we hypothesized that unbridled Notch activation was driving the secretory lineage defect in *Mtgr1*$^{-/-}$ mice and that Notch inhibition could reverse the phenotype. RNA analysis of *Mtgr1*$^{-/-}$ intestinal crypts revealed increased Notch activity and downregulation of secretory markers. Similarly, *Mucin2 (Muc2), Chromogranin a (Chga),* and *Growth factor independent 1 (Gfi1)* were downregulated in whole *Mtgr1*$^{-/-}$ intestines, consistent with Notch activation. We determined that MTGR1 interacts with CSL, a key Notch effector, and suppresses Notch-induced transcriptional activity *in vitro*. Pharmacologic

Notch inhibition using the gamma-secretase inhibitor dibenzazepine (DBZ) in *Mtgr1*$^{-/-}$ mice rescued the hyperproliferation observed in *Mtgr1*$^{-/-}$ intestine as well as the goblet and enteroendocrine lineages. GSI treatment did not rescue the Paneth cell deficiency, however, suggesting MTGR1 is required for GSI-dependent Paneth cell specification. In sum, our findings indicate that MTGR1, a previously identified transcriptional corepressor known to be critical in hematopoiesis, is an important regulator of intestinal lineage allocation.

Materials and methods

Mice and Treatments

Ten Wildtype (WT) and twelve *Mtgr1*$^{-/-}$ mice were treated with vehicle or GSI at 10 μmol/L/kg twice daily for 5 consecutive days. GSI was prepared as previously described[101] and made fresh daily. GSI and vehicle were administered intraperitoneally after mice were sedated using isoflurane. All *in vivo* procedures were carried out in accordance with protocols approved by the Vanderbilt Institutional Animal Care and Use Committee.

Mouse small intestinal epithelial (MSIE) WT and *Mtgr1*$^{-/-}$ cell lines were generated and validated by the Vanderbilt Digestive Disease Center (DDRC) Novel Cell Line Development Subcore according to core based protocols[102]. Microarray analysis of WT and *Mtgr1*$^{-/-}$ crypts was conducted as previously described[75].

Immunohistochemistry

After the mice were sacrificed, the small intestine was harvested and irrigated with phosphate-buffered saline. The small intestine was cut transversely and divided into three equal sections: proximal, middle, and distal. The intestinal segments were then opened longitudinally and rolled orienting the most distal region of intestine such that it was located in the innermost part of the roll. The tissues were then fixed in formalin (1:10 dilution buffered) overnight. The solution was subsequently changed to 70% ethanol before standard paraffin-embedding. Five micron sections were cut and stained with hematoxylin and eosin (H&E) and periodic acid schiff (PAS) by the Vanderbilt Tissue Core. Goblet cells were scored by PAS staining. Proliferation was measured by phospho-histone H3 (pH3) staining using anti-pH3 at 1:150 (Upstate/Millipore, Billerica, MA, USA) and incubated overnight at 4°C. Enteroendocrine cells were assessed by Chromogranin A (CgA) staining using anti-CgA at 1:1000 (Immunostar, Hudson, WI, USA) and incubated overnight at 4°C. Anti-Lysozyme antibody (Dako, Carpinteria, CA, USA) at 1:500 incubated at room temperature for 1 hour was utilized to identify Paneth cells. Vectastain ABC Kit (Vector Laboratories, Burlingame, CA, USA) was used to perform all immunohistochemistry reactions. Dewaxing and antigen retrieval processing of sections was conducted as previously described[103].

Quantitative Reverse Transcription Polymerase Chain Reaction

Intestinal tissue from mice was isolated and immediately placed into 350 ul RNALater (Qiagen, Valencia, CA, USA) and stored at -80°C. RNA from tissue or cells was isolated using the RNAEasy kit (Qiagen, Valencia, CA, USA) according to manufacturer's

"Animal Tissue" protocol. RNA was subsequently stored at -80°C. Twenty microliters of CDNA was synthesized using Iscript cDNA Synthesis Kit (BioRad, Hercules, CA, USA) from 1 ug of RNA per sample. All RT-PCR reactions were carried out using SYBR green reaction mix (BioRad, Hercules, CA, USA) according to manufacturer's protocol.

The following primers were used to measure expression levels: *Gfi1* (RealTimePrimers #2421, Elkins Park, PA, USA) amd *Notch3* (RealTimePrimers #4249, Elkins Park, PA, USA). The following sequences were used for *Muc2* (F:TGCCCACCTCCTC2AAAGAC and R: GTAGTTTCCGTTGGAACAGTGAA), *Chga* (F:CCACTGCAGCATCCAGTT and R: AGTCCGACTGACCATCATCTTTC), and *NeuroD1 (F:* ATGACCAAATCATACAGCGAGAG and R: TCTGCCTCGTGTTCCTCGT). Reaction conditions used were previously described [24].

Plasmids

The pCMV5 expression plasmids containing HA-tagged MTGR1 were previously described [69]. The pCDNA3-myc-CSL, pCDNA3-N1-ICD, and the Hes1-luciferase reporter were previously described[104,105].

Immunoprecipitation and Western Blot

Immunoprecipitations and western blot protocols were carried out as previously described [104]. Briefly, HA-tagged MTGR1 and myc-tagged CSL were transiently expressed in COS7L cells. Whole cell lysates were subjected to immune precipitation with anti-myc monoclonal antibody 9E10 (Vanderbilt Monoclonal Antibody Core,

Nashville, TN, USA) and immune complexes were collected on Protein-G sepharose beads (Sigma, St. Louis, MO, USA). The presence of myc:CSL and HA:MTGR1 was determined in immune complexes by western blot using anti-myc 9E10 (Santa Cruz, Dallas, TX, USA) and anti-HA rabbit polyclonal antibody Y-11 (Santa Cruz, Dallas, TX, USA) respectively. Expression of HA:MTGR1 was confirmed by western blot with anti-HA monoclonal antibody 12CA5 (Santa Cruz, Dallas, TX, USA). Detection of tubulin using anti-tubulin (Sigma, St. Louis, MO, USA) served as a loading control.

Luciferase Promoter Assay

All luciferase promoter assays were conducted as previously described[104]. Briefly, NIH 3T3 cells were grown on 6-well plates and transfected with Lipofectamine and lysed 48 hours later according to manufacturer's protocol (Promega, Madison, WI, USA). Luciferase activity was quantified in whole cell extracts by luminometry according to manufacturer's instructions. Results were normalized to an internal control constitutive reporter (pCMV-Renilla) and expressed as mean +/- standard deviation.

Flow Cytometry

Flow cytometry was conducted as previously described[106]. Briefly, single-cell suspensions were formed after the thymus was minced into fragments and passed through a 70-μm filter. Cells were labeled with the appropriate combination of fluorochrome-conjugated anti-CD4 and anti-CD8 (eBioscience, San Diego, CA, USA). Analysis was performed with a 3-laser BD LSR II using FACSDiva software.

Statistical Methods

Immunohistochemistry (number of positively stained cells) was analyzed by one-way ANOVA. If only two groups were being compared, a Student's *t* test was used. The observer was blinded to slide identity, and the slide was scored in an unbiased fashion.

Results

Notch signaling is hyperactive in the setting of Mtgr1 loss

Histologic examination of *Mtgr1*$^{-/-}$ mice revealed reduced secretory cells, but the molecular mechanism underlying this defect was unclear[70]. To identify whether hyperactive Notch was driving the reduction in secretory cells, we reviewed transcriptome analysis from laser capture microdissected small intestinal crypts from WT and *Mtgr1*$^{-/-}$ mice as reported previously[75] and identified *Notch3* and Notch-effector *Deltex-homolog 1 (Dtx1)* were upregulated 2-fold, while secretory markers and targets of Notch repression *Atonal homologue 1 (Atoh1)* and *Chromogranin b (Chgb)* were downregulated 2-fold (**Figure 2.1A**). Transcriptome analysis of whole *Mtgr1*$^{-/-}$ small intestines by qPCR revealed a similar hyperactive Notch profile with goblet cell-associated *Mucin2 (Muc2)*, enteroendocrine-associated *Chromogranin A (Chga)*, and Paneth/goblet-associated *Growth factor independent 1 (Gfi1)* all downregulated (*Muc2* 3.5-fold $p<0.05$; *Chga* 4-fold $p<0.01$*; Gfi1* 3.4-fold $p<0.05$ **Figure 2.1B**). To determine whether the changes in secretory markers were confined to the small intestine, we extended our analysis to the colon and observed similar decreases in secretory lineage markers such as *Muc2, Chga,* and *SAM pointed domain containing ETS transcription factor (Spedf)* (*Muc2* 2-fold $p<0.05$; *Chga* 10-fold $p<0.001$*; Spedf* 2.5-fold $p<0.01$ **Figure 2.1B**). We next employed an *ex vivo* approach to test whether loss of epithelial

Mtgr1 was sufficient to trigger Notch activation. We generated Mouse Small Intestinal Epithelial (MSIE) cell lines from *Mtgr1*$^{-/-}$ mice, and RNA analysis revealed transcriptome changes consistent with increased Notch signaling and a lack of differentiation. *Notch3* and stem cell marker *Lgr5* were upregulated 2.8 fold and upregulated 2-fold, respectively. Covernsely, differentiation markers *Muc2, Gfi1*, *Neuronal differentiation 1 (NeuroD)*, and *Chga* were downregulated 1.5, 2, 2.2, and 5-fold respectively (**Figure 2.1C**). In sum, the data indicate that *Mtgr1* loss results in Notch activation and preferential shunting to absorptive intestinal lineages.

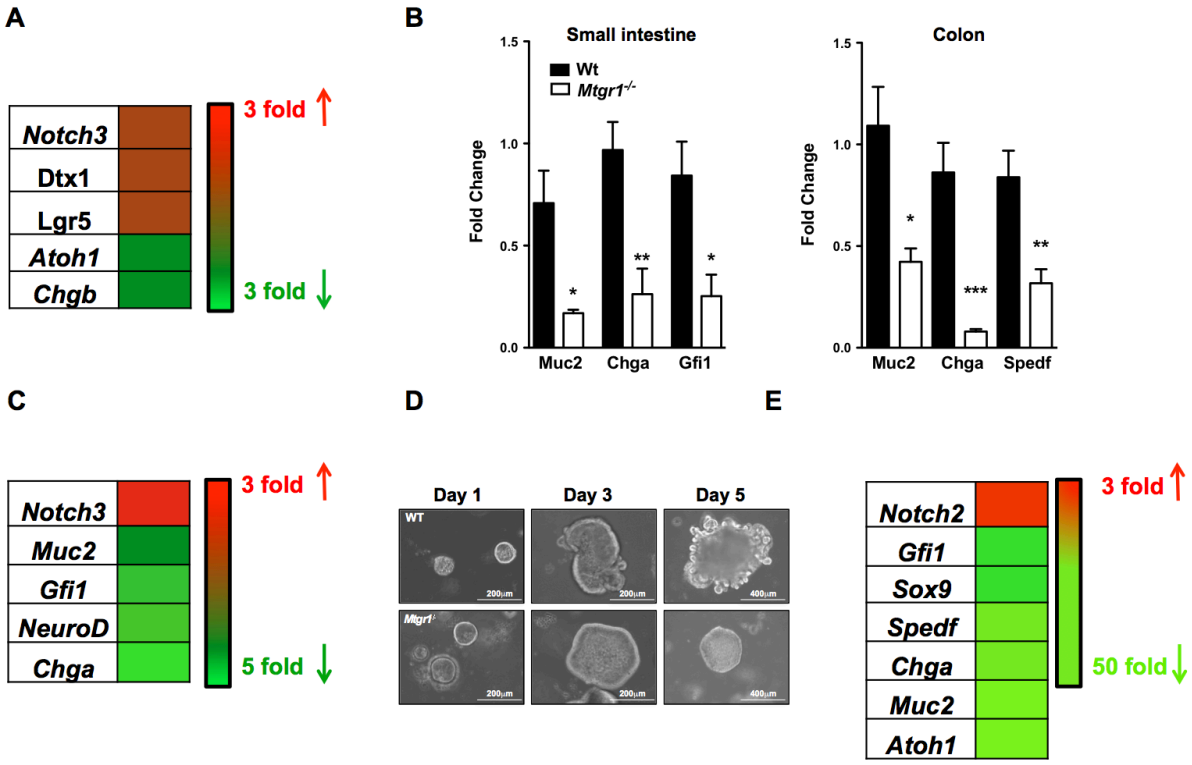

Figure 2.1. Notch signaling is hyperactive and secretory differentiation markers are downregultaed in the setting of *Mtgr1* loss. (**A**) Heatmap of dysregulated Notch-associated genes in microarray from laser captured small intestinal crypts from WT (N=2) and *Mtgr1*$^{-/-}$ (N=2) mice. (**B**) qPCR of the indicated lineage markers in small intestine of WT (N=4) and *Mtgr1*$^{-/-}$ (N=4) mice. Statistical test used was Student's *t* test. (**C**) Heatmap of secretory-associated transcripts in WT and *Mtgr1*$^{-/-}$ Mouse Small Intestinal Epithelial (MSIE) cells. (**D**) Representative images of enteroid cultures from WT and *Mtgr1*$^{-/-}$ mice 1 day and 3 days after plating. (**E**) Heatmap of Notch-associated genes in WT and *Mtgr1*$^{-/-}$ small intestinal derived enteroids. Red denotes increases fold expression relative to WT and green denotes decreased fold expression relative to WT. *P<0.05, **P<0.01

MTGR1 suppresses CSL-dependent transcription

Given that ectopic expression of Notch receptors or NICD resulted in a phenotype similar to deletion of *Mtgr1*[17,18,98], we hypothesized that MTGR1 could negatively regulate Notch-induced transcription. It has previously been reported that MTG family members can interact with the NICD and the key Notch effector CSL[104], but the functional consequence of this is unclear. To identify a molecular mechanism by which MTGR1 could regulate Notch activity *in vitro*, we tested whether MTGR1 could interact with NICD or CSL by co-immunoprecipitation. HA:MTGR1 was transiently transfected into COS7L cells either alone or with Flag:NICD. HA:MTG16 was used as a positive control. Whole cell lysates were immunoprecipitated with anti-Flag antibody, and MTGR1 was not detected in NICD containing immune complexes (**Figure 2.2A**). We then asked whether MTGR1 could interact with CSL. Similarly, HA:MTGR1 was co transfected with either an empty vector or myc:CSL. Immunopreciptating myc revealed MTGR1 complexes with CSL (**Figure 2.2B**). As the prototypic function of MTGR1 is transcriptional repression, we next used a luciferase reporter assay to examine the impact of MTGR1 on the Notch target gene *Hes1*. MTGR1 transfection into NIH 3T3 cells with or without N1-ICD co-expression resulted in dose-dependent repression of a *Hes1* luciferase reporter (**Figure 2.2C**). Overall, the data suggest MTGR1 acts as an upstream regulator of Notch-dependent transcriptional activity by interacting with CSL.

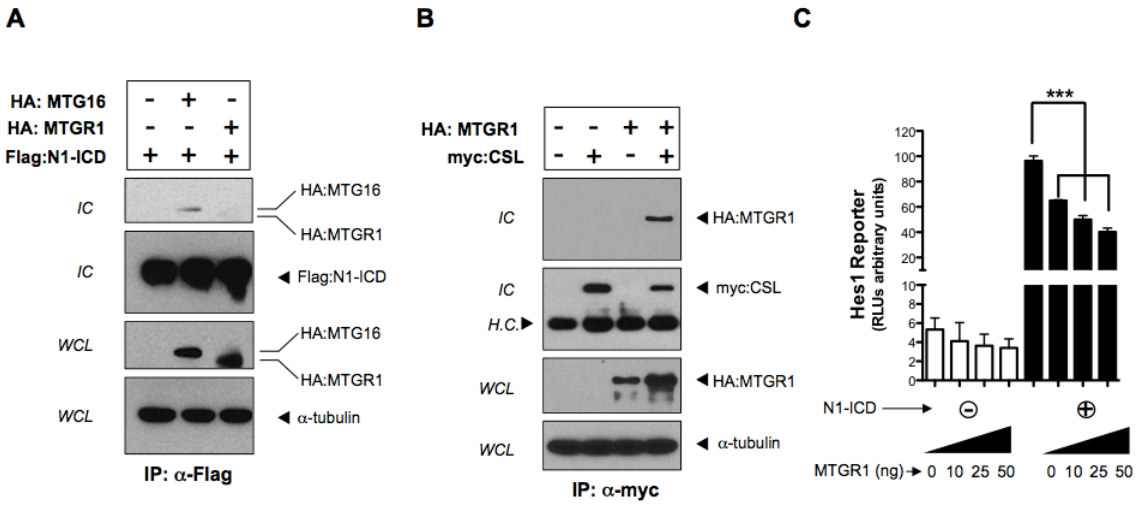

Figure 2.2 MTGR1 interacts with CSL and suppresses Notch-induced transcriptional activity. (**A**) HA-epitope tagged MTGR1 and Flag-epitope tagged N1-ICD were transiently expressed in COS7L cells. HA:MTGR1 was blotted for in immune complexes (IC) (Lane 3). HA-MTG16 and Flag-N1-ICD were also transiently transfected and immunopreciptated as a positive control (Lane 2). (**B**) HA:MTGR1 and myc-epitope tagged CSL were transiently expressed in COS7L cells in the combinations shown. The presence of myc:CSL and HA:MTGR1 was determined in immune complexes. (**C**) MTGR1, in the quantities shown, was transiently expressed in NIH3T3 cells with or without N1-ICD co-expression, along with the transcriptional reporter *Hes1*-Lux. Luciferase activity was quantified in whole cell extracts by luminometry. Results were normalized to an internal Renilla constitutive reporter. ***P<0.001. Statistical test used was Student's *t* test.

GSI rescues the hyperproliferative phenotype in Mtgr1$^{-/-}$ intestine

To test whether Notch inhibition was sufficient to rescue loss of secretory cells in the *Mtgr1*$^{-/-}$ mice, we treated 8-12 week-old *Mtgr1*$^{-/-}$ mice with dibenzazepine (DBZ), a Notch inhibitor/gamma-secretase inhibitor (GSI). GSI treatment effectively blocked Notch activation as we observed an increase in $CD4^-/CD8^-$ T cells and reciprocal decrease in $CD4^+/CD8^+$ T cells (**Figure 2.3**). *Mtgr1*$^{-/-}$ mice demonstrate increased intestinal proliferation and apoptosis at baseline[70], and we observed similar increases in vehicle treated WT and *Mtgr1*$^{-/-}$ mice (**Figure 2.4**). Apoptosis, as determined by cleaved caspase-3, was not significantly affected by GSI treatment (**Figure 2.4 A&B**). Immunohistochemical analysis for phospho-histone H3 (Ser10), however, showed that GSI reduced the number of proliferating cells per crypt in both WT and *Mtgr1*$^{-/-}$ small intestine (**Figure 2.4 C&D**), indicating that the previously reported basal increase in proliferation in *Mtgr1*$^{-/-}$ intestine[75] is at least partially due to Notch activation.

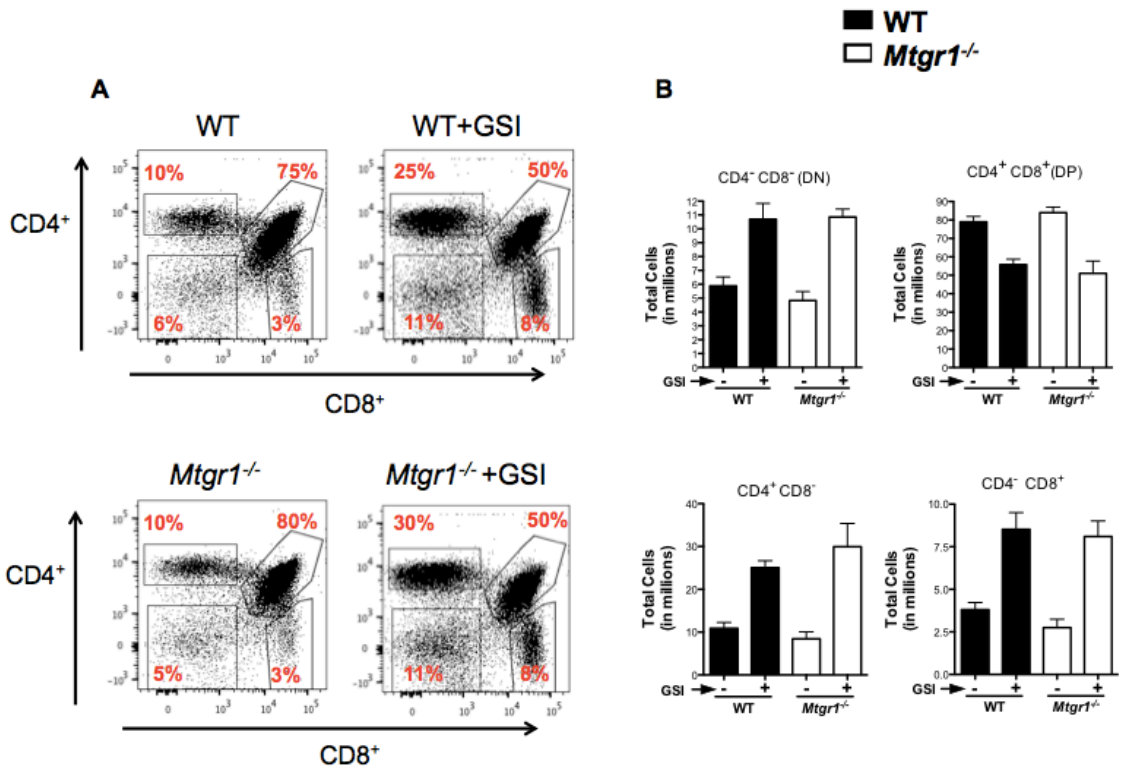

Figure 2.3 GSI treatment effectively increased CD4$^-$/CD8$^-$ (DN), CD4$^+$/CD8$^-$, and CD4$^-$/CD8$^+$ T cells and decreased CD4$^+$/CD8$^+$ (DP) T cells. (**A**) Thymic tissue from WT and *Mtgr1*$^{-/-}$ mice treated with vehicle or GSI treatment was harvested and single-cell suspensions were analyzed by flow cytometry using anti-CD4 and anti-CD8 antibodes. Using FACSDiva software, positive signal from anti-CD4 was plotted on the Y-axis while positive signal from anti-CD8 was plotted on the X-axis. Percentages of CD4$^-$/CD8$^-$ (DN), CD4$^+$/CD8$^-$, CD4$^-$/CD8$^+$, and CD4$^+$/CD8$^+$ (DP) were measured. (**B**) Absolute cell numbers of CD4$^-$/CD8$^-$ (DN), CD4$^+$/CD4$^-$, CD4$^-$/CD8$^+$, and CD4$^+$/CD8$^+$ (DP) cell populations for WT and *Mtgr1*$^{-/-}$ mice treated with vehicle or GSI.

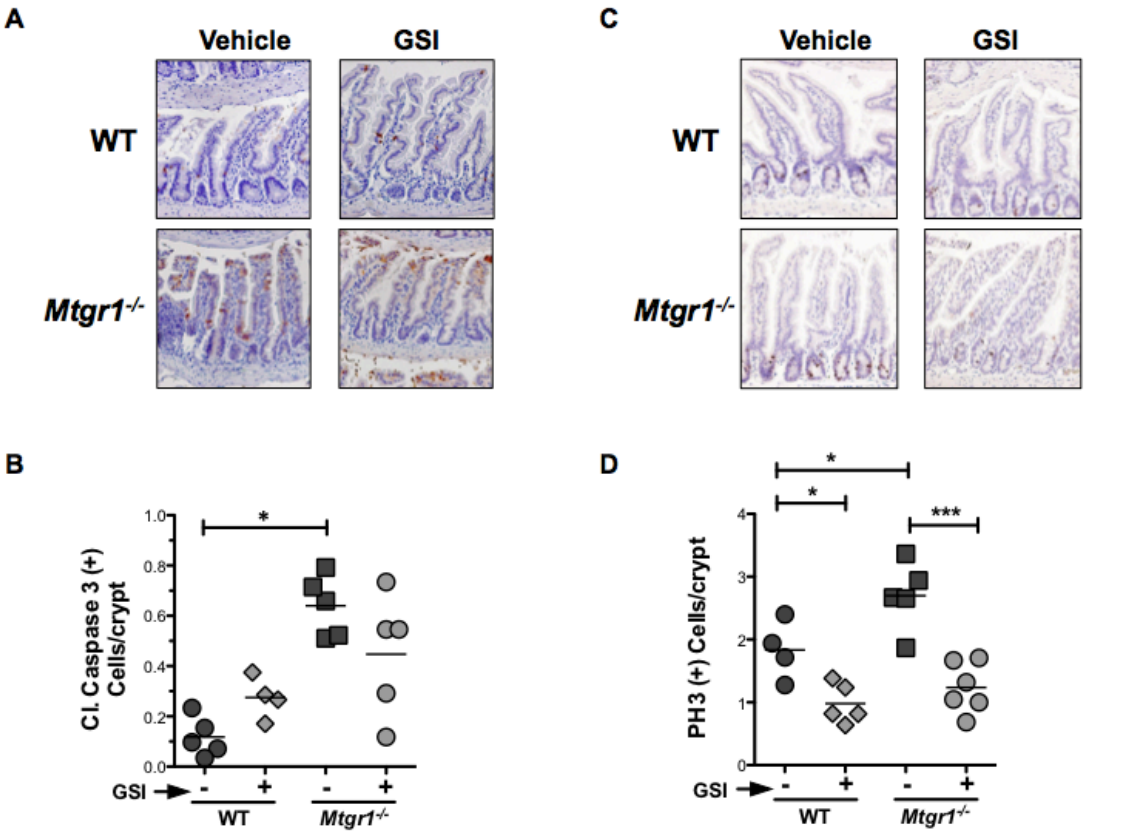

Figure 2.4 GSI reduces proliferation but has not effect on apoptosis in the *Mtgr1*$^{-/-}$ intestine. Representative sections of distal intestine (ileum) from vehicle or GSI-treated WT and *Mtgr1*$^{-/-}$ mice stained with (**A**) apoptosis marker anti-cleaved caspase 3 or (**C**) proliferation marker anti-phospho-histone H3. Positive staining cells were (**B, D**) quantified per crypt-villus unit. A minimum of 25 crypt-villus units was counted per mouse. *P<0.05, ***P<0.001. Statistical test used was One-way ANOVA.

Gamma secretase inhibition increases production of goblet and enteroendocrine cells in Mtgr1$^{-/-}$ intestine but fails to augment Paneth cell production

While histological architecture of both WT and *Mtgr1*$^{-/-}$ small intestine was unchanged by GSI treatment (**Figure 2.5A**), GSI treatment did increase WT and *Mtgr1*$^{-/-}$ goblet cell indices in comparison to vehicle-treated mice, (**Figure 2.5B**), with the most pronounced effects seen in the ileum (6.1 vs. 0.97 PAS^{+} cells/villus-crypt unit $p<0.001$ **Figure 2.6A, Figure 2.7**). To identify changes in enteroendocrine cell number, we stained for Chromogranin A (CgA) (**Figure 2.5C**). Similarly, GSI treatment significantly augmented the number of enteroendocrine cells compared to vehicle controls (ileum: 0.36 vs. 0.035 CgA^{+} cell/ villus-crypt unit $p<0.001$ **Figure 2.6B, Figure 2.7).** Interestingly, while anti-Lysozyme staining for Paneth cells (**Figure 2.5D**) revealed that GSI treatment increased the number of Paneth cells in WT mice, GSI treatment had no effect on Paneth cells in any segment of the small intestine in *Mtgr1*$^{-/-}$ mice (ileum: 1.4 vs. 0.96 Lys^{+} cell/ villus-crypt unit $p<1.0$ **Figure 2.6C, Figure 2.7**), revealing a previously unrecognized role for MTGR1 in Paneth cell differentiation. Taken together, our findings indicate MTGR1 is a key regulator of intestinal lineage allocation.

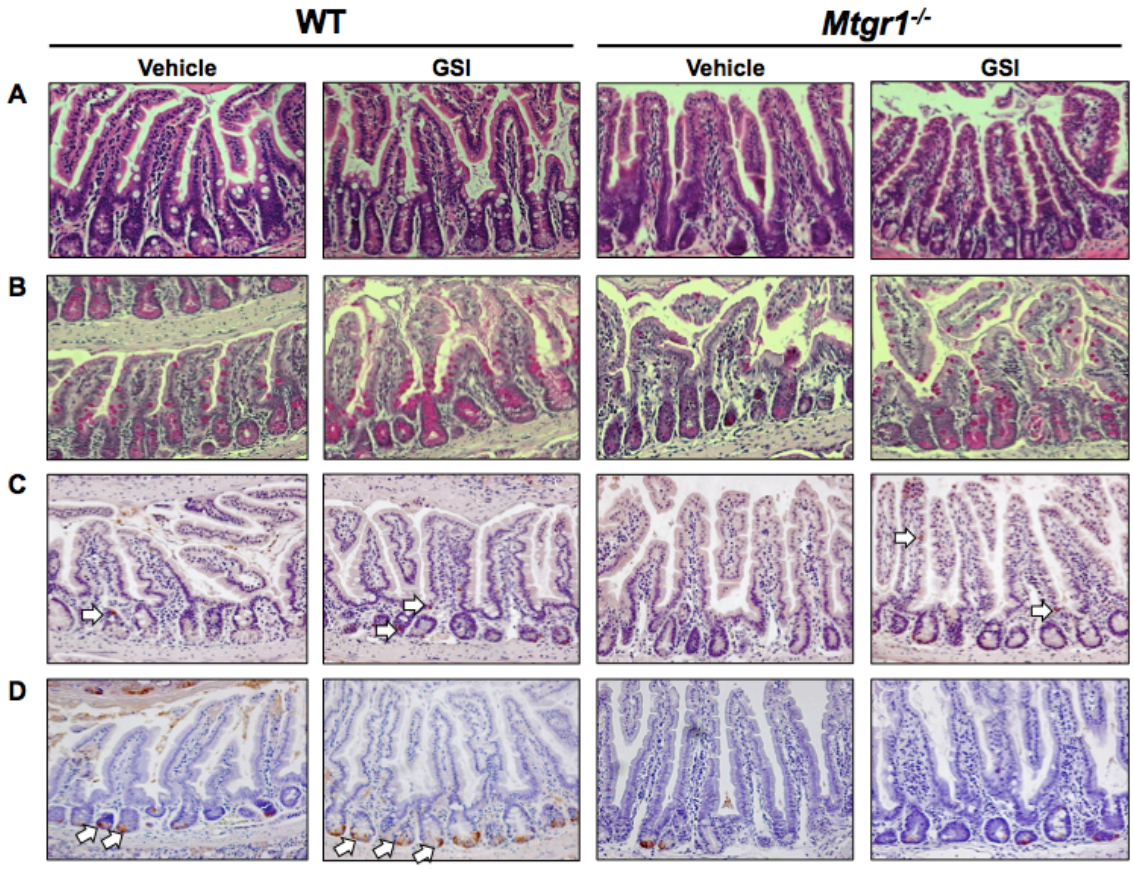

Figure 2.5 Notch inhibition increases goblet and enteroendocrine but not Paneth cells in *Mtgr1*$^{-/-}$ mice. Vehicle and GSI (DBZ, 10 mM/kg twice daily for 5 days) treated WT and *Mtgr1*$^{-/-}$ mice. (**A**) H&E staining of distal intestine sections. (**B**) PAS staining for goblet cells, (**C**) Chromogranin A (CgA) for enteroendocrine, and (**D***)* Lysozyme (Lys) staining for Paneth cells in the distal intestine. Images were captured using 20x objective. White arrows indicate positive staining cells.

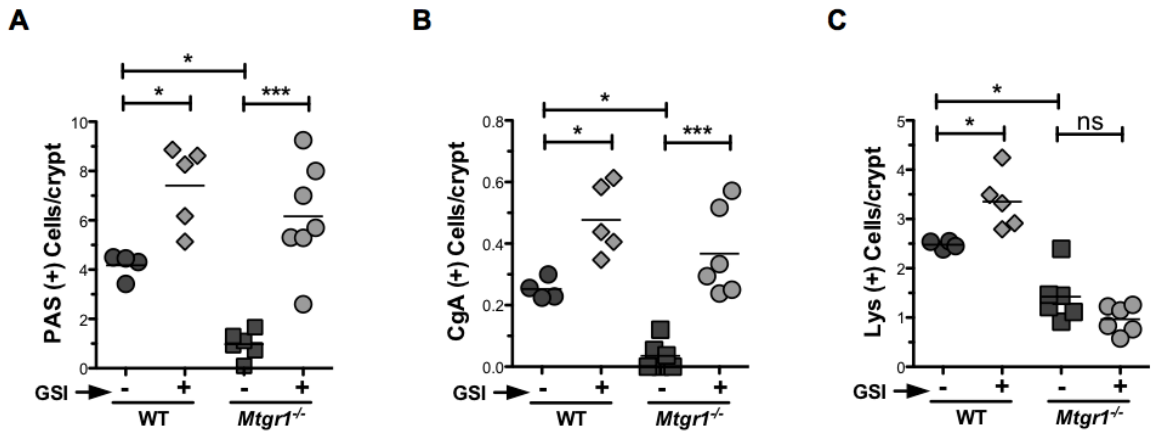

Figure 2.6 *Mtgr1* is required for Paneth lineage production after Notch inhibition. Quantification of (**A**) PAS^+ (**B**) CgA^+ and (**C**) Lys^+ cells per intestinal crypt/villus structure in WT and *Mtgr1*$^{-/-}$ mice treated with vehicle or GSI. A minimum of 25 crypt-villus units was counted per mouse. *P<0.05, **P<0.01, ***P<0.001. Statistical test used was One-way ANOVA.

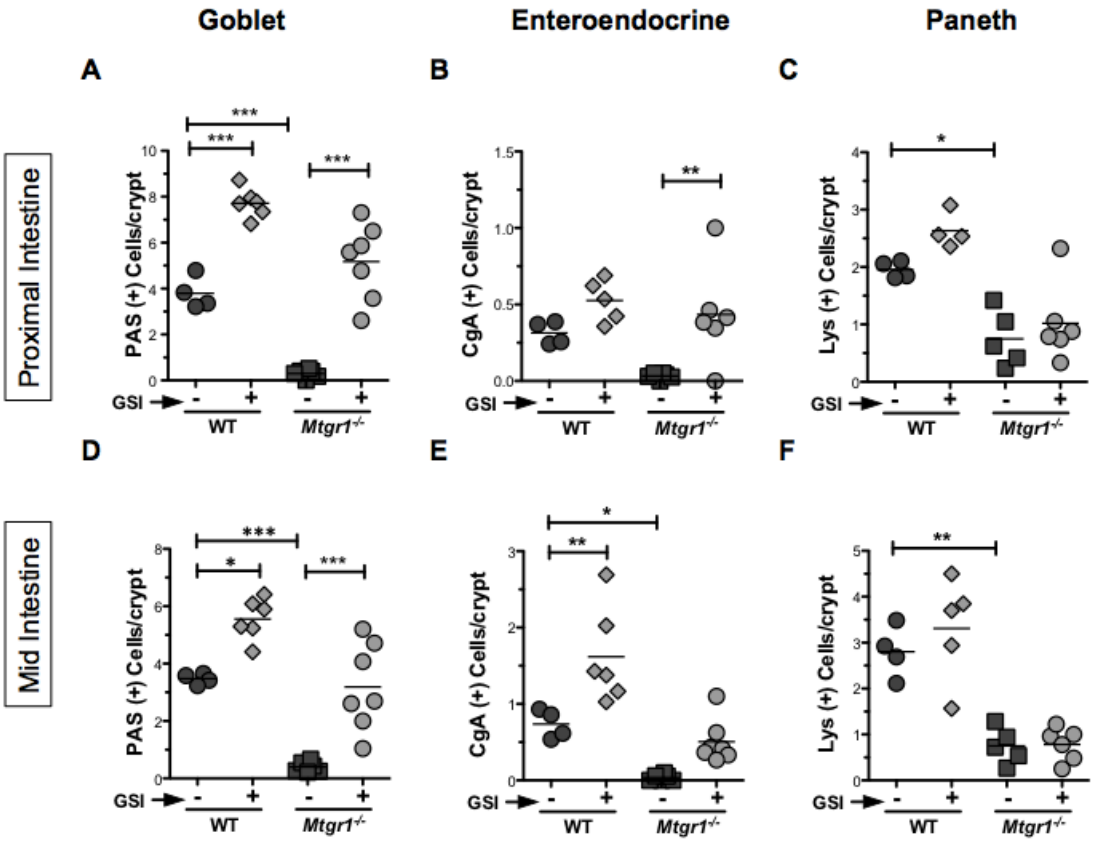

Figure 2.7. GSI treatment increases goblet and enteroendocrine but not Paneth cells in the *Mtgr1*$^{-/-}$ intestine. Quantification of goblet (**A, D**), enteroendocrine (**B, E**), and Paneth (**C, F**) cells per crypt-villus in proximal and mid sections of the intestine. Goblet cells were identified by PAS staining. Anti-CgA and anti-Lysozyme stains were used to identify enteroendocrine and Paneth cells, respectively. One-way ANOVA was used for statistical analysis. *P<0.05, **P<0.01, ***P<0.001.

MTGR1 interacts with GFI1 and can repress GFI1 targets

MTGR1 has been shown to interact with a variety of transcriptional corepressors[70,75]. Gfi1 is a transcriptional corepressor important in Paneth cell differentiation[27]. To determine whether Mtgr1 could interact with GFI1, we performed a co-immunoprecipitation and observed that Mtgr1 interacts with GFI1 (**Figure 2.8A**). Analysis of our laser capture microdissection array indicated that a subset of Gfi1 targets such as Satb1, E2f5, and Jak3 were upregulated in *Mtgr1*$^{-/-}$ intestine (**Figure 2.8B**), suggesting Mtgr1 could facilitate Gfi1-mediated repression. We subsequently asked whether Mtgr1 was capable of repressing a reporter construct containing a 2XSatb1 promoter element upstream of luciferase. Overexpression of Mtgr1 reduced luciferase by 50%, indicating Mtgr1 can repress Gfi1 targets (**Figure 2.8C**). *Satb1* and E2Fa transcriptional analysis of *Mtgr1*$^{-/-}$ intestine indicated *Atoh1* transcripts were increased and *Hes1* transcripts were decreased, confirming the increase toward secretory cells seen histologically (**Figure 2.9**).

Figure 2.8. MTGR1 interacts with transcriptional corepressor GFI1 and can repress GFI1-targets. (**A**) HA:MTGR1 and Flag:GFI1 were transiently expressed in COS7L cells. Flag:GFI1 was immunoprecipitated, and HA:MTGR1 was blotted for in immune complexes (IC). (**B**) GFI1 repression targets *Satb1, E2f5, and Jak3* were upregulated in laser captured crypts from WT (N=2) and *Mtgr1*$^{-/-}$ (N=2) mice. (**C**) HA:MTGR1 was transfected into NIH3T3 cells with the transcriptional reporter *Satb1*-Lux. Luciferase activity was quantified in whole cell extracts by luminometry. Results were normalized to an internal Renilla constitutive reporter. ***P<0.001. Statistical test used was Student's *t* test.

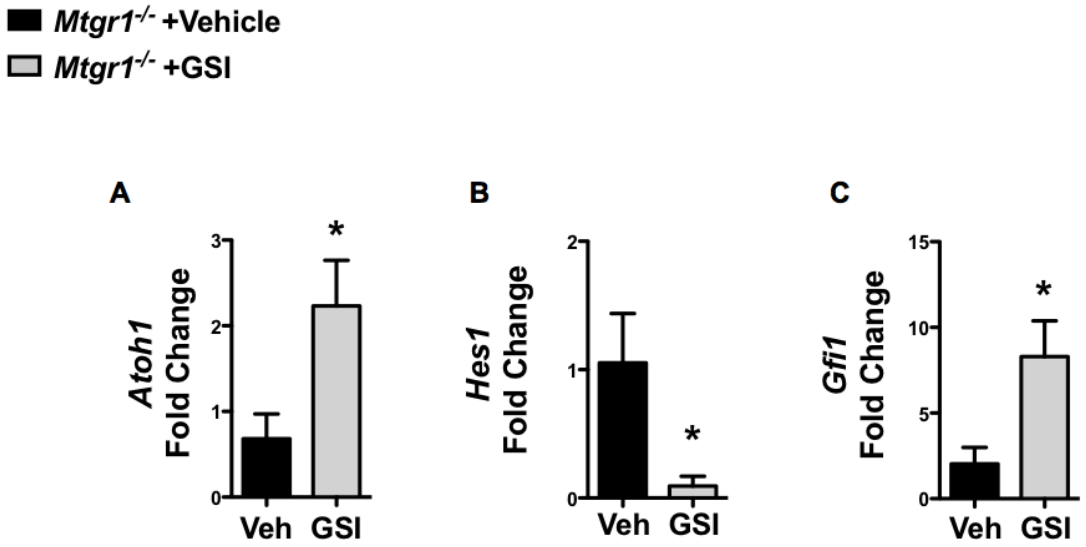

Figure 2.9. GSI treatment increased *Atoh1* and *Gfi1* expression and decreased *Hes1* expression in *Mtgr1*$^{-/-}$ mice. qPCR for (**A**) *Atoh1*, (**B**) *Hes1*, and (**C**) *Gfi1*. (*Mtgr1*$^{-/-}$ vehicle treated N=4 and *Mtgr1*$^{-/-}$ GSI treated N=4) *P<0.05.

Discussion

Notch signaling plays a critical yet incompletely understood role in determining intestinal cell fate[16,17]. When *Mtgr1*$^{-/-}$ mice were generated and examined for intestinal phenotypes, they had unexpected characteristics: 1) increased proliferation in the small intestine and colon and 2) the progressive depletion of the secretory lineage in the small intestine[70,73], suggesting hyper-Notch tone and identifying MTGR1 as an important regulator of fate determination in the intestine. Here we show that Notch inhibition by GSI treatment rescued the goblet and enteroendocrine lineages in the *Mtgtr1*$^{-/-}$ intestine but failed to rescue the Paneth lineage. The results suggest a model in which MTGR1 endogenously represses Notch activation through an interaction with CSL (**Figure 2.10**) and in its absence, unbridled Notch signaling drives the intestinal epithelium to a predominantly absorptive phenotype. Inhibiting Notch, as we did with a gamma-secretase inhibitor, increases the production of secretory cells, with the exception of the Paneth lineage, suggesting that in addition to acting at the Notch/CSL interface, MTGR1 also regulates downstream lineage allocation.

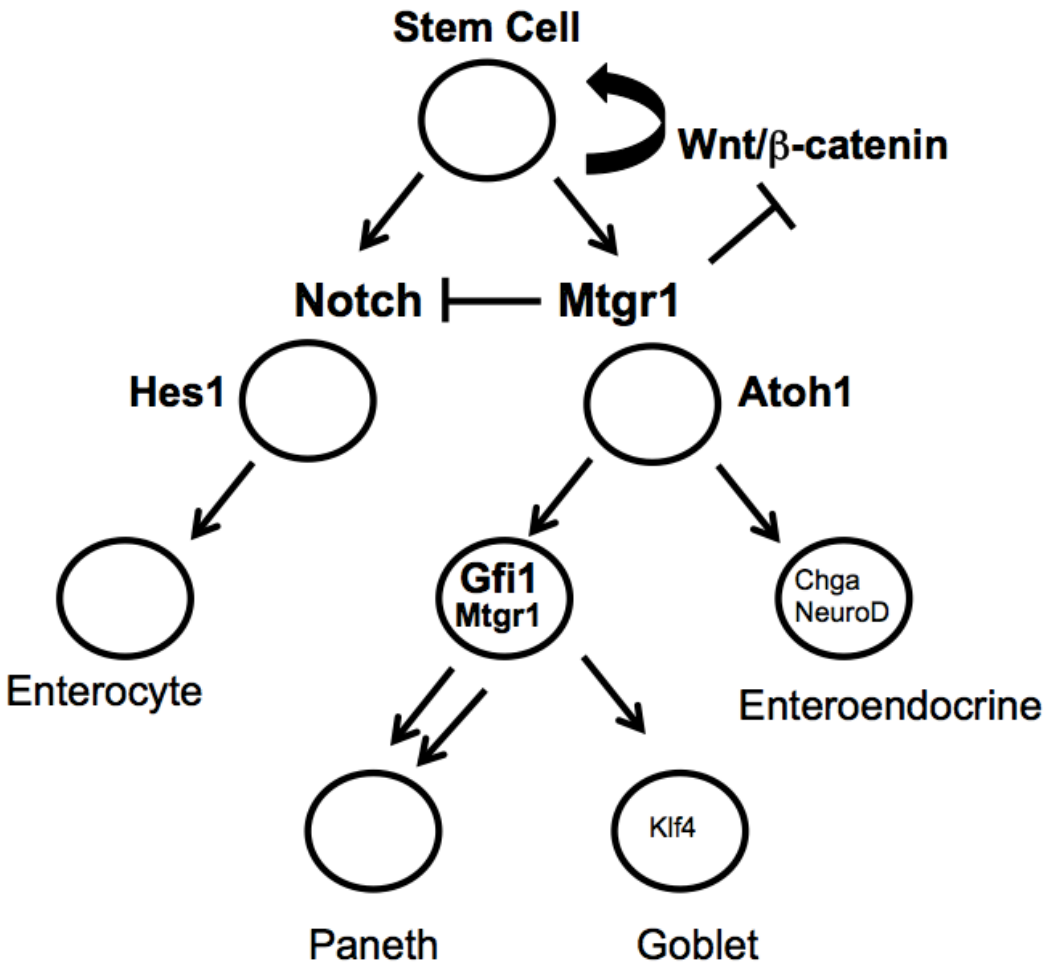

Figure 2.10 Schematic of MTGR1 regulating multiple branch points in intestinal lineage differentiation. We propose that MTGR1 acts at multiple levels in regulating intestinal epithelial differentiation. MTGR1 negatively regulates Wnt signaling by competing with β-catenin for TCF4 occupancy. As the stem cell divides and moves along the crypt-villus axis, MTGR1 acts as a negative regulator of Notch signaling by interacting with CSL and repressing Notch-induced transcriptional activity. As cells differentiate into either $HES1^{+}$ enterocytes or $ATOH1^{+}$ secretory progenitors, MTGR1 is also required downstream for Paneth cell differentiation.

While the role of MTGs in hematopoiesis is well characterized, studies using knockout animal models revealed that MTGs have unexpected roles in the gut. MTGs regulate intestinal development and lineage allocation programs, but each family member appears to regulate different differentiation programs. A small percentage of *Mtg8*$^{-/-}$ mice show a deletion of their midgut, and those that survive postnatally demonstrate severe intestinal architectural disruption[71]. *Mtg16*$^{-/-}$ mice show normal gut architecture, but they have decreased goblet cells (unpublished observations). *Mtgr1*$^{-/-}$ mice, on the other hand, show a marked reduction in all secretory cells [70]. Given the importance of Notch signaling in the intestine, the phenotypes strongly suggested MTGs modulate Notch. Components of the Notch pathway can interact with MTG16 *in vitro* [104], but no *in vivo* Notch studies have been conducted until now. Our results are the first to show that reversal of Notch signaling can partially generate secretory lineages in *Mtgr1*$^{-/-}$ intestine.

The balance between absorptive and secretory cell fate in the intestine is largely governed in a reciprocal fashion by the Notch and Atoh1 signaling pathways. Notch ligands activate Notch receptors which are subsequently cleaved by gamma secretase to produce NICD, resulting in NICD tranlsocating to the nucleus where it increases the expression of *Hes1*, a repressor of the pro-secretory cell transcription factor *Atoh1*. Consistent with this model, inhibiting Notch using GSI had no effect on the expression of Notch ligands but did reduce *Hes1* expression and increase *Atoh1* expression in *Mtgr1*$^{-/-}$ mice (**Figure 2.9**). It is interesting to note that *Mtgr1*$^{-/-}$ mice phenocopy *Atoh1* mutants, which also lack secretory cells, suggesting some interplay between MTGR1 and ATOH1. Because GSI treatment increased *Atoh1* transcript levels in *Mtgr1* mice (**Figure 2.9**), Mtgr1 most likely acts downstream of Atoh1. In support of this, we recently identified

that Atoh1 ChIPs to the Mtgr1 promoter, suggesting that Mtgr1 could be an important downstream effector of Atoh1 (unpublished data). How Atoh1 and Mtgr1 interact is an outstanding question for future investigation.

The inability of Notch inhibition to induce Paneth cell differentiation in the *Mtgr1*$^{-/-}$ mice identifies MTGR1 as a new Paneth cell allocation constituent. Paneth cell differentiation is controversial, but it is believed that a goblet/Paneth cell progenitor is marked by *Gfi1* expression[26,27] (**Figure 2.10**). *Gfi1* deficient mice have increased enteroendocrine cells, suggesting that loss of GFI drove supernumerary enteroendocrine cells because of the inability of the progenitor to differentiate into mucous and Paneth cells [27]. Alternatively, GFI1 may repress *Neurog3* and by doing so "stabilizes" the Paneth and mucous cell lineages[26]. In *Gfi1*-deficient mice, unchecked *Neurog3* expression drives progenitor cells towards enteroendocrine cells. How Mtgr1 fits into this model is unclear, but Gfi1 transcripts were increased after GSI administration in *Mtgr1*$^{-/-}$ intestine (**Figure 2.9**) suggesting Mtgr1 is not required to regulate Gfi1 expression. Alternatively, GFI1 could require MTGR1 to repress and therefore initiate programming to properly form Paneth cells in the setting of Notch inhibition. Indeed, we determined that MTGR1 and GFI1 can complex and that MTGR1 can repress two GFI1 reporters, suggesting MTGR1 could interact with and enable GFI1-mediated repression (**Figure 2.8**). Interestingly, we found several GFI1 targets such as SATB1 and E2F5 were upregulated in *Mtgr1*$^{-/-}$crypts (**Figure 2.8**), suggesting that GFI1 may require MTGR1 to initiate differentiation programs.

Paneth cell function is an intense area of investigation because of its potential supporting role in crypt stem cell biology[32,107,108]. Understanding transcriptional programs

regulating Paneth allocation is critical to defining their function in the intestinal stem cell niche. More broadly, intestinal secretory cell differentiation is still incompletely understood. MTGR1, a transcriptional corepressor originally discovered to be critical in hematopoiesis, appears to be an important and heretofore unidentified contributor to intestinal cell lineage allocation.

Chapter 3

Myeloid translocation genes differentially regulate colorectal cancer programs

Introduction

Colorectal cancer (CRC) is one of the leading causes of cancer mortality in the United States[33]. More than 80% of CRCs feature mutational inactivation of the *Adenomatous Polyposis Coli* (APC) gene, a tumor suppressor that acts as a regulator of the Wnt/β-catenin signaling pathway[6,35]. Inactive APC allows β−catenin to accumulate and redistribute to the nucleus activating TCF4-dependent transcriptional programs, promoting tumor development[2,6–8,36]. Similar to Wnt signaling, upregulation of the Notch pathway promotes intestinal carcinogenesis[17,96,98,109]. Notch signaling is a critical mediator of intestinal differentiation and is activated when its ligands, Jagged and Delta-like, bind to Notch receptors and induce intracellular proteolytic cleavage by gamma-secretase. This releases the Notch Intracellular Domain (NICD) allowing its translocation to the nucleus, where it binds to the transcription factor CSL to block secretory lineage specification and promote stem cell programs[109,97]. While dysregulation of the Wnt and Notch pathways promotes intestinal tumorigenesis[19,110,111], how each signaling network escapes regulation in this process and becomes activated is incompletely understood.

The Myeloid Translocation Gene (MTG) family consists of three members: *MTG8 (ETO*), *MTGR1* (*CBFA2T2*), and *MTG16* (*CBFA2T3*)[76]. MTGs associate with DNA binding proteins and recruit other corepressors and histone deacetylases (HDACs) to form repression complexes that downregulate the transcription of target genes[70]. MTG8 and MTG16 are pathologically disrupted by chromosomal translocations in acute myeloid leukemia (AML), highlighting their importance in regulating stem cell

programs[100]. Given their prominent role in hematopoietic malignancies and hematopoiesis and that stem cell programs are frequently activated in tumorigenesis, it was postulated that MTG dysfunction may cooperate with other mutations in driving epithelial tumorigenesis. In support of this hypothesis, MTG8 mutations have been identified as statistically significant "drivers" in breast cancer[112]. Similarly, 97 MTG16 and 80 MTGR1 mutations have been identified in The Cancer Genome Atlas (TCGA) database[113,114]. Furthermore, animal models have revealed unexpected pivotal roles for MTGs in regulating stem cell and differentiation programs in the gut. Genetic deletion of any one of the MTG family members results in striking intestinal phenotypes. A portion of *Mtg8*$^{-/-}$ mice fail to develop the midgut[71], *Mtgr1*$^{-/-}$ mice have pan-secretory lineage loss[70], and *Mtg16*$^{-/-}$ mice have decreased goblet cells indices[72]. Moreover, both *Mtgr1*$^{-/-}$ and *Mtg16*$^{-/-}$ mice have augmented intestinal epithelial proliferation[70,72,74,115], further suggesting dysregulated stem cell programs. The mechanism underlying their intestinal phenotypes is not deduced, but may reflect alterations in Wnt or Notch signaling levels.

Here we formally tested the roles of MTGs in spontaneous colon tumorigenesis. To accomplish this aim, we employed the *Apc*$^{1638/+}$ mouse polyp model and determined that genetic ablation of MTGR1, but not MTG16, increased tumor multiplicity. This was associated with progression to more advanced disease with conversion to high grade dysplasia and even invasive adenocarcinoma, a feature not observed in this model. Examination of a murine erythroid cell ChIP-seq dataset[116] revealed that MTGR1 and MTG16 co-occupy 356 genes, but MTGR1 uniquely occupies an additional 1,063 specific genes and analysis of these targets predicted MTGR1, but not MTG16, would regulate the Wnt and Notch pathways. Using immunohistochemical and RNA-seq

analysis, we determined that both Wnt and Notch signaling were hyperactive in *Mtgr1*$^{-/-}$ tumors. Lastly, we demonstrate downregulation of MTGR1 in CRC. Overall, our report defines a unique role for MTGR1 as a critical regulator of colorectal cancer programs through dual regulation of Wnt and Notch signaling.

Materials and methods

Mouse experiments and analysis

Mice were housed, maintained, and then euthanized using isoflurane and cervical dislocation according to a protocol approved by the Vanderbilt Institutional Animal Care and Use Committee. The small intestine was removed and divided into equal thirds. Each segment, along with the large intestine, was then bisected longitudinally. Tumor number was counted grossly. Tumor samples and normal, non-malignant tissue were collected for RNA and stored in RNAlater (Invitrogen). The remaining intestinal segments were "Swiss rolled" so that the distal most segment was innermost[103]. Microscopic analysis was performed by a gastrointestinal pathologist (MKW) for dysplasia on haematoxylin and eosin (H&E) stained sections (processed by the Vanderbilt Translational Pathology Shared Resource core). All *in vivo* procedures were carried out in accordance with protocols approved by the Vanderbilt Institutional Animal Care and Use Committee.

qPCR mRNA analysis

RNA was made from tumor tissue stored in RNAlater using the RNeasy Mini kit (Qiagen), according to the manufacturer's directions. cDNA was then made using the SuperScript cDNA kit (Invitrogen). qPCR was then performed using SYBR Green

(Biorad) with primers for *Gapdh* (Realtimeprimers). Primers for *CgA* and *Muc2* were previously described[115]. Reactions were performed according to the manufacturer's recommendations.

Immunohistochemistry

Five micrometer sections were cut, dewaxed, hydrated and endogenous peroxidase activity quenched with 0.03% hydrogen peroxide in MeOH. Antigen retrieval was performed using the boiling sodium citrate method in a microwave (20 mmol sodium citrate pH 6.5) for 16 minutes at 30% power. After blocking, primary antibodies were incubated overnight at 4°C at the following concentrations: α-phosphohistone-H3 (Millipore), 1:150 and α-β-catenin (BD Transduction Laboratories), 1:1000. Isotype-matched antibodies were included as negative controls. The Vectastain ABC Elite System (Vector Labs) was used to visualize staining for immunohistochemistry. Identification of intratumoral and crypt apoptotic cells was performed using the ApopTag Plus Peroxidase *in situ* Apoptosis Kit (Chemicon) according to the manufacturer's protocol. Control stains were obtained by omitting the terminal transferase (TnT) enzyme. Apoptosis and proliferation indices were generated by counting the number of positive cells per high-powered field (HPF; 40× objective) within each tumor by a blinded observer. A β-catenin index was employed, as previously reported[103]. This index is generated by multiplying the staining intensity (on a scale of 1-5) by percentage of the cells demonstrating nuclear staining.

RNA Sequencing and Analysis

Tumor RNA from *Mtgr1*$^{-/-}$ (n=3) and WT (n=3) mice was sequenced by the Vanderbilt Sequencing Core Facility. Initial raw sequencing data was aligned to a reference mouse genome (mm9) using TopHat (version 1.3.1) software[117]. The transcript of mouse genome (mm9) was downloaded from UCSC as implemented in the Bioconductor package *GenomicFeatures*. Then, the Bioconductor packages *Rsamtools* and *DESeq* were used to estimate the read count for expression of each gene and to detect differentially expressed (DE) genes. For count based gene expression data, *DESeq* uses a model based on the negative binomial distribution which includes a dispersion parameter to better estimate variance[118]. The p-values from *DESeq* were adjusted by Benjamini and Hochberg's method to control false discovery rate (FDR)[119].

Tissue Microarrays

All tissue samples were collected, coded, and de-identified in advance, and their use in this work was approved by the Institutional Review Board. Tissues were stained with H&E and representative regions were selected for inclusion in a tissue array. Tissue cores with a diameter of 0.6 mm were retrieved from the selected regions of the donor blocks and punched to the recipient block using a manual tissue array instrument (Beecher Instruments); samples were punched in duplicate. Control samples from normal epithelial specimens were punched in each sample row. Five micrometer sections were transferred to polylysine-coated slides (Menzel-Glaser) and incubated at 37°C for 2 hours. The resulting tumor tissue array was used for immunohistochemical analysis. Further clinical information regarding samples is described (**Table 3.1**).

	CRC (n=102)	Normal (n=25)
Average Age (± sd)	64 ± 14.9	48 ± 21.2
Gender	Female (n=53) Male (n=49)	Male (n=14) Female (n=11)
Average BMI	n/a	24.5 ± 2.8
Race	White (n=83) Black (n=19)	White (n=23) Black (n=2)
Grade if applicable	1 (n=14) 2 (n=62) 3 (n=26)	n/a

Table 3.1 Clinical characteristics of patient samples.

Antigen retrieval was conducted by boiling in citrate pH 6.0 at 104°C for 20 min. Slides were then cooled down at room temperature for 10 min before being quenched with 0.03% H_20_2 with sodium azide for 5 min. Serum-free protein was used to block for 20 min. Primary antibody (MTGR1/CBFA2T2 Proteintech CAT# 11336-1-AP) was used at a 1:200 dilution and incubated for 60 min. Envision HRP Labeled Polymer was applied for 30 minutes for detection. DAB was used as a chromogen after incubation for 5 min. Cores were scored for the proportion of epithelial cells that stained positive and for the intensity of the stain using an index from 1-4. The index was generated by multiplying the two scores together.

Moffitt/Vanderbilt-Ingram Cancer Center Expression Array

The array was previously described[120]. The source of the data: GSE17538.

RNA Scope

RNA *in situ* probes for *MTGR1* were ordered from Advanced Cell Diagnostics and sequences are available on their online database. Tissue microarrays were processed and stained exactly according to manufacturer's protocol. Staining was scored as percentage of positive cells per core. All cores were also stained with a positive control probe for housekeeping gene Peptidylprolyl Isomerase B (Cyclophilin B, *PPIB)*. Cores that did not stain robustly with positive control were omitted.

Statistical Methods

A student's t-test was used when comparing two groups such as apoptosis, proliferation, and tumor counts. Data is presented as the mean +/- the standard error of the mean (SEM) in bar graphs and a line identifying the mean is shown when all data points are plotted. All of these analyses were performed using GraphPad Prism®5.0c.

Results

Loss of MTGR1 augments intestinal tumorigenesis

Cancer programs often co-opt normal cellular processes. We have identified MTGs as regulators of intestinal proliferation, self-renewal and wound healing processes[70,71,73,74,103]. It is reasonable to postulate that MTGs may also play key roles in other non-hematopoietic malignancies. Consistent with this hypothesis, MTG16 has been identified as a putative tumor suppressor in breast cancer[121] and mutation of MTG8 is postulated to be a "driver" in breast cancer[112]. Examination of TCGA data identified 80 non-synonymous mutations in MTGR1 and 97 in MTG16[113,114], some of which were predicted to impair function by MutationAssessor algorithms[122]. We thus postulated that inactivation of MTGR1 or MTG16 would augment tumorigenesis.

To test this hypothesis we crossed *Mtgr1*$^{-/-}$ or *Mtg16*$^{-/-}$ mice with *Apc*$^{1638/+}$ polyp-prone mice. *Apc*$^{1638/+}$;*Mtgr1*$^{-/-}$ had decreased survival throughout the duration of the experiment (**Figure 3.1**), suggesting increased tumor burden.

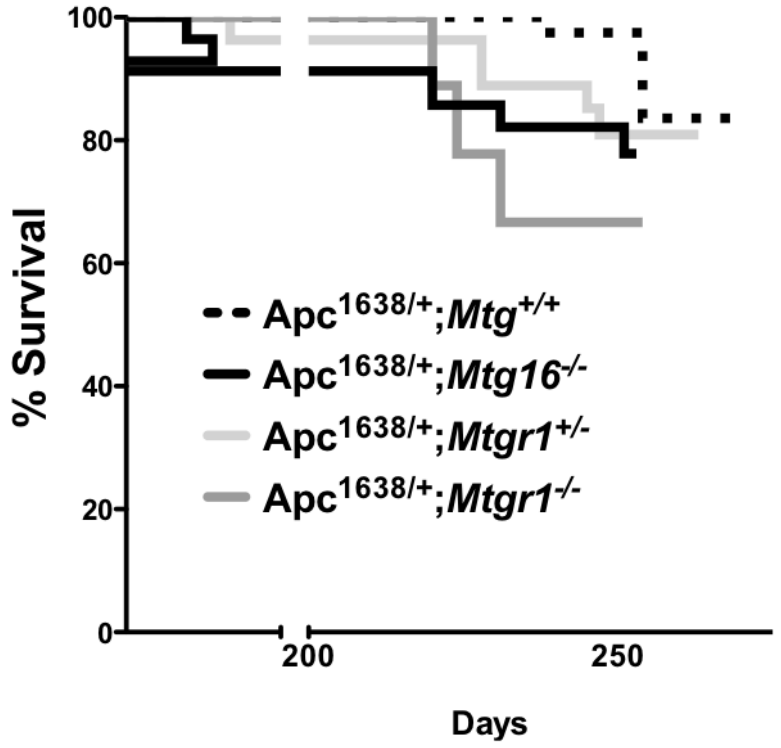

Figure 3.1 Survival curves of *Mtg* deficient mice and *Apc*$^{1638/+}$

Indeed, after aging the mice for 36 weeks, we observed increased tumor multiplicity with gene dose-dependent loss of *Mtgr1*, but surprisingly loss of *Mtg16* did not modify tumorigenesis (*Apc*$^{1638/+}$;*Mtg*$^{+/+}$ 4.3 ± 0.5 vs. *Apc*$^{1638/+}$;*Mtg16*$^{-/-}$ 2.4 ± 0.5 vs. *Apc*$^{1638/+}$;*Mtgr1*$^{-/+}$ 7.1 ± 1.1 vs. *Apc*$^{1638/+}$;*Mtgr1*$^{-/-}$ 28.9 ± 4.5 tumors per mouse, **Figure 3.2A**). *Apc*$^{1638/+}$;*Mtgr1*$^{-/-}$ mice had more tumors in every segment of the small intestine, with the most pronounced effect being in the distal small intestine (**Figure 3.2B**). Histopathological analysis indicated tumors from *Apc*$^{1638/+}$;*Mtgr1*$^{-/-}$ and *Apc*$^{1638/+}$;*Mtgr1*$^{-/+}$ were more dysplastic with progression to invasive adenocarcinoma in some cases (**Figure 3.3A**). Indeed, 43% of *Apc*$^{1638/+}$;*Mtgr1*$^{-/-}$ mice showed evidence of invasive adenocarcinoma or high grade dysplasia while *Apc*$^{1638/+}$;*Mtg*$^{+/+}$ tumors had only low grade dysplastic changes (**Figure 3.3B**). Overall, our data indicates that loss of MTG16 has no effect on tumorigenesis. Loss of MTGR1, however, substantially augments tumorigenesis in a gene dose-dependent fashion.

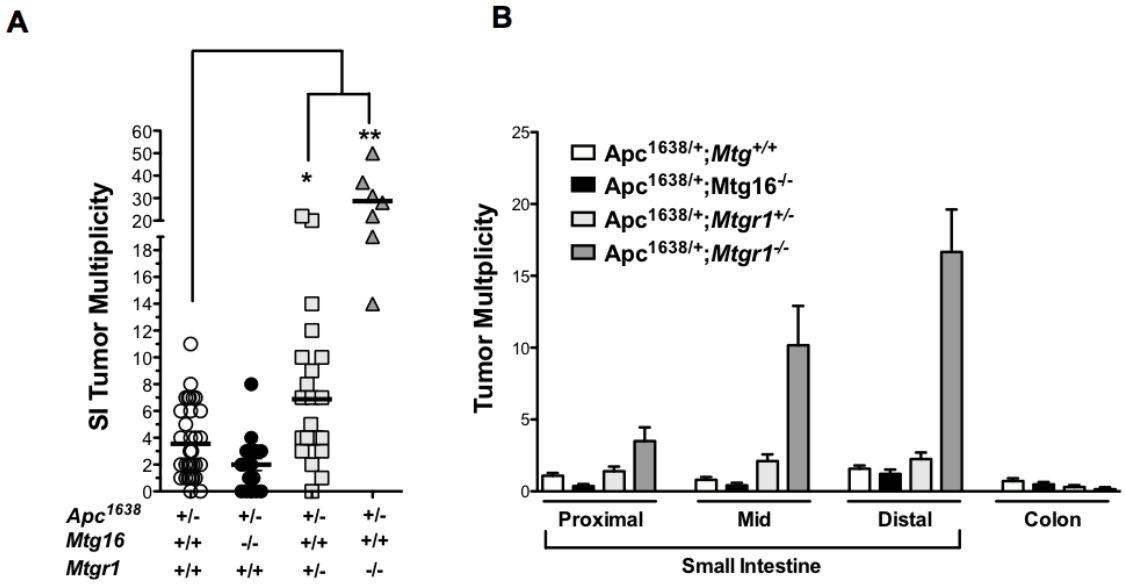

Figure 3.2 Loss of MTGR1, not MTG16, augments intestinal tumorigenesis. (**A**) Tumor multiplicity and (**B**) distribution in *Apc*$^{1638/+}$;*Mtg*$^{+/+}$, *Apc*$^{1638/+}$;*Mtg16*$^{-/-}$, *Apc*$^{1638/+}$;*Mtgr1*$^{-/+}$, *Apc*$^{1638/+}$;*Mtgr1*$^{-/-}$ mice. *P < 0.05, **P < 0.01

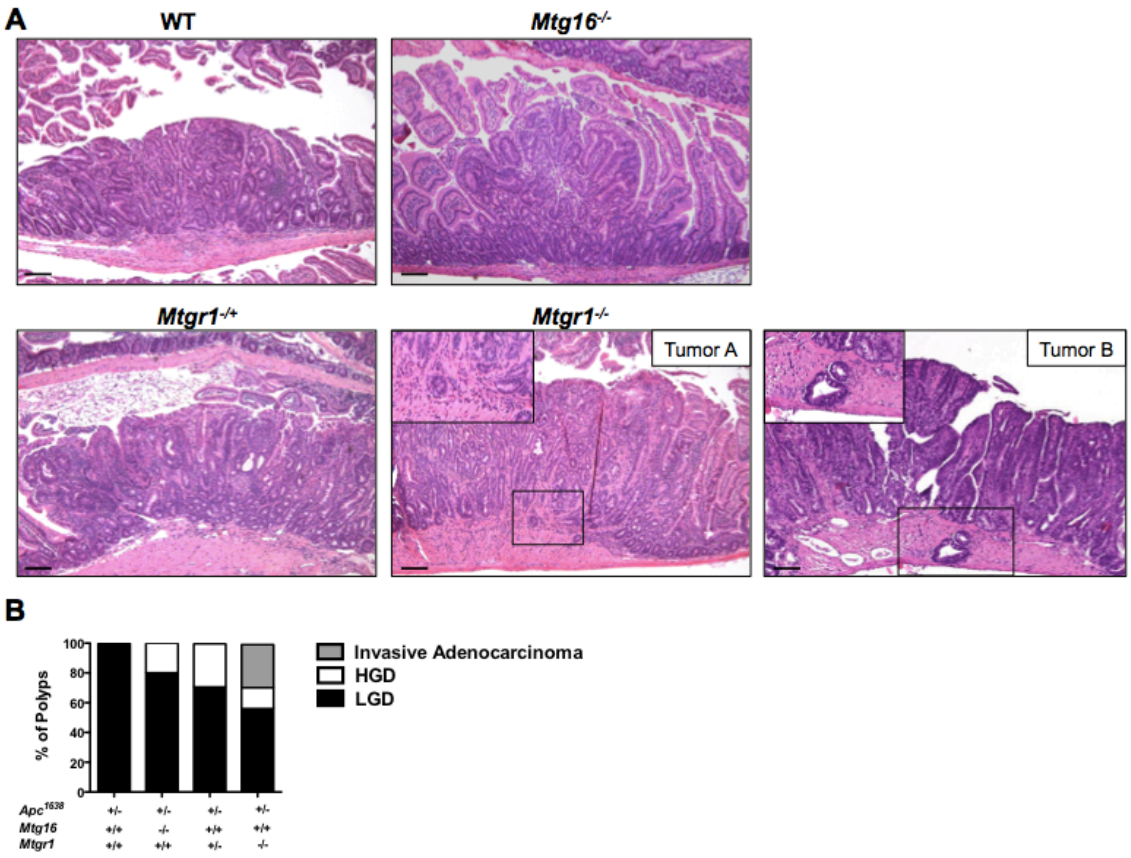

Figure 3.3 *Mtgr1*$^{-/-}$ tumors exhibit a higher degree of dysplasia. (**A**) Representative H&E images of tumors from *Apc*$^{1638/+}$;*Mtg*$^{+/+}$, *Apc*$^{1638/+}$;*Mtg16*$^{-/-}$, *Apc*$^{1638/+}$;*Mtgr1*$^{-/+}$, *Apc*$^{1638/+}$;*Mtgr1*$^{-/-}$ mice. Two examples (Tumor A and B) of invasive adenocarcinoma from *Apc*$^{1638/+}$;*Mtgr1*$^{-/-}$ mice. Black boxes highlight invasive carcinomas. Size standard is 100 microns. (**B**) Quantification of degree of dysplasia by histopathological analysis of H&E stained sections.

MTGR1 preferentially associates with Wnt and Notch genes

As MTGR1 and MTG16 associate with genomic regions to repress transcription, we reasoned that MTG genomic occupancy differences may underlie these disparate phenotypes. We therefore examined ChIP-seq datasets generated from a murine erythroleukemic cell line (MEL) to compare MTGR1 and MTG16 genomic binding sites[116]. Using a false discovery rate of 5%, we determined that MTGR1-containing complexes occupy sites proximate to 1,388 specific genes and MTG16-containing complexes occupy 353, of which there was overlap with 325 genes. Thus, there were a significant number of unique MTGR1 targets (MTGR1 exclusive: 1,063; MTG16 exclusive: 28, **Figure 3.4A**). Protein analysis through evolutionary relationships (PANTHER)[123] of the non-overlapping ChIP binding sites predicted that MTGR1, but not MTG16, regulates Wnt and Notch signaling (**Figure 3.5**). These results suggest that while MTGR1 and MTG16 share occupancy of a subset of targets, the majority of MTGR1 targets are unique to MTGR1.

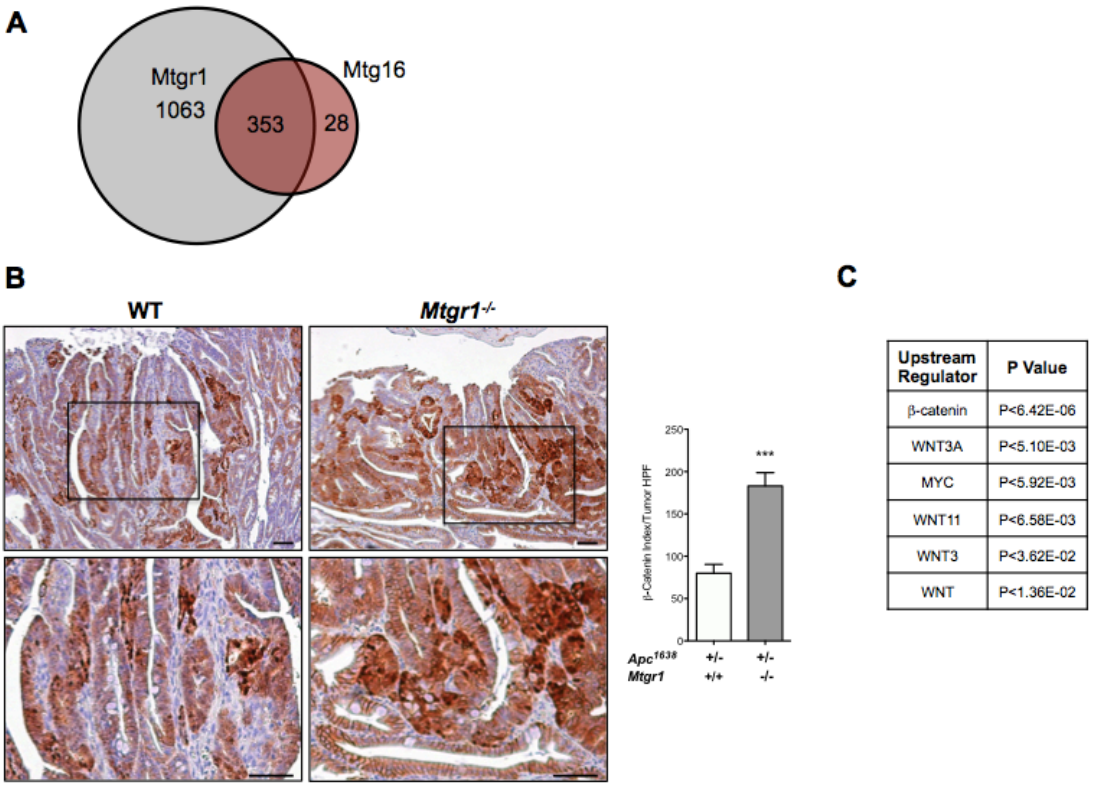

Upstream Regulator	P Value
β-catenin	P<6.42E-06
WNT3A	P<5.10E-03
MYC	P<5.92E-03
WNT11	P<6.58E-03
WNT3	P<3.62E-02
WNT	P<1.36E-02

Figure 3.4 *Mtgr1*$^{-/-}$ tumors demonstrate dysregulated Wnt signaling. (**A**) Venn diagram of MTGR1 and MTG16 genomic occupancy based on ChIP-seq analysis. (**B**) Representative images of β-catenin immunohistochemistry and quantification of β-catenin nuclear localization and intensity. (**C**) RNA-seq analysis of *Apc*$^{1638/+}$*;Mtgr1*$^{+/+}$ (n=3*)* and Apc$^{1638/+}$;*Mtgr1*$^{-/-}$ (n=3) tumors identifying Wnt-perturbed signaling networks. ***P<0.001

Notch and Wnt Signaling Targets

Arrb1	Ep400
Ctbp2	Gnb4
Plcb2	Arrb2
Prcka	Chd1
Ctnna3	Plcb4
Ppp2cb	Bcl9
Tcf712	Nfatc1
Tle3	Ppp3ca
Btrc	Hes1
Gna15	Prkci
Gnaq	Prkcq
Cdh23	Siah1b

Figure 3.5 MTGR1 and MTG16 regulates specific genomic subsets. MTGR1 Wnt and Notch targets.

Mtgr1$^{-/-}$ tumors demonstrate hyperactive Wnt and Notch signaling

Because the ChIP-seq data predicted MTGR1 regulation of Wnt targets (**Figure 3.5**), we used immunohistochemistry to examine the subcellular localization of β-catenin, which is used as a surrogate for Wnt activation. We identified increases in both nuclear β-catenin and extent of its staining, suggesting hyperactive Wnt signaling in the *Mtgr1*$^{-/-}$ background (**Figure 3.4B**). We further evaluated Wnt pathway activation by performing RNA-seq followed by Ingenuity Pathways Analysis (IPA)[124] and identified hyperactive Wnt regulatory networks, including *β-catenin*, *Wnt3A,* and *Myc*, supporting the hypothesis that MTGR1 regulates Wnt targets (**Figure 3.4C**).

As the ChIP-seq data also suggested preferential Notch regulation by MTGR1 and because we previously determined that the secretory lineage deficiency observed in the *Mtgr1*$^{-/-}$ intestine was rescued by Notch inhibition[115], we next determined if Notch signaling was perturbed in *Mtgr1*$^{-/-}$ tumors. As active Notch signaling will increase absorptive enterocyte production at the expense of secretory lineages, we stained tumors with periodic acid Schiff (PAS) to identify goblet cells. *Mtgr1*$^{-/-}$ tumors had dramatically fewer intratumoral goblet cells, consistent with increased Notch signaling *Apc*$^{1638/+}$;*Mtg*$^{+/+}$ 120 ± 14.5 vs. *Apc*$^{1638/+}$;*Mtgr1*$^{-/-}$ 39.4 ± 3.1, PAS positive cells per tumor HPF, **Figure 3.6A**). Supporting this, IPA analysis of intratumoral RNA-seq data indicated activation of Notch signaling (**Figure 3.6B**). To confirm Notch activation, we performed qPCR for *Muc2* and *Cga,* two Notch repression targets, and observed a 2-fold reduction in both in *Mtgr1*$^{-/-}$ tumors, further supporting increased Notch tone (**Figure 3.6C**). We next reasoned that if Wnt and Notch signaling were increased in *Mtgr1*$^{-/-}$ tumors, then cellular processes such as proliferation and apoptosis should be affected. We

measured intratumoral proliferation by immunohistochemical staining for phosphohistone H3 and apoptosis by TUNEL staining and observed increases in both indices in *Mtgr1*$^{-/-}$ tumors (pH3: *Apc*$^{1638/+}$;*Mtg*$^{+/+}$ 76 ± 7.4 vs. *Apc*$^{1638/+}$;*Mtgr1*$^{-/-}$ 139 ± 10.3 positive cells per tumor HPF and TUNEL: *Apc*$^{1638/+}$;*Mtg*$^{+/+}$ 26 ± 3.3 vs. *Apc*$^{1638/+}$;*Mtgr1*$^{-/-}$ 50 ± 3.5 positive cells per tumor HPF) (**Figure 3.7**). These data support the hypothesis that MTGR1 is a coregulator of Notch and Wnt signaling.

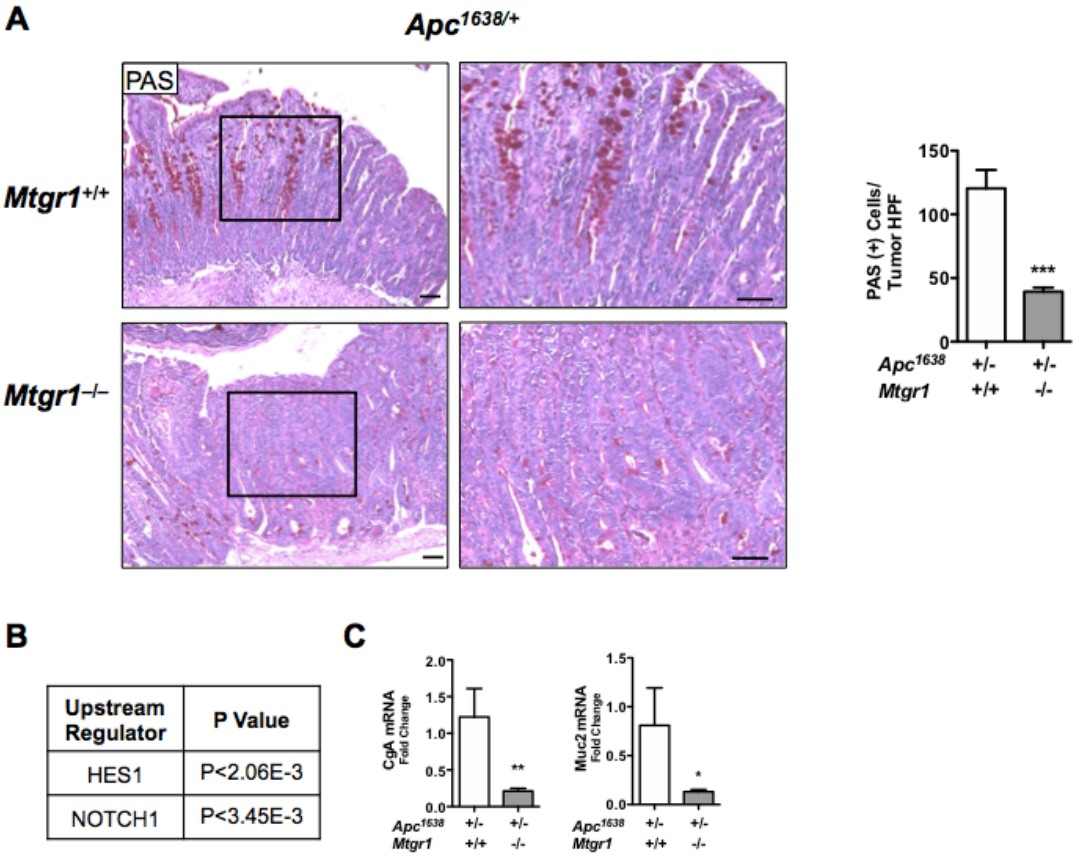

Upstream Regulator	P Value
HES1	P<2.06E-3
NOTCH1	P<3.45E-3

Figure 3.6 Intratumoral Notch signaling is hyperactive upon MTGR1 inactivation. (**A**) Periodic Acid Schiff (PAS) staining for goblet cells in tumors from *Apc*$^{1638/+}$;*Mtgr1*$^{+/+}$ and Apc$^{1638/+}$;*Mtgr1*$^{-/-}$ and quantification of PAS positive cells per tumor HPF. Size standard=50 microns. (**B**) RNA-seq analysis of *Apc*$^{1638/+}$;*Mtgr1*$^{+/+}$ (n=3*)* and Apc$^{1638/+}$;*Mtgr1*$^{-/-}$ (n=3) tumors identifying perturbed Notch signaling networks. (**C**) qPCR for *Cga* and *Muc2* in *Apc*$^{1638/+}$;*Mtgr1*$^{+/+}$ and Apc$^{1638/+}$;*Mtgr1*$^{-/-}$ tumors *P<0.05,**P<0.01, ***P<0.001

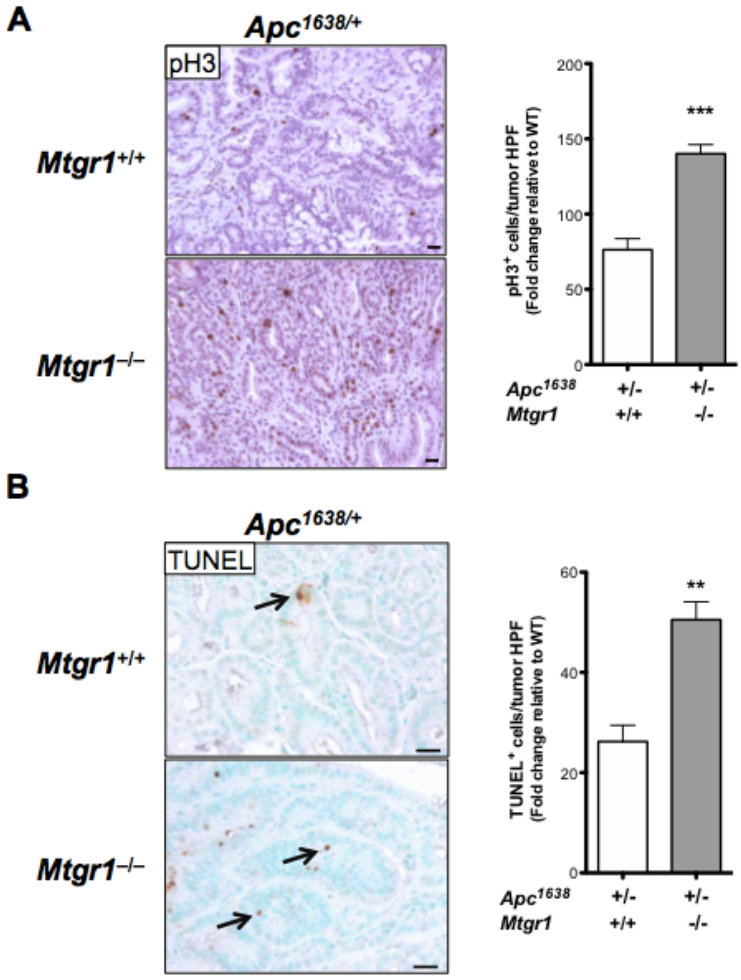

Figure 3.7. Increased intratumoral proliferation and apoptosis in *Mtgr1*$^{-/-}$ animals. (**A**) Proliferation (phospho-histone H3) and (**B**) apoptosis (TUNEL) immunohistochemical assessment per tumor high power field. Size standard=20 microns, **P<0.01, ***P<0.001

MTGR1 is underexpressed early in CRC progression

Because our data implicates MTGR1 as a tumor suppressor, we reasoned that its levels may be reduced in CRC. Therefore, we assessed *MTGR1* levels in CRC in the Moffitt/Vanderbilt-Ingram Cancer Center expression array dataset consisting of 10 normal controls, 6 adenomas, and 250 carcinomas[89,120]. *MTGR1* message was significantly reduced in both the adenoma and carcinoma stages (**Figure 3.8A).** To corroborate this decrease in *MTGR1* mRNA, we used high-resolution *in situ* hybridization (RNAscope) to measure its expression in a separate CRC tissue microarray consisting of 17 normal colon controls and 102 carcinomas. We observed that *MTGR1* RNA was also reduced in carcinomas compared to normal colons (normal colons: 68% ± 7.5% vs. carcinomas: 13% ± 2.5% *MTGR1* expressing epithelial cells per core, **Figure 3.8B**). We then asked if MTGR1 was also decreased at the protein level. Using immunohistochemistry, we detected less MTGR1 protein in carcinomas compared to normal colons (normal colons: 1.8 ± 0.15 vs. carcinomas: 1.3 ± 0.09 MTGR1 staining protein index, **Figure 3.8C**). While MTGR1 expression was decreased in carcinomas, MTGR1 expression did not correlate with disease outcome, survival, or grade (data not shown). Taken together, our data demonstrate that MTGR1 is underexpressed at an early stage in CRC.

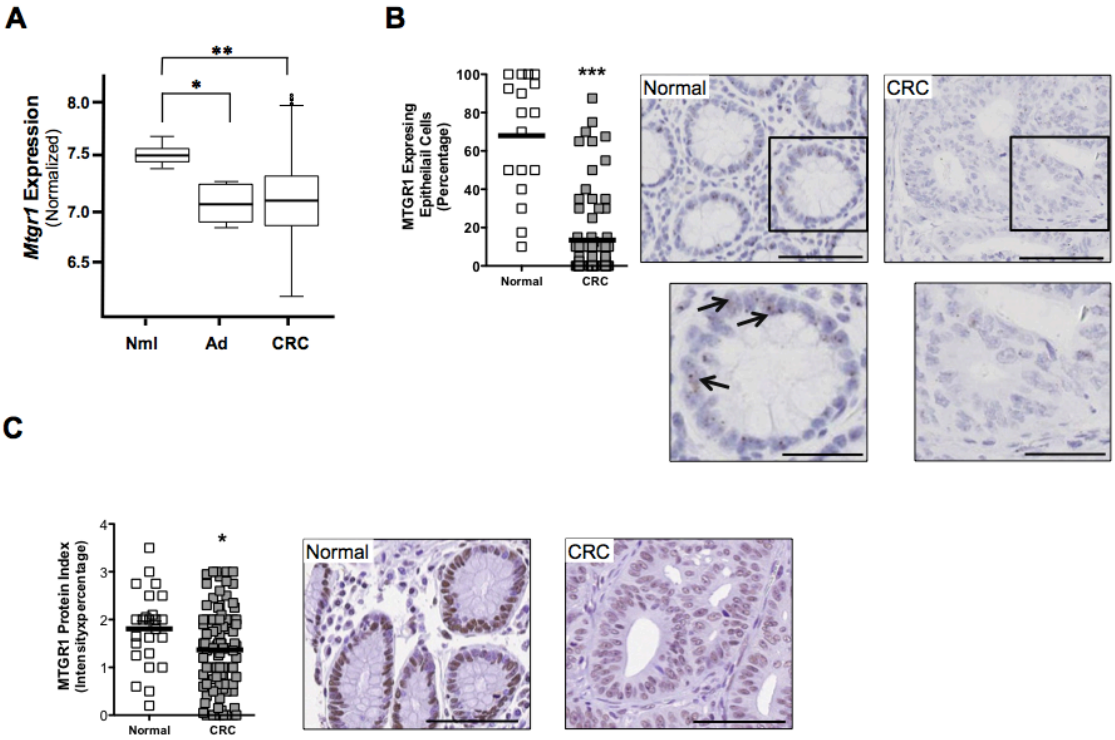

Figure 3.8 MTGR1 is underexpressed in Human CRC. (**A**) *Mtgr1* mRNA expression in Moffitt/Vanderbilt Ingram Cancer Center expression array. (**B**) *MTGR1* RNA expression (size standard=100 microns; inset size standard=50 microns) and (**C**) MTGR1 protein expression (size standard=100 microns) in Vanderbilt Tissue Microarray of CRC and. *P<0.05, **P<0.01, ***P<0.001

Discussion

In this report, we show that while MTGR1 and MTG16 are 65% homologous at the protein level, genetic inactivation of MTGR1, but not MTG16, increased tumorigenesis 10-fold in the *Apc*$^{1638/+}$ mouse model of CRC. Moreover, *Mtgr1*$^{-/-}$ tumors had a higher degree of dysplasia and had increased proliferation and apoptosis. Immunohistochemical and RNA-seq analysis of *Mtgr1*$^{-/-}$ tumors indicated Wnt and Notch pathway activation. In support of its role as a tumor suppressor, MTGR1 was underexpressed in CRC and this appears to occur at an early stage primarily driven by a change in mRNA levels. Overall, our data demonstrate that loss of MTGR1 augments tumorigenesis through dysregulation of Wnt and Notch signaling.

The Myeloid Translocation Gene family consists of three members: *Mtg8*, *Mtgr1*, and *Mtg16*[76]. While the MTGs were initially discovered as a foundational translocation in AML, their genetic deletion in mice has revealed a unique intestinal role for each family member. *Mtg8*$^{-/-}$ mice demonstrate a severe mid-gut deletion phenotype[71]; *Mtgr1*$^{-/-}$ mice have pan-secretory cell loss and are smaller than their wild type counterparts [70]; and *Mtg16*$^{-/-}$ mice have decrease goblet cell indices[72]. The mechanisms underlying the various phenotypes remains unclear. Our analysis of previously published ChIP-Seq data revealed that MTGR1, but not MTG16, uniquely occupies Wnt and Notch targets. Thus, a possible explanation is that MTGR1 and MTG16 differentially associate at genomic loci and have non-overlapping regulatory roles. As MTGs lack the ability to bind DNA directly, their target specificity is determined by the trans-acting DNA binding factors with which they associate[76]. MTGR1 and MTG16 are 65% homologous and share four highly conserved domains termed *Nervy Homology Domain*[76]. The regions between these

domains are variable and likely are important factors in explaining the unique genomic associations of each family member.

Our report identifies MTGR1 as a Modifier of Min (MOM) similar to *Muc2, Mom2*, and *Rassf1a*[125–127]. Where inactivation of MTGR1 fits in the multistep model of CRC mutations is unclear, but our data suggests that loss of MTGR1 plays an important role in both tumor initiation and progression. We propose that because *Mtgr1* loss leads to basal elevation of Wnt and Notch activation, the threshold to trigger tumorigenesis is reduced. Indeed, as MTGR1 regulates two key CRC pathways, it is an important tumor suppressor, and even partial loss of MTGR1 can reduce this tumorigenesis threshold. This is underscored by the fact that MTGR1 haploinsufficiency increased tumor multiplicity and progression (**Figure 3.2A** and **Figure 3.3**). Moreover, that *Mtgr1*$^{-/+}$ mice show increased tumor multiplicity suggests that MTGR1 levels are tightly regulated to restrict Wnt and Notch signaling.

The inflammatory milieu is an important component of colorectal tumorigenesis. *Mtgr1*$^{-/-}$ mice were more susceptible to DSS-induced colitis, but in the setting of inflammatory tumorigenesis, *Mtgr1*$^{-/-}$ mice had fewer AOM/DSS-induced polyps. At face value, this would suggest that loss of MTGR1 expression does not contribute to inflammatory carcinogenesis[103]. It was postulated that perhaps, in the setting of injury, *Mtgr1*$^{-/-}$ initiated tumor cells were hypersensitive to DSS, resulting in their clearance and decreased polyp formation. This hypothesis was supported by the observation that in the absence of DSS mediated injury, *Mtgr1*$^{-/-}$ mice had increased incidence of aberrant crypt foci with AOM treatment[103]. Our report strongly supports this hypothesis, as we show that loss of MTGR1 does indeed augment sporadic CRC. Taken together, we propose a

model in which *Mtgr1*$^{-/-}$ cells, in the setting of injury, are predisposed to undergo apoptosis. In the absence of injury, however, the elevated Wnt and Notch tone observed in *Mtgr1*$^{-/-}$ cells synergizes with *Apc* loss and accelerates tumorigenesis.

In conclusion, we have identified MTGR1 as a modifier of Wnt dependent tumorigenesis and as a potential tumor suppressor. The clinical importance of this observation is underscored by our finding that MTGR1 is downregulated at both the transcript and protein level in CRC. Patients who have reduced MTGR1 expression may be at risk for more aggressive disease. Indeed, given that even partial loss of MTGR1 promoted tumor formation, MTGR1 could serve as a valuable biomarker for patients at risk for CRC.

Chapter 4

BVES is an essential regulator intracellular signaling in inflammatory carcinogenesis

Introduction

Chronic inflammation promotes the development of colorectal cancer (**CRC**)[57,128]. Patients with inflammatory bowel disease (**IBD**), for example, have an elevated risk of developing CRC[58], particularly those who have extensive disease or long disease duration[129]. Although the pathogenesis of inflammatory carcinogenesis remains unclear, it has been postulated that at least a component of malignant degeneration is a consequence of chronic inflammation disrupting intestinal epithelial function[130,131]. Indeed, pathologic changes in adherens and tight-junction proteins have been described in colitis and colitis-associated cancer (**CAC**)[48,131,132]. In addition to providing junctional integrity between cells, adherens and tight-junctional complexes also transduce extracellular signals to direct intracellular programs ("outside-in" signaling[133]), such as those controlling cellular proliferation and differentiation. For example, E-cadherin can sequester β-catenin and at the cell membrane, preventing its nuclear localization and transcriptional activity[134]. Given that dysregulation of junctional proteins commonly occurs in CAC, it is imperative to understand how junctional proteins regulate intracellular signaling networks in normal biology in order to understand how their dysfunction can drive carcinogenesis.

Blood vessel epicardial substance (**BVES/POPDC1**) is a tight-junction associated protein with diverse functions and is silenced in carcinomas secondary to promoter hypermethylation[89,91]. Restoration of BVES expression in CRC cell lines promotes epithelial-like morphology and decreases proliferation, migration, invasion, xenograft

tumor growth, and metastasis[89]. Conversely, knockdown of BVES in epithelial-like cells induces a mesenchymal-like phenotype characterized by increased proliferation, altered morphology, and disorganized cell-cell contacts[89]. Yet how BVES regulates these phenotypes is incompletely understood. Indeed, while several BVES interacting proteins have been identified, their known functions do not explain fully the role of BVES in maintaining epithelial phenotypes. Moreover, how BVES contributes to tumor development has not been tested using genetic approaches.

The transcription factor c-Myc is overexpressed in a variety of cancers including colorectal[135] and gastric[136] malignancies. c-Myc regulates genes involved in proliferation, differentiation, and apoptosis, and its expression can induce epithelial-to-mesenchymal transition[137]. In sporadic CRC, c-Myc plays a central role in APC-driven tumorigenesis[138]. In IBD, c-Myc is overexpressed in inflamed tissues and upregulated in CAC[139]. Indeed, a network analysis of CAC samples indicated that c-Myc protein dysregulation plays a key role in CAC progression[140]. Similarly, c-Myc levels are also increased in the azoxymethane (**AOM**)/dextran sodium sulfate (**DSS**) mouse model of CAC[141]. Yet how c-Myc is deregulated in inflammatory carcinogenesis is not entirely clear. To date, a complex mechanistic network of proteins—including protein phosphatase 2A (PP2A), Axin1, and GSK3β—has been identified that regulate c-Myc protein levels by modifying the phosphorylation status of c-Myc at two residues, threonine 58 (**T58**) and serine 62 (**S62**)[142]. Ubiquitylation of c-Myc is initiated by phosphorylation at T58, leading to its ultimate degradation. Given the prominent role of c-Myc in driving oncogenic programs, understanding how PP2A mediates c-Myc destruction may identify new therapeutic targets in inflammatory carcinogenesis.

Here we report that BVES is an important regulator of inflammatory carcinogenesis programs and promotes c-Myc degradation through an interaction with the PR61α-PP2A complex. We observed that *BVES* was downregulated in human CAC samples, which also show hypermethylation of the *BVES* promoter within the tumors and at distant sites, suggesting a field effect. Using genetic approaches we show that *Bves*$^{-/-}$ mice developed greater tumor incidence and multiplicity as well as a higher degree of dysplasia and intratumoral proliferation in an inflammatory carcinogenesis model. Furthermore, molecular analysis of *Bves*$^{-/-}$ tumors revealed increased c-Myc protein and dysregulated c-Myc signaling. c-Myc protein was also elevated in *Bves*$^{-/-}$ mice intestinal crypts. Knockdown of BVES *in vitro* increased c-Myc stability and consequently key c-Myc targets *ODC* and *CAD*. Conversely, BVES overexpression reduced c-Myc stability and increased c-Myc ubiquitylation. Using a yeast two-hybrid (**Y2H**) screen, we identified that BVES interacts with PR61α, the PP2A regulatory subunit that is critical in degrading c-Myc, and that this interaction is required for BVES to modulate cellular c-Myc levels. Thus, we demonstrate that BVES, a tight-junction associated protein, coordinates PR61α-containing PP2A phosphatase complexes to restrict c-Myc protein levels and that BVES is a key suppressor of inflammatory carcinogenesis whose promoter methylation status may define patients with ulcerative colitis (**UC**) who are at risk for colon cancer.

Materials and methods

Mice, treatments, and analysis

AOM and DSS were prepared as previously described[103]. *Bves*$^{-/-}$ mice have been previously described[87]. Over the course of two experiments, 15 wildtype (8 female and 7 male) (WT) C57BL/6 and 15 *Bves*$^{-/-}$ (7 female and 8 male) mice were treated with 7.5 mg/kg of AOM by intraperitoneal injection and placed on 3 cycles of 5 day treatments with 2.5% DSS. Mice were between 8-12 weeks of age before AOM treatment. All mice were bred and housed in the same facility throughout the duration of the experiment. All *in vivo* procedures were carried out in accordance with protocols approved by the Vanderbilt Institutional Animal Care and Use Committee.

After the mice were sacrificed, colons were irrigated with phosphate-buffered saline (PBS). The colons were then opened longitudinally and rolled orienting the most distal region of the colon such that it was located in the innermost part of the roll. The tissues were then fixed in formalin (1:10 dilution buffered) overnight. The solution was subsequently changed to 70% ethanol before standard paraffin-embedding. Five micron sections were cut and stained with hematoxylin and eosin (H&E) by the Vanderbilt Translational Pathology Shared Resource Core. Proliferation was measured by phospho-histone H3 (pH3) staining using anti-pH3 at 1:150 (Upstate/Millipore) and incubated overnight at 4°C. β-catenin was measured using anti-β-catenin at 1:150 (BD Transduction Laboratories). c-Myc was stained using Abcam at 1:1000 (Y69). Vectastain ABC Kit (Vector Laboratories) was used to perform all immunohistochemistry reactions. Dewaxing and antigen retrieval processing of sections was conducted as previously

described[103]. For intratumoral c-Myc staining, high power fields were scored according to an index from 1-4 (a score of 1 denotes less than 25% of positive cells per high power field; a score of 2 denotes 25-50%; a score of 3 denotes 50-75%; a score of 4 denotes 75-100%).

For RNA analysis, colonic tissue from mice was isolated and immediately placed into 350 μl RNALater (Qiagen) and stored at -80°C. RNA from tissue or cells was isolated using the RNAEasy kit (Qiagen) according to the manufacturer's "Animal Tissue" protocol. RNA was subsequently stored at -80°C.

For RNA-seq experiments, RNA from WT colons (n=3), *Bves*$^{-/-}$ colons (n=3), WT tumors (n=3), and *Bves*$^{-/-}$ tumors (n=3) was sequenced by the Vanderbilt Technologies for Advanced Genomics (VANTAGE) core facility. Initial raw sequencing data were aligned to a reference mouse genome (mm9) using TopHat (version 1.3.1) software[48]. The transcript of mouse genome (mm9) was downloaded from UCSC as implemented in the Bioconductor package *GenomicFeatures*. Then the Bioconductor packages *Rsamtools* and *DESeq* were used to estimate the read count for expression of each gene and to detect differentially expressed (DE) genes. For count based gene expression data, *DESeq* uses a model based on the negative binomial distribution which includes a dispersion parameter to better estimate variance[49]. The p-values from *DESeq* were adjusted by Benjamini and Hochberg's method to control false discovery rate (FDR)[50].

BVES promoter methylation analysis

The tissue samples were obtained from colectomy specimens from individuals without UC, individuals with UC without dysplasia or cancer as well as from individuals with UC and high-grade dysplasia and/or colon cancer. Clinical information about the specimens is described in **Table 4.1.**

Patient	Biopsy dx	UC NP/P	biopsy dx	Location	Distance to Dysplasia(f/ anal verge)	Age	Gender	Disease Duration(mo.)	PSC?	Disease Activity	Inflammation
1	neg	NP	neg	distal		67	M	30	no		3-4+
2	neg	NP	neg	distal		70	F	16	no		3-4+
3	tumor	P	tumor	distal	0 cm	55	F	20	no		4+
4	neg	NP	neg	distal		56	F	10	no		
5	tumor	P	tumor	proximal	0 cm	47	M	8	no		?
6	tumor	P	tumor	proximal	0 cm	31	M	10	no		?
7	neg	NP	neg	distal		48	M	9	no		3-4+
8	neg	P	neg	distal		67	M	30	no		0
9	neg	NP	neg	distal		41	F	20	no		2-3+
10	neg	NP	neg	distal		63	M	39	no		
11	neg	NP	neg	distal		31	M	8	no		3-4+
12	neg	NP	neg	distal		49	F	20	no		1-2+
13	HGD	P	HGD	83 cm	0 cm	36	M	8	yes	marked activity	4+
14	HGD	P	HGD	(C2)next to rectal pieces	0 cm	53	F	NA	no?		4+
15	neg	NP	neg	7 cm		59	M	0.25		no data	active
16	neg	NP	neg	14 cm		51	F	20	no	no data	3+
17	neg	NP	neg	15 cm		46	F	17	no	no data	0
18	neg	P	neg	3.4 cm	78.3 cm	36	M	11	yes	no data	0
19	HGD	P	HGD	92 cm	0 cm	58	M	29	yes	focal activity	0
20	HGD	P	HGD	3 cm	0 cm	32	M	16	no	active	1+
21	HGD	P	LGD +HGD	19 cm	0 cm	48	M	10	no	focal activity	0
22	HGD	P	HGD	4 cm	0 cm	33	M	13	no	focal active	4+
23	HGD	P	HGD	70.4 cm	6.4cm to CA	51	F	13	yes	active	1+
24	HGD	P	HGD	31.2 cm	0 cm	33	F	22	no	no data	1+
25	neg	P	neg	14.4 cm	18.4 cm	34	M	17	yes	active	1+

Table 4.1 Clinical characteristics of patients samples.

1) Primary Human Tissue Samples

Fresh frozen epithelial cell layers were isolated from each specimen using the epithelial "shake off" technique[51] and the DNA was extracted using Qiagen DNA extraction kits (Qiagen) following the manufacturer's instructions. DNA was extracted from the following groups: 1) 17 control samples of normal colon mucosa from patients who did not have UC (**Control-No UC**) 2) non-neoplastic cells from 11 UC patients without cancer/dysplasia (**Normal—no HGD/CAC**) 3) non-neoplastic cells from 10 UC patients with concurrent cancer/dysplasia located at least 20 cm away (**Normal—concurrent HGD/CAC**) 4) cancerous or dysplastic cells from 10 UC patients (**HGD/CAC**). The specimens were obtained from the pathology archives at University of Washington (Seattle, WA) following protocols approved by the Institutional Review Board.

2) Methylation array analyses

300 ng of epithelial cell DNA was bisulfite converted using the EZ Meth DNA kit following the manufacturer's instructions (Zymo Research, #D5002). Converted DNA was applied to Infinium HumanMethylation450 BeadChips (Illumina) which were then processed in the Genomics Shared Resource Core at the Fred Hutchinson Cancer Research Center according to the manufacturer's specifications. Data was normalized and filtered as described by our group previously[52]. Differentially methylated loci (DML) were determined after converting beta values, which range from 0.0 (no methylation) to 1.0 (100% methylation), to M values, where the M value is the $\log_2$ ratio of the intensities of the methylated probe versus unmethylated probe. For the purposes of this study, we were interested in loci that demonstrated both 1) differential methylation between **UC—**

no HGD/CAC and **UC—concurrent HGD/CAC** cases and 2) similar methylation patterns between **UC—concurrent HGD/CAC** and **HGD/CAC** cases. Loci with p values ≤ 0.0008 (adjusted p value ≤ 0.260) were considered differentially methylated.

The differentially methylated probes in the *BVES* promoter region were cg17398252 (located within a CpG island 1500 base pairs upstream from the transcription start site), cg25280433 (located within a CpG island in the 5' UTR/exon 1), and cg20624391 (located in a CpG island in 5' UTR/exon 1).

3) Pyrosequencing of DNA samples

Pyrosequencing assays were designed to confirm methylation differences seen on the HM450 arrays. Assays were designed to target the same promoter CpG island that contained the DML from the arrays. The same DNA samples that were used on the HM450 array were used for pyrosequencing, except for one UC—no HGD/CA and one UC—concurrent HGD/CAC case, both of which did not have enough DNA remaining for these assays. Primers and reaction conditions used have been previously described[89].

RNAScope

RNA scope was conducted according to manufacturer's protocol (ACD, www.acdbio.com) with probes directed against *BVES* (catalog number 410346), positive control Hs-PPIB (catalog number 313901), and negative control DapB (catalog number 310043Tissue microarrays were scanned digitally and uploaded to a digital image hub. The percentage of epithelium per core that stained positive was scored and quantified. Only cores that stained robustly with the positive control probe were scored. Clinical information of specimen is described in **Table 4.2**.

	Ulcerative Colitis Patients With Cancer (N=14)	UC Patients with Dysplasia (N=6)	Normal (N=14)
Average Age (sd)	51.4 ± 18.3	50.2 ± 17.5	57.9 ± 15.5
Gender	6 Males, 8 Females	5 Males, 1 Female	8 Males, 6 Females
BMI	26 ± 9.2	n/a	27.6 ± 3.1
Race	White (N=14)	n/a	Black (N=2), White (N=12)
Tumor Grade	Grade 1 (N=3), Grade 2 (N=2), Grade 3 (N=9)	n/a	n/a
Location if known	Descending (N=2), Transverse (N=2), Left (N=1), Ascending (N=1), Sigmoid (N=2), Rectum (N=4), Hepatic fixture (N=1)	n/a	n/a
Lymph Node Involvement	Positive (N=9), Negative (N=5)	n/a	n/a
Average Tumor Size	4.2 ± 2.9 cm	n/a	n/a
Mesenteric Deposits	Absent (N=7), Present (N=8)	n/a	n/a

Table 4.2 Clinical characteristics of TMA patients samples.

Enteroid cultures

Enteroid cultures were derived according to previously published protocols[47].

Yeast two-hybrid assays

*BVES (*hgx2637v_pB29*)* and *PR61a* (pB20_A-197) constructs were obtained from Hybrigenics. Y2H assays were conducted as previously described[48].

Cell Culture

Unless otherwise indicated, all HEK 293T and Caco2 cells were cultured in DMEM with 10% serum and 1% Penn/strep. Polyethylenimine (PEI) at a concentration of 1 mg/ml was used for all transfection experiments. An empty vector was used to ensure equal quantities of cDNA were transfected. Cycloheximide (Sigma) was used at 100 mg/ml and cells were lysed at the indicated intervals. MG132 (CalBiochem) was used at 10 mM for 4 hours for ubiquitylation experiments.

For immunoprecipitation assays, cells were grown in 100-mm cell culture dishes. Once desired confluence was reached, cells were rinsed with ice-cold PBS and incubated for 15 min at 4°C in 1 ml of cell lysis buffer (Sigma) containing 1X Phosphatase inhibitor cocktail 2 and 3 (Sigma) and 1X Protease Inhibitor cocktail (Sigma). Samples were sonicated for 10 seconds at 4°C. Cellular debris was removed by centrifugation; protein concentration was measured by Bradford method. For immunoprecipitation, approximately 1 mg of total protein was incubated with 3 μg of the respective antibodies overnight at 4°C followed by a 3 hour incubation with 25 μl of protein A/G magnetic

beads (Millipore). The immunoprecipitates were collected by magnetic separation and washed three times with 0.5 ml of cell lysis buffer. Washed beads were suspended in 50 μl of 2X Laemmli buffer and samples were resolved on a reducing 10% SDS-PAGE gel and probed with respective antibodies.

Proximity ligation assays (PLA) were performed according to manufacturer's protocol (Sigma, #DUO92101). Primary antibodies were incubated for 30 minutes in a 37°C humidified chamber at the following concentrations: V5 (Abcam) 1:1500, c-Myc (cell signaling) 1:750, and PPP2R5A (Bethyl labs) 1:750.

For western blots, cells were washed with ice-cold PBS before being scraped and collected. Cells were pelleted by centrifugation and resuspended in 2X Laemmli buffer and boiled for 10 minutes before analysis by SDS-PAGE electrophoresis. Membranes were blocked using Odyssey blocking buffer for 30 minutes and then blotted with anti-PPP2R5A (Bethyl labs, #A300-967A), anti-c-Myc (Cell Signaling #D84C12), anti-V5 (Abcam #ab27671), anti-His (Abcam #ab18184), or anti-HA (Vanderbilt Antibody and Protein Resource). All antibodies were used at 1:1000 concentration in Odyssey blocking buffer with 0.1% Tween-20. Primary antibodies were incubated for 1 hour at room temperature (RT) before being washed three times in PBS-Tween. LiCor secondary antibodies were used at 1:30,000 dilution and incubated for 30 minutes at room temperature. Quantification of western blot band intensity was conducted using LiCor Image Studio.

BVES and PR61α expression plasmids were generated using Gateway cloning (Invitrogen). pENTR vectors containing either BVES (HsCD00368575, Harvard Plasmid Prep) or PPP2R5A (HsCD00041318, Harvard Plasmid Prep) were shuttled into pcDNA3.1 V5/His using LR clonase (Invitrogen). The HA-tagged PP2Ac expression plasmid was graciously provided by Peter Howley who deposited the plasmid into Addgene repository (plasmid #35005). WT-c-Myc and T58A-c-Myc plasmids were previously described[143].

For quantitative reverse transcription polymerase chain reactions, twenty microliters of cDNA was synthesized using iScript cDNA Synthesis Kit (Bio-Rad) from 1 μg of RNA per sample. All RT-PCR reactions were carried out using SYBR green reaction mix (Bio-Rad) according to the manufacturer's protocol.

The following primers were used to measure expression levels: human *CAD*: (F: AGTGGTGTTTCAAACCGGCAT and R:CAGAGGATAGGTGAGCACTAAGA), human *ODC* (F:TTTACTGCCAAGGACATTCTGG and R: GGAGAGCTTTTAACCACCTCAG) and mouse *Odc* (F: AGCAGGCTTCTCTTGGAAC and R: CATGCATTTCAGGCAGGTTA). All qPCR reactions were normalized to GAPDH (Human GAPDH, Realtime Primers #3541 and Mouse Gapdh, Realtime Primers #7317).

Statistical Methods

Immunohistochemistry (number of positively stained cells) was analyzed by one-way ANOVA. If only two groups were being compared, a Student's *t* test was used. The observer was blinded to slide identity, and the slide was scored in an unbiased fashion.

Results

BVES is downregulated and its promoter is hypermethylated in CAC

As *BVES* is underexpressed via promoter hypermethylation in CRC[89] and epithelial junctional dysfunction is thought to underlie the progression of CAC, we asked whether the *BVES* promoter was hypermethylated in CAC. To determine this, we analyzed an Infinium HumanMethylation450 array screen of samples from patients without UC (**Control—No UC**), patients with UC who did not have cancer (**UC—no HGD/CAC**), and patients with UC who developed colon cancer. Two different groups of samples were analyzed from the patients with UC who developed colon cancer: non-malignant tissue (**UC—concurrent HGD/CAC**) and tissue with high-grade dysplasia and/or cancer (**HGD/CAC**). These analyses demonstrated that three loci in the *BVES* promoter were unmethylated in the normal colon of the controls–No UC (0.1% $\pm$ 0.016%), modestly methylated in UC–no HGD/CAC (16% $\pm$ 4.7%), and hypermethylated in the HGD/CAC among patients with colitis-associated carcinoma (HGD/CAC, 53% $\pm$ 2.6%) (**Figure 4.1A**). Furthermore, remote non-neoplastic, mucosal samples (UC-Concurrent HGD/CAC) from the same patients who had CAC (HGD/CAC) were hypermethylated (50% $\pm$ 2.6%) to a similar degree as that observed in cancerous tissue, suggesting that *BVES* promoter methylation may represent a field effect in CAC

and that *BVES* promoter methylation status may identify UC patients with concurrent malignancy. To confirm the results derived from the HM450 methylation array studies, we pyrosequenced the *BVES* promoter using the same samples and again demonstrated low levels of methylation in the UC—no HGD/CAC cases and higher methylation in the UC—concurrent HGD/CAC and HGD/CAC cases (**Figure 4.1B**).

It is possible that *BVES* promoter methylation, while increased, may not be sufficient to silence its expression. To determine whether *BVES* promoter methylation reduced its transcription, we tested whether *BVES* mRNA was downregulated in CAC using high resolution *in situ* hybridization (RNAScope[144]) in a tissue microarray consisting of normal and CAC samples. *BVES* RNA showed low levels of expression in the normal colon, but it was present throughout the epithelium (**Figure 4.1C**). In CAC samples, however, *BVES* message was rarely detected and quantification of epithelial staining indicated a 5-fold decrease ($p<0.001$). Taken together, *BVES* RNA expression is downregulated in CAC, and the *BVES* promoter is hypermethylated in both tumor and non-malignant mucosa in patients with CAC, implicating *BVES* promoter methylation as a potential biomarker associated with dysplasia or neoplasia in the colons of patients with IBD.

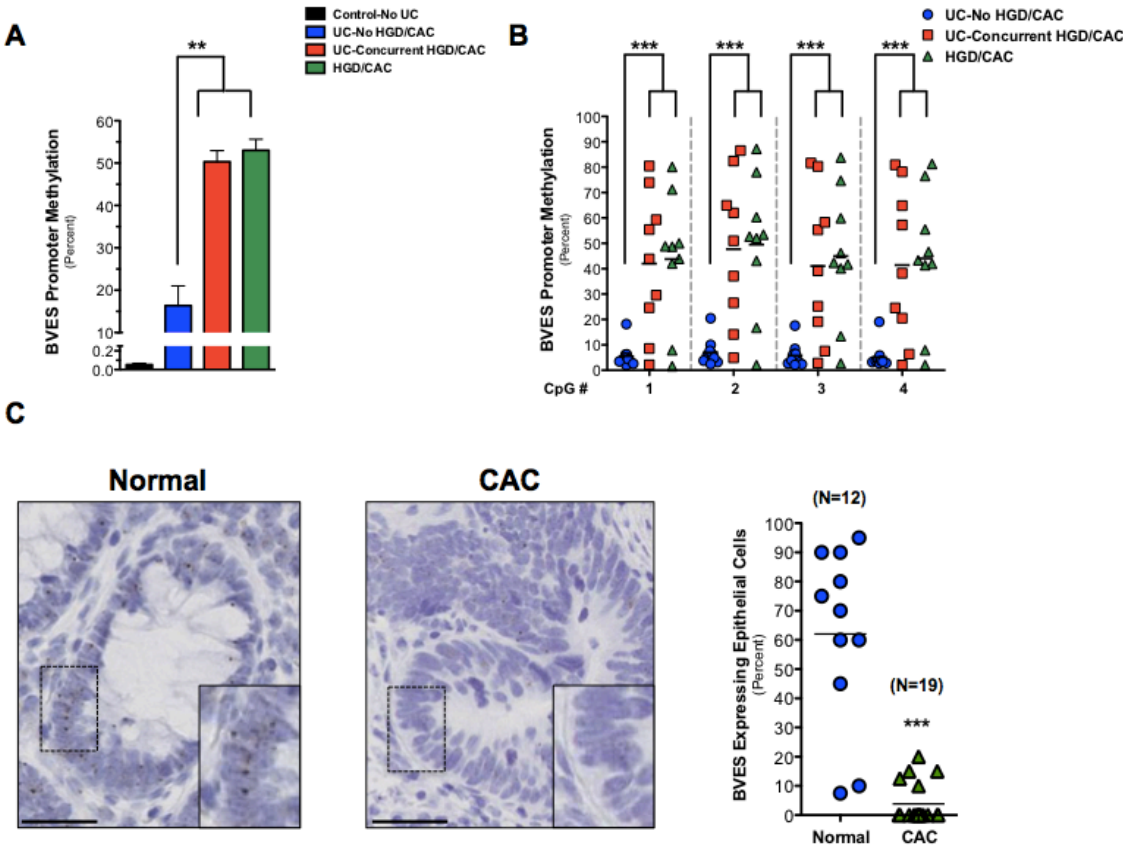

Figure 4.1 A field effect of *BVES* promoter hypermethylation in colitis-associated cancer. (A) Average *BVES* promoter methylation status in the indicated sample from the Infinium HumanMethylation 450 Array. Methylation was measured in four sample types: colon epithelia from patients who did not have UC (Control—No UC); colon epithelia from UC patients who did not have dysplasia or carcinoma (UC—no HGD/CAC); non-malignant colon epithelia (UC—concurrent HGD/CAC) and malignant colon epithelia (HGD/CAC) from UC patients who had dysplasia/carcinoma. Control—No UC, n=17; UC—no HGD/CAC, n=11; UC—concurrent HGD/CAC, n=10; HGD/CAC, n=10. **p<0.01. **(B)** Pyrosequencing at four sequential CpG dinucleotides in the *BVES* promoter. Each shape represents a separate individual, with mean methylation values depicted with black bars. ***p<0.001. **(C)** Representative images of RNA scope analysis of *BVES* message in normal colons (n=12) and CAC (n=19). Right: Quantification of BVES expressing epithelial cells per tissue microarray core. Size standard=50 microns. ***p<0.001

Bves loss promotes CAC development

Because *BVES* was underexpressed in CAC we next determined the functional significance of its underexpression using reverse genetic approaches. We hypothesized that genetic deletion of *BVES* might modify CAC in experimental modeling. To test this hypothesis, we used the AOM/DSS murine model of inflammatory carcinogenesis (**Figure 4.2A**). We first profiled the transcriptome of AOM/DSS-induced tumors and observed that *Bves* transcripts were downregulated 5-fold in tumors compared to normal colon (**Figure 4.2B).** As expected**,** we also observed changes in other tight-junction constituents, supporting previous reports of tight-junctional dysregulation in colitis and CAC[44]. We confirmed that *Bves* message was decreased in AOM/DSS tumor tissue by qPCR in an independent sample set (**Figure 4.2B**). As a result, we hypothesized that complete loss of *Bves* might promote inflammatory carcinogenesis.

To test whether *Bves* expression could modify CAC, we compared tumor burden in WT and *Bves*$^{-/-}$ mice subjected to the same inflammatory carcinogenesis protocol. *Bves*$^{-/-}$ mice lost a greater fraction of body weight compared to WT mice, most notably during cycle 3 (**Figure 4.2C**). Endoscopy one-week prior to sacrifice demonstrated increased tumor multiplicity in *Bves*$^{-/-}$ mice (**Figure 4.2D**). Enhanced tumorigenesis in the setting of *Bves* loss was confirmed at necropsy where we observed 100% tumor penetrance in *Bves*$^{-/-}$ mice compared to 60% in WT mice and increased tumor multiplicity (6.5 tumors per *Bves*$^{-/-}$ mouse vs. 2.2 tumors per WT mouse, $p<0.001$, **Figure 4.2E**). Furthermore, *Bves*$^{-/-}$ tumors demonstrated more advanced dysplasia compared to WT tumors (**Figure 4.2F**). Control mice treated with DSS-only or a single AOM injection did

not develop tumors during this time frame (data not shown). In sum, BVES is underexpressed in CAC and its genetic deletion augments inflammatory carcinogenesis.

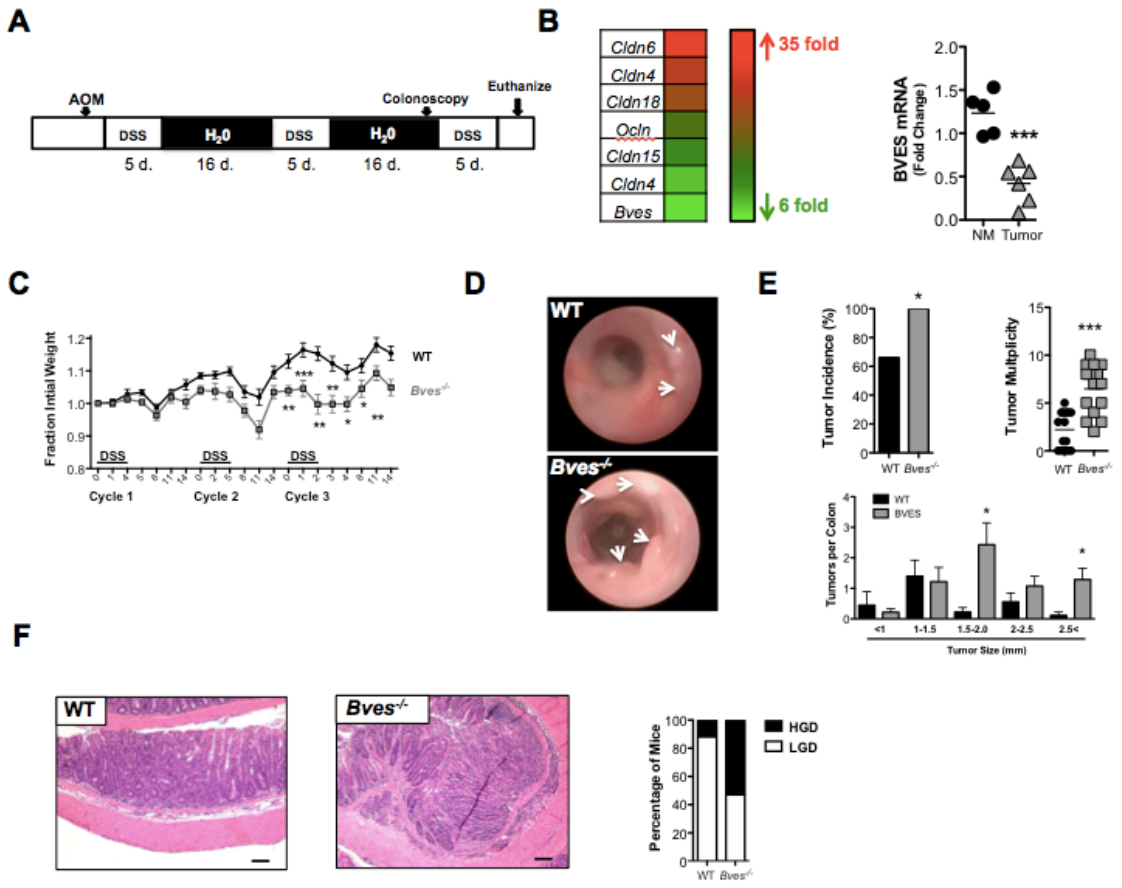

Figure 4.2. **BVES modifies inflammatory carcinogenesis.** **(A)** Schematic of AOM/DSS protocol and timeline. Mice were injected with 7.5 mg/kg of AOM and treated with 2.5% DSS at the indicated time. **(B)** Left: Heat map of RNA-seq data derived from WT colons (n=3) and WT AOM/DSS tumors (n=3). Red indicates genes increased and green indicates genes decreased in tumors compared to normal colon. Right: Quantitative RT-PCR of *Bves* message levels in normal adjacent/non-malignant (NM, n=5) and tumor (Tumor, n=6). Tissue harvested from WT mice after AOM/DSS treatment. ***p<0.001.
(C) Weights of *Bves*$^{-/-}$ and WT mice during AOM/DSS treatment. Weights are presented as fraction of initial weight. *Bves*$^{-/-}$ (n=15) and WT (n=15). *p<0.05, ***p<0.01, ***p<0.001. **(D)** Representative colonoscopy images of WT and *Bves*$^{-/-}$ colons after the second cycle of DSS treatment. **(E)** Tumor incidence, multiplicity, and size distribution in WT and *Bves*$^{-/-}$ mice. *p<0.05, ***p<0.001. **(F)** Left: Representative H&E stained sections demonstrating the histologic features of WT and *Bves*$^{-/-}$ tumors. Size standard=100 microns. Right: Blinded histological scoring of degree of dysplasia of tumors from WT and *Bves*$^{-/-}$ mice. Percentage of mice with intratumoral low or high-grade dysplasia.

Increased proliferation and enhanced Wnt activation in Bves$^{-/-}$ tumors

To identify BVES-directed mechanisms responsible for modifying tumorigenesis, we examined proliferation and apoptosis in the tumors of AOM/DSS treated *Bves*$^{-/-}$ mice. Proliferation, as measured by phospho-histone H3 staining, was increased in *Bves*$^{-/-}$ tumors (**Figure 4.3A)**. Conversely, staining for cleaved caspase-3 indicated no difference in intratumoral apoptosis between *Bves*$^{-/-}$ and WT mice (**Figure 4.4**). As Wnt activation can drive proliferation, we postulated that Wnt signaling might be perturbed in *Bves*$^{-/-}$ tumors. β-catenin dysregulation is a key indicator of hyperactive Wnt signaling[6], and β-catenin is also a mutational target in AOM/DSS carcinogenesis, resulting in increased levels and altered subcellular distribution[145]. We observed excessive cytoplasmic and nuclear β-catenin localization in *Bves*$^{-/-}$ tumors compared to WT tumors (**Figure 4.3B**), suggesting hyperactive Wnt signaling. Furthermore, intratumoral transcriptome profiling followed by Ingenuity Pathway Analysis (**IPA**)[124] indicated upregulation of Wnt target genes in *Bves*$^{-/-}$ tumors (**Figure 4.3C**). Immunoblotting also demonstrated greater expression of Cyclin D1 and c-jun, two well-characterized Wnt target genes[4,5] in *Bves*$^{-/-}$ colons (**Figure 4.3D**). While previous experiments demonstrated that BVES could regulate Wnt signaling using *in vitro*, cell-based assays[89], these current findings provide the first *in vivo* and only genetic evidence supporting the hypothesis that BVES regulates Wnt activity.

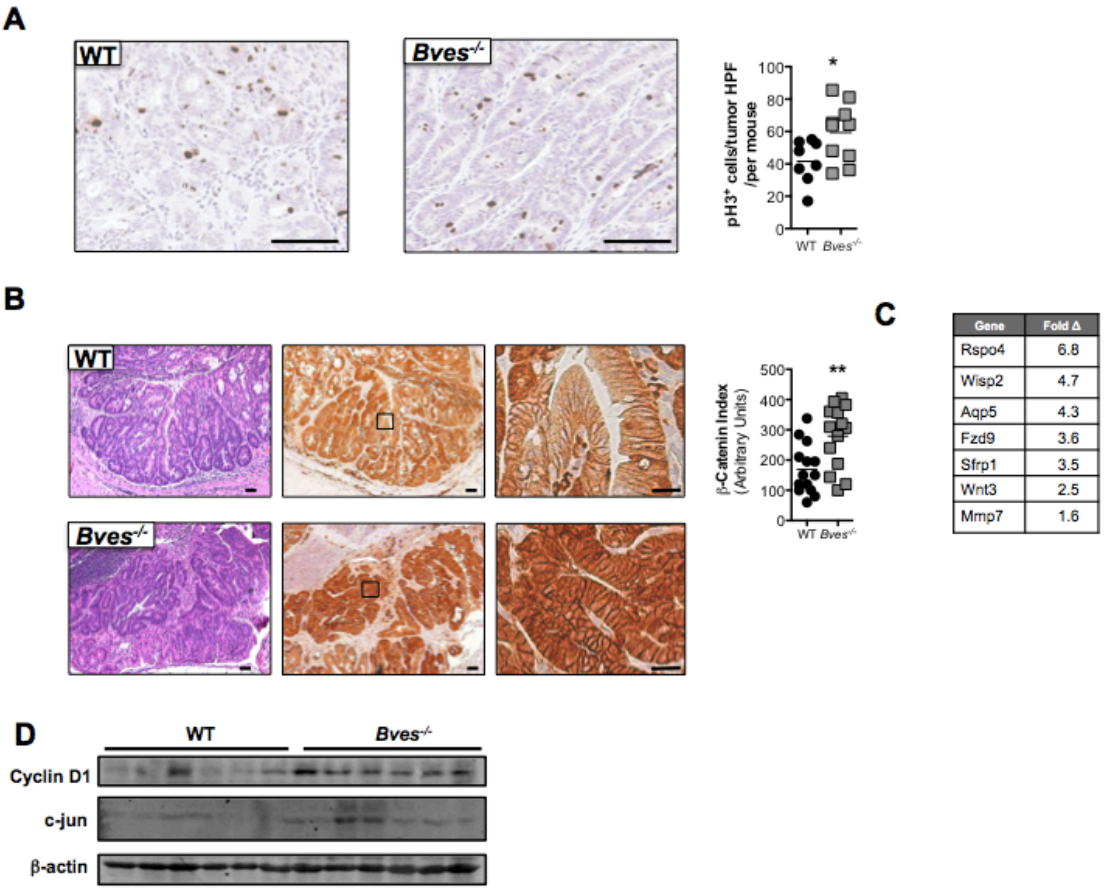

Figure 4.3. Dysregulated Wnt signaling in *Bves*$^{-/-}$ tumors. (A) Left: Representative images of phospho-histone H3 (pH3) immunohistochemistry in WT and *Bves*$^{-/-}$ tumors. Size standard=50 microns. Right: Quantification of pH3 positive cells per tumor HPF. *p<0.05. **(B)** Representative images of β-catenin immunohistochemistry. Left: H&E stained sections, size standard=50 microns. Middle: Low magnification, size standard=50 microns. **Right**: High magnification, size standard=20 microns. Quantification of intratumoral β-catenin immunohistochemistry. Staining was quantified according to cytoplasmic localization as well as intensity[103]. **(C)** Wnt target genes upregulated in *Bves*$^{-/-}$ tumors identified in RNA-seq dataset (WT, n=3; *Bves*$^{-/-}$, n=3). **(D)** Immunoblot of Cyclin D1 and c-jun in *Bves*$^{-/-}$ and WT colons. β-actin was used as a loading control.

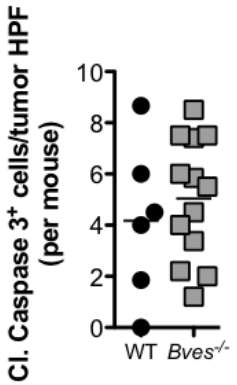

Figure 4.4 Quantification of cleaved caspase 3 positive cells per tumor high-powered field.

BVES regulates c-Myc degradation

As c-Myc is a *bona-fide* Wnt transcriptional target[138], has been identified as a potential biomarker in patients with IBD at risk for CAC[140], and is overexpressed in AOM/DSS tumors[141], we postulated that c-Myc was dysregulated in *Bves*$^{-/-}$ tumors. Indeed, IPA analysis of intratumoral transcriptomes identified causal dysregulation[124] of c-Myc networks (**Figure 4.5A**). While analysis of RNA-seq datasets showed a modest increase in c-Myc transcripts in *Bves*$^{-/-}$ tumors compared to WT tumors (**Figure 4.5B**), immunohistochemical staining for c-Myc demonstrated a more striking increase in c-Myc protein in *Bves*$^{-/-}$ tumors (**Figure 4.6A**). Moreover, immunoblotting in tumor-adjacent mucosa indicated that c-Myc was increased prior to tumor formation and suggested BVES might regulate c-Myc levels in the gut at baseline (**Figure 4.6B**). To test this, we isolated crypts from untreated *Bves*$^{-/-}$ and WT mice and observed greater c-Myc protein in *Bves*$^{-/-}$ samples (**Figure 4.6C**). Consistent with elevated c-Myc, qPCR for *Ornithine decarboxylase (Odc)*, a c-Myc transcriptional target, indicated a 4-fold increase in *Bves*$^{-/-}$ colons (**Figure 4.7**). We also observed increased mRNA of c-Myc targets *Odc* and *E2f transcription factor 2 (E2f2)* (**Figure 4.6D**) in "mini-gut" 3D cultures, demonstrating that BVES regulation of c-Myc activity was epithelial cell-autonomous.

As we observed increased c-Myc protein in *Bves*$^{-/-}$ tumors, we postulated that BVES could regulate c-Myc protein stability. Using RNA interference, we suppressed BVES expression in HEK 293T cells, a non-malignant cell line, and Caco2 cells, a CRC cell line that expresses BVES and can form a polarized epithelium[89]. BVES knockdown both increased c-Myc protein levels and reduced threonine 58 phosphorylation (T58), a key post-translational modification which signals for c-Myc degradation by the ubiquitin-

proteasome system (**Figure 4.8A**). This increase in c-Myc levels was functionally relevant as transcript levels of c-Myc targets *ODC* and *Carbamoyl-Phosphate Synthetase 2 Aspartate Transcarbamylase and Dihydroorotase* (*CAD*) were increased with *BVES* knockdown (**Figure 4.8B**). Knockdown of BVES doubled c-Myc half-life compared to non-targeting control samples (**Figure 4.8C**). Conversely, overexpressing BVES reduced c-Myc protein while increasing T58 c-Myc species (**Figure 4.8D**) and reduced c-Myc protein half-life (**Figure 4.8E**, lower panel). We then tested whether BVES could regulate c-Myc ubiquitylation, a central post-translational event targeting its destruction. Indeed, by overexpressing BVES we observed increased c-Myc polyubiquitylation (**Figure 4.8F).** Moreover, inhibiting the proteasome using MG132 blocked BVES-induced reduction of c-Myc. (**Figure 4.8F**). Hence, our results suggest that BVES promotes the post-translational degradation of c-Myc.

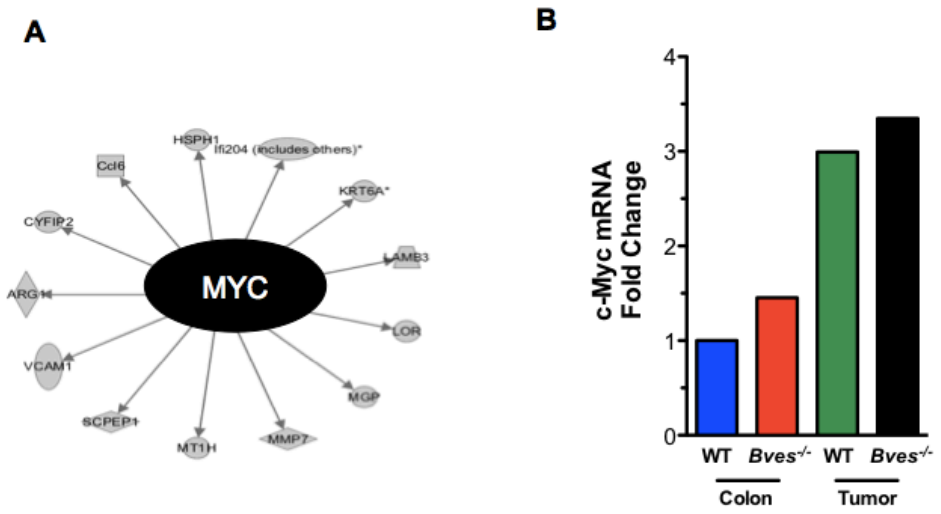

Figure 4.5 RNA seq analysis of tumors. (**A**) IPA generated schematic of dysregulated c-Myc network in *Bves*$^{-/-}$ tumors compared to WT tumors. (**B**) c-Myc mRNA levels relative to WT colon.

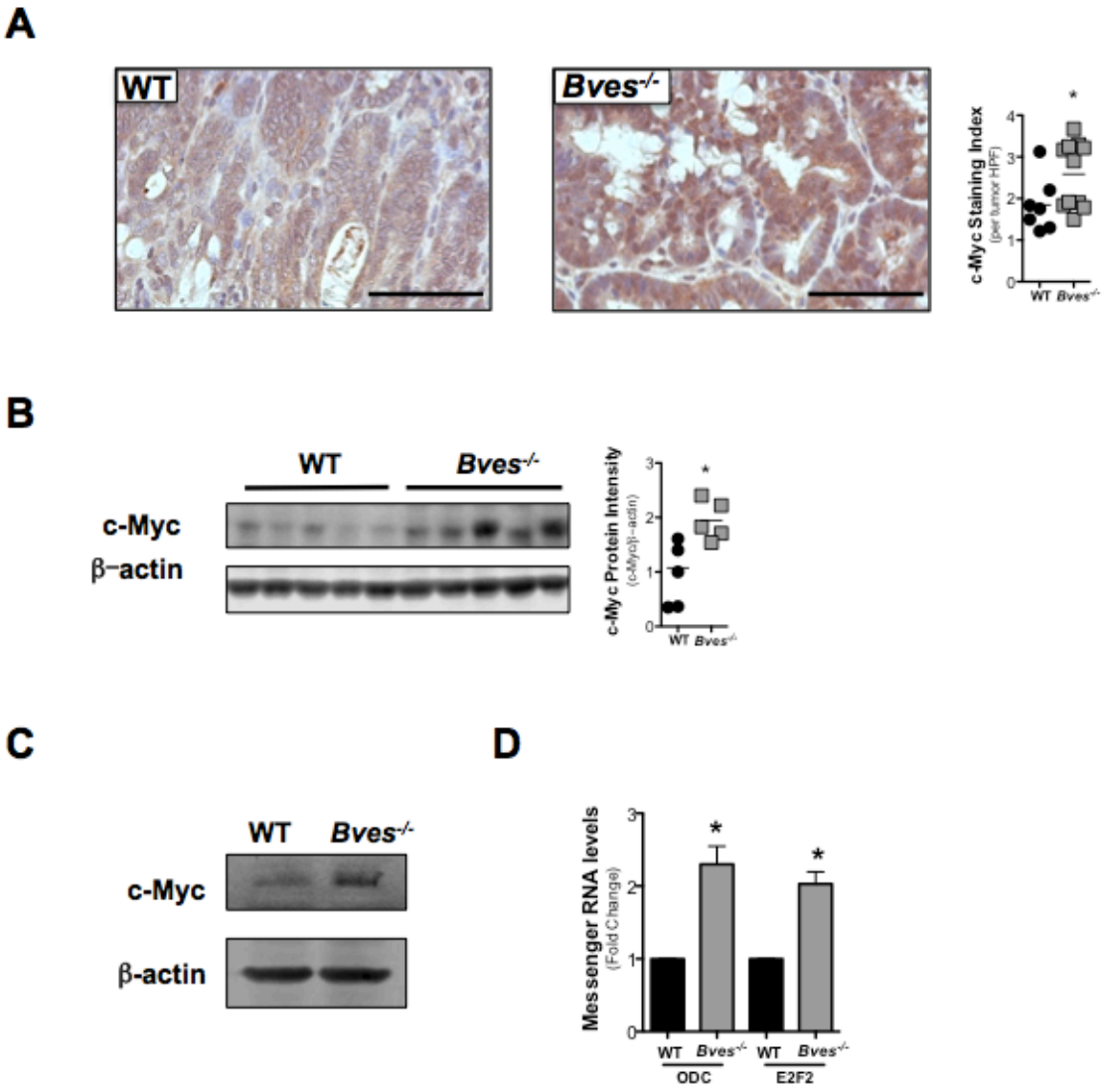

Figure 4.6 c-Myc signaling is dysregulated in *Bves*$^{-/-}$ mice in inflammatory carcinogenesis. (A) Left: Representative intratumoral c-Myc immunohistochemistry images. Size standard=50 microns. Right Quantification of c-Myc positive cells per tumor high power field. *p<0.05. **(B)** Immunoblot of c-Myc in WT and *Bves*$^{-/-}$ whole colons. *p<0.05. **(C)** c-Myc immunoblot in WT (n=3) and *Bves*$^{-/-}$ (n=3) intestinal crypts. **(D)** qRT-PCR for *Odc* and *E2f2* in enteroid cultures. *p<0.05. In all immunoblots, β-actin served as loading control.

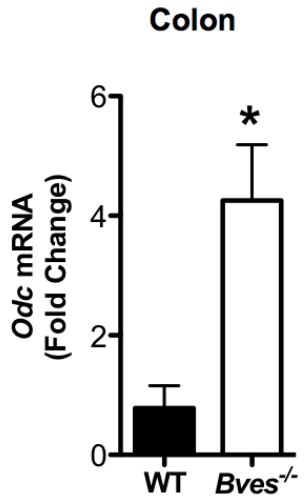

Figure 4.7 *Odc* is upregulated in *Bves*$^{-/-}$ colons.

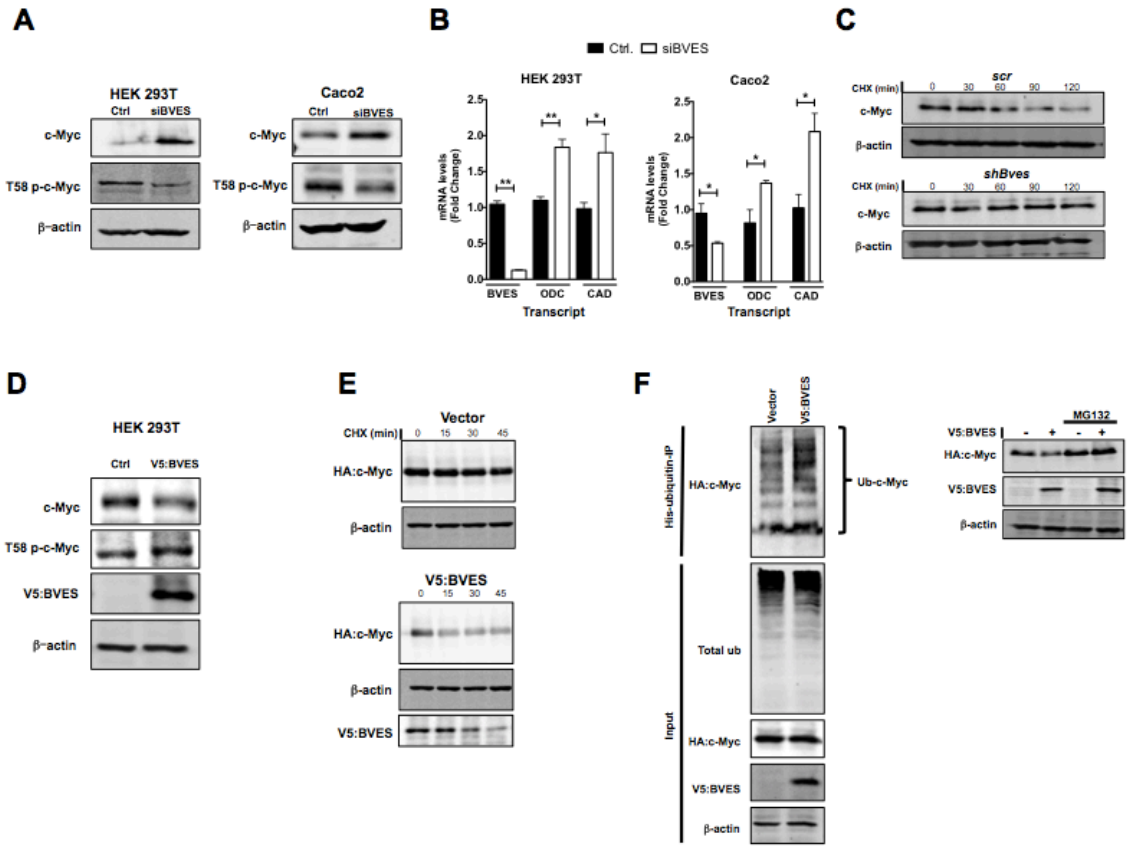

Figure 4.8. BVES regulates c-Myc stability and activity. (A) c-Myc and T58 phospho-c-Myc protein levels after *BVES* knockdown in HEK 293T or Caco2 cells after 48 hr serum starvation. **(B)** qRT-PCR assay for c-Myc targets *ODC* and *CAD* following *BVES* knockdown in the indicated cell lines. Data are presented as mean $\pm$ SEM and in triplicates. *p<0.05, **p<0.01. **(C)** Cycloheximide treatment (100 μg/ml) of HEK 293T cells with and without *Bves* knockdown followed by immunoblotting for c-Myc. **(D)** c-Myc and T58 phospho-c-Myc protein levels after BVES overexpression in HEK 293T cells. **(E)** HEK 293T cells co-transfected with HA:c-Myc and V5:BVES were then treated with cycloheximide (100 μg/ml) followed by immunoblotting for the indicated protein. **(F)** Left: His:Ubiquitin and HA:c-Myc were co-transfected into HEK 293T cells along with V5:BVES. Cells were treated with proteasome inhibitor MG132 (20 μm) for 4 hours before His:Ubiquitin complexes were immunoprecipitated and resolved by SDS-PAGE. Ubiquitylated HA:c-Myc complexes were visualized by immunoblotting (Ub-c-Myc). Total ubiquitylated protein (Total ub) was examined as a control. **Right**: HEK 293T cells co-transfected with HA:c-Myc and V5:BVES were treated with proteasome inhibitor MG132 (20 μm) for 4 hours. Whole cell lysates were analyzed for HA:c-Myc expression. In all immunoblots, β-actin was used as a loading control.

BVES interacts with PR61α, PP2Ac, and c-Myc

To identify a molecular mechanism by which BVES orchestrates c-Myc degradation, we conducted a Y2H screen to define the BVES interactome. Characterization of this interactome using the PANTHER (Protein ANalysis THrough Evolutionary Relationships) Classification System[123] identified a number of biologic processes influenced by BVES (**Figure 4.9A)**. Interestingly, the screen identified that BVES interacted with four of the five members of the B' family of PP2A regulatory subunits (PPP2R5A, PPP2R5B, PPP2R5D, and PPP2R5E). PPP2R5A/PR61α is a key regulator of PP2A mediated c-Myc dephosphorylation. PR61α directs the heterotrimeric PP2A complex, consisting of a regulatory, catalytic, and structural subunit, to associate with doubly phosphorylated (T58/S62) c-Myc and dephosphorylate S62, resulting in increased levels of monophosphorylated T58 c-Myc species, which signals c-Myc to be degraded by the proteaosome[146].

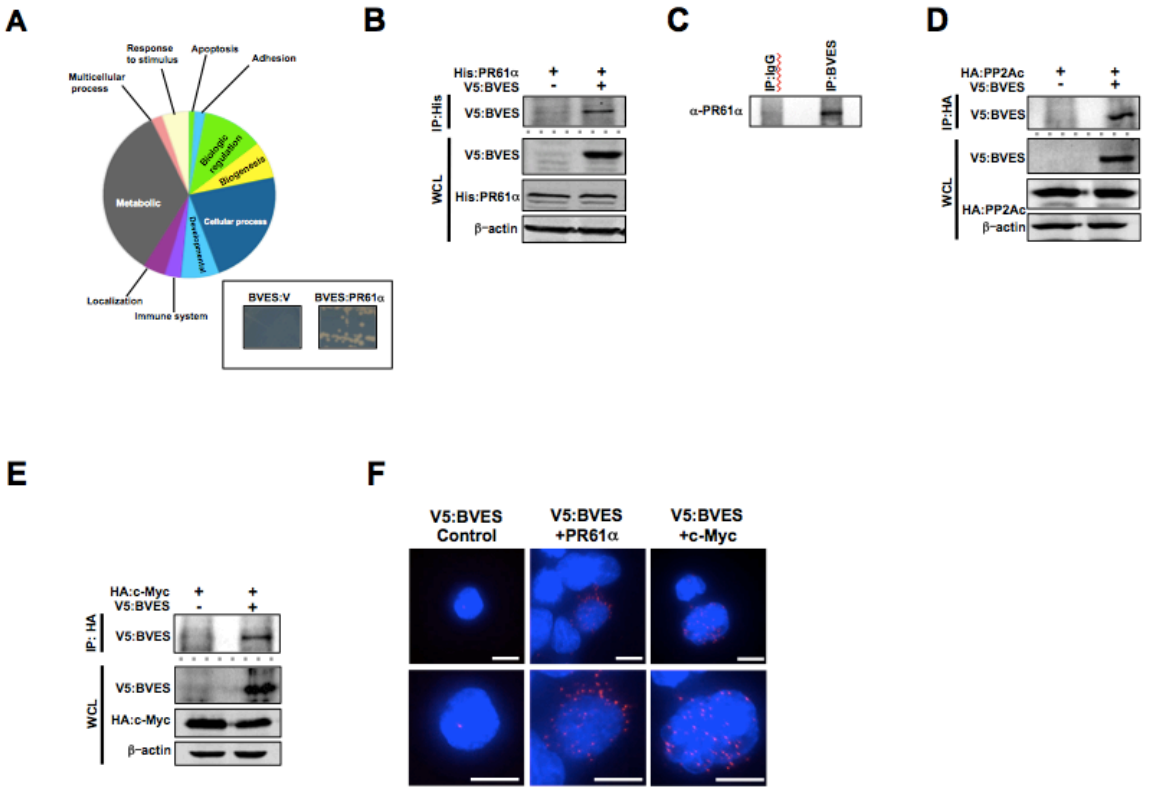

Figure 4.9 BVES interacts with PR61α, PP2A, and c-Myc. (A) PANTHER Biologic Process Analysis of BVES interactome. Inset: Directed yeast two-hybrid of BVES and PR61α. **(B)** Co-immunoprecipitation of exogenous and (**C**) endogenous PR61α:BVES complexes in HEK 293T cells. **(D)** Co-immunoprecipitation of V5:BVES and HA:PP2Ac or (**E**) HA:c-Myc. **(F)** Proximity ligation assay in HEK 293T cells transfected with V5:BVES. Left: control, middle: anti-PR61α, right: anti-c-Myc. Size standard=10 microns. In all immunoblots blots, β-actin was used to ensure loading consistency.

The BVES:PR61α interaction was confirmed by directed Y2H (**Figure 4.9A**) and by exogenous and endogenous co-immunoprecipitation in HEK 293T cells (**Figure 4.9 B and C)**. If BVES were interacting with PR61α to promote c-Myc degradation, we reasoned BVES should complex with both the PP2A catalytic subunit (PP2Ac) and c-Myc, which was demonstrated by co-immunoprecipitation (**Figure 4.9 D and E and Figure 4.10)**. We further confirmed BVES interaction with endogenous PR61α and c-Myc utilizing the proximity ligation assay (PLA) (**Figure 4.9).** Overall, our data indicates that BVES complexes with c-Myc, PR61α, and the PP2A catalytic subunit.

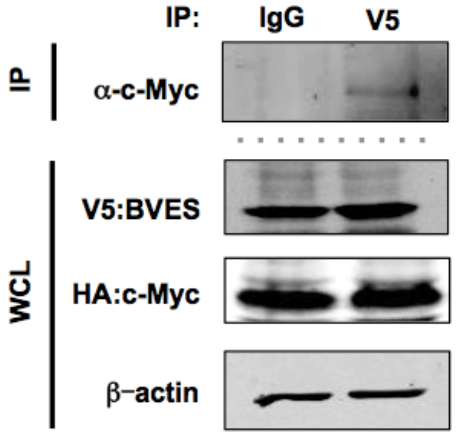

Figure 4.10 HEK 293T cells were transfected with HA:c-Myc and V5:BVES. V5:BVES was immunoprecipitated and HA:c-Myc was immunoblotted for. Non-specific IgG was used as a control.

BVES is essential for PR61α-mediated c-Myc degradation

PP2A dephosphorylation of S62 requires c-Myc to be phosphorylated at residue T58[147]. If BVES reduces c-Myc through PP2A, we reasoned c-Myc^{T58A}, a c-Myc mutant resistant to T58 phosphorylation, would escape BVES-induced degradation. Indeed, BVES expression consistently reduced c-Myc^{WT} but had no effect on c-Myc^{T58A} (**Figure 4.11A**). We next hypothesized that knockdown of BVES would ablate PR61α-PP2A induced c-Myc degradation. Overexpression of PR61α reduced c-Myc protein subtly but consistently as previously reported[146] (**Figure 4.11B**; compare lane 1 and 3). Knocking down BVES, however, rescued PR61α-induced degradation (**Figure 4.11B**; compare lanes 3 and 4). We then tested whether BVES could enhance PR61α-mediated c-Myc degradation. Indeed, overexpression of BVES and PR61α substantially reduced c-Myc protein compared to PR61α or BVES alone (**Figure 4.11C**; compare lane 4 to 2 or 3).

To determine whether BVES requires PR61α to degrade c-Myc, we first mapped the PR61α interaction domain. Deleting the carboxy-terminal 30 residues, but not the last 15 residues, disrupted the BVES:PR61α interaction as demonstrated by Y2H and by co-IP, thus mapping the interaction domain to residues 330-345 (**Figure 4.11D**). Similarly, the uncoupling mutant (BVES-330 mutant) demonstrated reduced affinity for c-Myc (**Figure 4.11E**) and was unable to reduce c-Myc levels as compared to WT-BVES (**Figure 4.11F).** Overall, our results demonstrate that BVES, through PR61α, promotes c-Myc dephosphorylation, destabilization, and destruction.

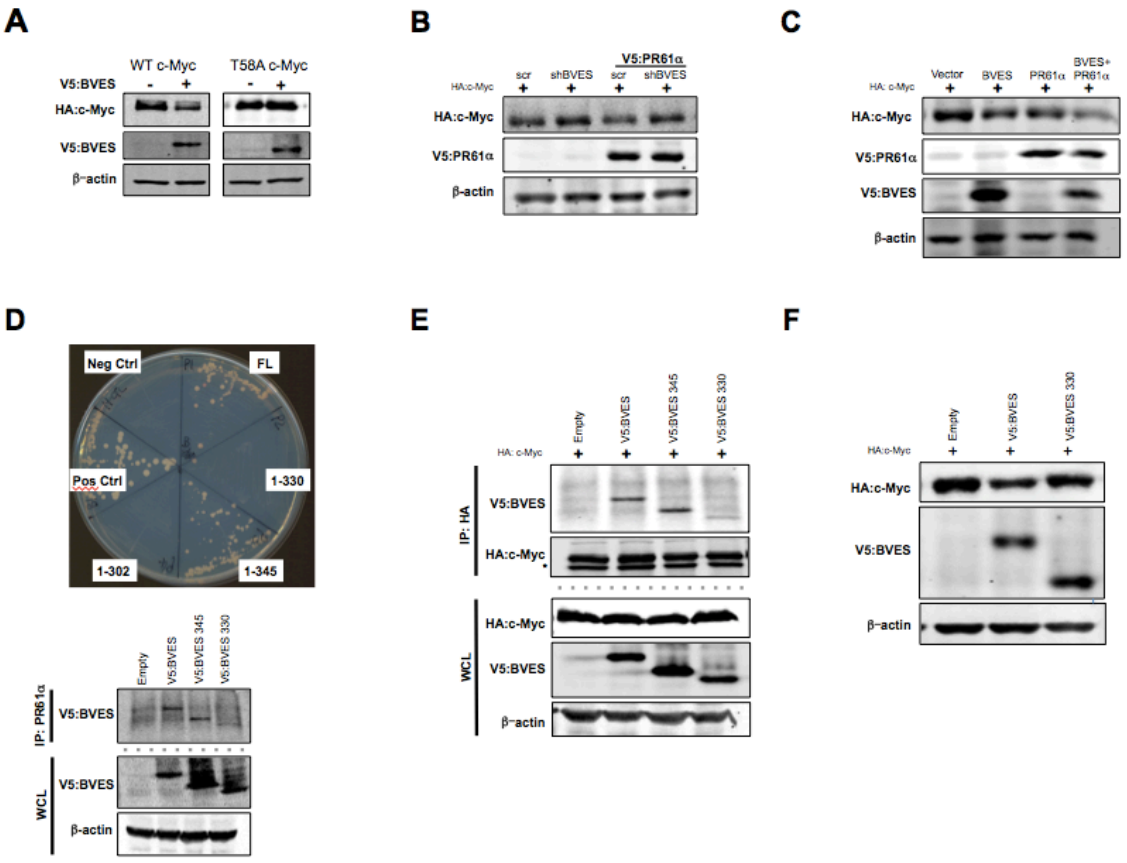

Figure 4.11 The BVES:PR61α interaction is required to promote c-Myc degradation. (**A**) WT HA:c-Myc or phospho-mutant HA:T58A c-Myc levels after V5:BVES transfection. (**B**) Immunoblotting for HA:c-Myc levels following PR61α overexpression in the setting of BVES knockdown or (**C**) when both PR61α and BVES are present. (**D**) Top: Mapping the PR61α BVES binding interface via directed yeast two-hybrid (Full length BVES, residues 1-345, 1-330, 1-302, negative control (Neg Ctrl), and positive control (Pos Ctrl)). Below: Co-immunoprecipitation of the indicated BVES mutants and PR61α or (**E**) HA:c-Myc. (**F**) HA:c-Myc protein levels after transfection of the indicated BVES construct. In all immunoblots, β-actin was used as a loading control.

Discussion

We, and others, have shown that BVES is underexpressed in gastrointestinal cancers and that restoration of BVES in cancer cell lines induces epithelial features. Here we provide the first genetic evidence that BVES modifies cancer phenotypes, as we demonstrate that mice lacking *Bves* have increased tumor multiplicity and dysplasia after establishment of inflammatory carcinogenesis. Further, we show *Bves*$^{-/-}$ tumors have increased c-Myc protein resulting in activation of c-Myc regulated networks. Moreover, we identify that BVES interacts with PR61α, a key regulatory subunit of the PP2A phosphatase complex, and promotes PP2A-mediated c-Myc dephosphorylation leading to c-Myc degradation. Uncoupling the BVES:PR61α interaction blocks BVES-dependent reduction of cellular c-Myc levels. To our knowledge, this is the first junctional-associated protein identified that regulates post-translational c-Myc status. The potential clinical relevance is demonstrated as we observed that *BVES* is downregulated in CAC likely secondary to promoter methylation, and perhaps most importantly, that the *BVES* promoter is also aberrantly methylated in distant, normal appearing tissues in patients with CAC/HGD—suggesting a field effect. Thus, our findings not only reveal that deletion of BVES promotes CAC, but also that *BVES* promoter methylation status may be a clinically important surrogate marker of colitis-associated dysplasia or CAC in IBD patients.

Chronic colitis has been shown to accelerate genome-wide methylation changes[148]; it has been hypothesized that this greater rate of methylation contributes to the increased cancer risk in patients with colitis by silencing tumor suppressors. Our report identifies that the *BVES* promoter is hypermethylated in UC patients who have

CAC. Interestingly, *BVES* promoter hypermethylation is observed not only in the cancerous tissue but also in the non-malignant mucosa in these patients. Currently, the standard method of cancer screening in IBD patients, who are at up to a 10-fold elevated risk of developing CAC[128], is surveillance colonoscopy performed with the hope that cancer will be detected at an early, treatable stage. Yet the detection of neoplasia in the colon can be challenging in individuals with IBD as the lesions are frequently flat and difficult to detect in a background of acute and chronic inflammatory changes. Our data suggest that aberrant *BVES* promoter methylation may be a useful biomarker for the presence of CAC, or even dysplasia, and that measuring *BVES* promoter methylation status could serve as a clinically useful tool to identify patients at risk for colon dysplasia or cancer.

While the molecular pathogenesis of CAC remains incompletely understood, recent work has shown the importance of NF-κB signaling[62], the intestinal microbiota[64], the tumor microenvironment[63], and the innate immune system[149] in regulating inflammatory tumorigenesis. A growing body of evidence also supports the important role of epithelial junctional constituents in inflammation and CRC. Mice expressing a dominant negative form of adherens-junction associated *N-cadherin* develop severe inflammation, most prominently in areas underlying epithelial disruption, as well as colitis-associated dysplasia[47]. Knocking out *Junctional adhesion molecule* (*Jam-A*) results in a dramatic increase in susceptibility to DSS-induced colitis[48]. Here we show that deletion of *Bves*, a tight-junction associated protein, augments inflammatory carcinogenesis. Our results further strengthen the model that junctional constituents are important regulators of colitis-induced tumor initiation and progression.

In the last decade, BVES has been shown to regulate a variety of cellular processes. For example, a Y2H screen of a mouse heart library identified an interaction between BVES and GEFT, a guanine nucleotide exchange factor[93]. Indeed, it was shown that expression of BVES modulated cell shape and locomotion, linking BVES to Rho-family GTPase signaling[93]. BVES has also been shown, via an interaction with ZO-1, to regulate GEF-H1-mediated RhoA activity, thus influencing cytoskeletal dynamics and cellular motility[89]. More recently, it was reported that BVES plays a regulatory role in cardiac pacemaking through binding of cAMP and interacting with potassium channel TREK-1[95]. Further, BVES interacts with CAV3, a caveolin expressed in the muscle tissue, and cardiac myocytes in *Bves*$^{-/-}$ mice have altered calveolar number and size[150]. Thus, BVES, through scaffolding with protein complexes, regulates a wide variety of basic, yet essential, cellular processes.

Our results now expand the known regulatory roles of BVES to include maintaining appropriate c-Myc protein levels. We show that BVES, through its interaction with the PR61α-containing PP2A phosphatase complex, can promote c-Myc degradation. Silencing BVES prevents PR61α-induced degradation of c-Myc. Moreover, mutating BVES so that it is unable to associate with PR61α renders BVES unable to initiate c-Myc destruction. The post-translational regulation of c-Myc requires coordination of numerous proteins to modify its phosphorylation and ubiquitylation status[142]. Precisely how BVES coordinates the PR61α-PP2A complex remains to be understood, but given that analysis of BVES structure shows no apparent enzymatic motifs in BVES, it is likely that BVES acts as a scaffold allowing for complex formation, similar to AXIN1[142]. Interestingly, in addition to the membranous staining of the

BVES:PR61α complex, there also appears to be peri-nuclear and cytoplasmic localization (**Figure 4.9F**), which is consistent with previous reports describing the dynamic subcellular localization of BVES and its family members[83]. The PP2A family has been associated with tight-junctional complexes regulating cellular permeability, but their exact role remains controversial[151]. BVES may serve as a link connecting PP2A complexes to tight-junctions and adds a new molecular mechanism for "outside-in" signaling.

Because c-Myc regulates thousands of genes, even subtle changes in c-Myc expression can have profound effects on cellular transcriptomes that promote tumorigenesis[152]. Indeed, strict regulation of c-Myc is an important component of homeostasis, and this is particularly true in the intestine. Acute expression of c-Myc, for example, dramatically expands the intestinal crypts and results in loss of differentiated cells[153]. Moreover, it has been shown that c-Myc is essential for APC-mediated intestinal tumorigenesis[138]. Thus, BVES may serve as an important suppressor of inflammatory tumorigenesis via attenuating excessive c-Myc levels. More broadly, BVES could act as a regulator of c-Myc in a variety of tissues, as BVES is expressed in most epithelial tissues, such as lung, stomach, and breast, and its downregulation or promoter hypermethylation has been documented in diverse epithelium[89,91].

Taken together, our data indicate that BVES suppresses CAC by complexing with PR61α-PP2A to regulate c-Myc post-translational phosphorylation status. Furthermore, *BVES* promoter methylation status may serve as a clinical biomarker for patients at risk for CRC. Our data implicate BVES as a key regulator of intracellular signaling in inflammation-induced cancer.

Chapter 5

Conclusions and Future Directions

The role of MTGR1 in intestinal lineage allocation

In Chapter 2 of my dissertation, we confirmed and expanded on the previous report that *Mtgr1*$^{-/-}$ mice have reduced goblet, enteroendocrine, and Paneth cells[70]. By manipulating cell lines and enteroids, we showed that loss of MTGR1 reduced secretory lineage transcripts *in vivo*. Furthermore, we identified that MTGR1 does not interact with NICD but does interact with the Notch effector, CSL. Moreover, MTGR1 can repress NICD-induced transcriptional activation of *Hes1*. As transcription of *Hes1* is a key upstream event in Notch signaling, our findings place MTGR1 as an important upstream regulator of intestinal lineage allocation (**Figure 2.10**). In the absence of MTGR1, CSL can activate *Hes1* expression and shift cells toward an enterocyte fate, potentially explaining the *Mtgr1*$^{-/-}$ intestinal phenotype.

MTGs have been shown to have overlapping roles and share binding partners. For example, MTGR1, MTG16, and MTG8 all interact with TCF4 and N-CoR[70,75] to regulate Wnt signaling and repress transcription *in vitro*, respectively. Yet each MTG-deficient mouse has a distinct intestinal phenotype, suggesting non-redundant functions for the MTGs. For example, *Mtgr1*$^{-/-}$ mice have pan-secretory cell loss while *Mtg16*$^{-/-}$ mice have only a modest decrease in goblet cell formation. What explains this difference in lineage allocation? Presumably these distinct phenotypes are due in large part to unique Notch binding partners. MTG16 has been shown to negatively regulate Notch signaling by interacting with NICD and displacing its interaction with CSL[104]. We showed that MTGR1 does not interact with NICD but does interact with CSL. It is worth speculating

whether this difference in associating with CSL versus NICD is an underlying explanation for why *Mtgr1*$^{-/-}$ mice lack all secretory cells but *Mtg16*$^{-/-}$ mice have only decreased goblet cells. Identification of new binding partners is key in advancing our understanding of how each MTG functions uniquely. A useful experiment would be to immunoprecipitate MTGR1 or MTG16 out of either enteroid cultures or isolated intestinal epithelium and perform mass spectrometry. If this technique can be established, then an even more informative experiment would be to immunoprecipitate MTGR1 or MTG16 from enteroids at various time points (for example, after 24, 48, and 72 hours of plating). This would help identify whether the composition of MTG complexes change as intestinal epithelial cells mature. A complementary experiment would be to also immunoprecipitate MTGs from intestinal villi and crypts and perform mass spectrometry. My expectation is that there are many lineage allocation proteins that MTGR1 and MTG16 bind to uniquely of which we currently unaware, and the composition of these complexes is dynamic and changes throughout the differentiation process.

Understanding how MTGR1 contributes to Paneth cell differentiation

In addition to demonstrating that MTGR1 acts as an upstream negative regulator of Notch signaling in Chapter 2, we also determined that MTGR1 acts at a lineage-specific branchpoint. We showed that while inhibition of Notch signaling using GSI increased goblet, enteroendocrine, and Paneth cell number in WT mice, GSI treatment did not increase Paneth cells in *Mtgr1*$^{-/-}$ mice, revealing MTGR1 is essential for GSI-induced Paneth cell differentiation. The precise mechanism of this is unclear. We found that MTGR1 can interact with GFI1, a transcriptional repressor previously shown to be important in determining Paneth/goblet cell vs. enteroendocrine cell differentiation[26,27].

Moreover, expression of MTGR1 repressed GFI1 targets. Whether this interaction is required for Paneth cell differentiation remains an important question for future work. The aims of future studies should focus on two key aspects. What is the MTGR1-GFI1 binding domain? Second, are Paneth cells observed in enteroid cultures expressing MTGR1 mutants that uncouple the GFI1 interaction?

A key observation made in Chapter 2 was that *Mtgr1*$^{-/-}$ enteroids fail to survive after a week in culture. Why do *Mtgr1*$^{-/-}$ enteroids die after 7 days? One possible explanation is that this is due to the absence of Paneth cells in *Mtgr1*$^{-/-}$ intestines. Indeed, it has been suggested that Paneth cells are required for maintenance of enteroids[31], and it would be intriguing to test this in *Mtgr1*$^{-/-}$ cultures. Paneth cells from WT mice can be isolated by flow cytometry and co-cultured with *Mtgr1*$^{-/-}$ enteroids[31]. While this could be technically challenging, the experiment would elucidate whether Paneth cells are sufficient to maintain *Mtgr1*$^{-/-}$ cultures. Another important experiment should be to determine whether *Mtgr1*$^{-/-}$ enteroids can be rescued by lenti-viral transduced expression of MTGR1. If they can be rescued, then expression of MTGR1 mutants that are unable to associate with CSL or GFI1 would be highly informative. It is possible that the *Mtgr1*$^{-/-}$ enteroids will crash before they are successfully manipulated genetically or that MTGR1 expression is unable to rescue the enteroids. In this case WT enteroids can be manipulated with CRISPR-Cas9 technology to delete MTGR1 or knock-in MTGR1 mutants. Manipulation of MTGR1 in WT enteroids has important value in that it will test the immediate effects of MTGR1 loss. Indeed, *Mtgr1*$^{-/-}$ mice could display compensation from other MTG family members. In this vein, the generation of MTGR1-floxed mice would be a critical tool in advancing our understanding of how MTGR1 affects intestinal

lineage allocation. This would be useful because it will not only allow us to test the tissue-specific function of MTGR1, but also the temporal role of MTGR1 in lineage allocation.

MTGR1 as a tumor suppressor in CRC

In Chapter 3 of my thesis, we showed that loss of MTGR1 promotes tumorigenesis in the *Apc*$^{1638/+}$ mouse model. *Mtgr1*$^{-/-}$ tumors were more dysplastic, and there was evidence of invasive adenocarcinoma. The findings demonstrate that loss of MTGR1 promotes tumorigenesis and progression. Given that the *Mtgr1*$^{-/-}$ mice were global knockouts, it will be important going forward to test whether tissue-specific MTGR1 loss impacts intestinal tumorigenesis. I predict that intestinal specific deletion of MTGR1 will phenocopy the results from Chapter 3 because in two previous reports, WT bone marrow transplantation had no effect on intestinal phenotypes observed in *Mtgr1*$^{-/-}$ mice[73,103]. The development of an MTGR1-floxed mouse would provide the tools to test this formally, and an MTGR1-floxed mouse crossed with an inducible Cre driver would also provide the opportunity to test the effect of MTGR1 within specific intestinal epithelial populations. For example, does loss of MTGR1 in Lrig1^{+} or Lgr5^{+} stem cell populations have a different effect on Apc-mediated tumorigenesis than if MTGR1 is deleted throughout the intestinal epithelium using a Villin-Cre driver?

BVES promoter methylation as biomarker of colitis-associated cancer

In Chapter 4 of my dissertation, we showed that BVES is an important negative regulator of colitis-associated cancer. BVES mRNA is downregulated in patients with CAC. Moreover, we found that the BVES promoter is hypermethylated in patients with CAC in both their normal, non-malignant mucosa as well as their cancers. Importantly,

patients with ulcerative colitis who did *not* have cancer did not show evidence of BVES promoter hypermethylation. The findings make BVES promoter methylation status an attractive biomarker identifying which IBD patients are at high risk for CAC. The utility of BVES as a clinical biomarker needs to be confirmed by investigating BVES promoter hypermethylation in another cohort of IBD patients with and without CAC. The biological implications are also not entirely clear. Is BVES promoter hypermethylation a biomarker because the loss of BVES function is critical? Or does BVES promoter hypermethylation simply reflect a level of such advanced methylation that cancer is likely? Indeed, greater genomic methylation is observed in IBD patients[148], and it is possible that BVES promoter hypermethylation is an indirect marker of CAC. Our current understanding of BVES promoter methylation, and more fundamentally, our understanding of BVES transcriptional regulation is limited. Studying how BVES is transcriptionally regulated is important to not only further understand BVES function, but also to develop therapies that could potentially restore BVES function.

The biological role of BVES in colitis and colitis-associated cancer

Chapter 4 showed that BVES loss augmented colitis-associated cancer as *Bves*$^{-/-}$ mice had increased tumorigenesis after AOM/DSS treatment. We observed that *Bves*$^{-/-}$ tumors had a greater degree of dysplasia and showed evidence of dysrgulated Wnt signaling. The precise mechanism of how loss of BVES promotes CAC is not entirely clear, but given the known cellular functions of BVES, the phenotype is likely due to alterations in numerous signaling pathways. For example, BVES immunoprecipitates with ZO-1, and BVES expression restores ZO-1 complex formation in cancer cell lines[89,92]. Similarly, BVES expression has been shown to restore E-cadherin junctional

complexes in cancer cell lines, and conversely, interfering with BVES in epithelial cell lines has been shown to disrupt E-cadherin localization[89]. Alterations in ZO-1 and E-cadherin in colitis and colitis-associated carcinoma are well documented[43,45,52,130]. Not only could impaired junctional complexes result in a "leaky" epithelium, but impaired junctional complexes can result in dysregulated signaling pathways that promote oncogenesis. Thus, it is critical to examine whether *Bves*$^{-/-}$ mice have impaired junctional complexes, and this is question can be addressed easily. Immunofluorescence for E-cadherin and ZO-1 can be conducted on *Bves*$^{-/-}$ mice at baseline and after AOM/DSS treatment. Additionally, electron microscopy can be used to determine whether tight or adherens junctions are disrupted in *Bves*$^{-/-}$ intestines.

A considerable amount of work has also found that BVES is a cAMP binding protein and can interact with the potassium-voltage protein TREK1[95]. The effect of BVES loss on cAMP signaling has yet to be studied in the gut, but it should be tested. Dysregulation of cAMP signaling in the intestinal epithelium has been linked to IBD and even suggested as a potential therapeutic target, although there is controversy regarding its merits[154–156]. Thomas Brand's group has generated BVES mutants that have reduced affinity for cAMP binding. These mutants can be used to test whether BVES-dependent phenotypes in colon cancer cell lines require cAMP binding. For example, are the BVES mutants able to increase trans-epithelial resistance in Caco2 cells? Do the BVES mutants unable to bind cAMP decrease Lim2405 cell migration? These would be simple, yet informative experiments.

The functional role of BVES in promoting c-Myc degradation

In Chapter 4, we identified that BVES can interact with c-Myc through binding to PR61α, a regulatory subunit of the PP2A family, to destabilize and degrade c-Myc. c-Myc post-translational regulation is dynamic and complex. The current model holds that c-Myc is reversibly phosphorylated at two residues threonine 58 and serine 62 through the coordination of Pin1, Axin1, PP2A, and GSK3β before being shuttled to the ubiquitylation pathway through the E3 ubiquitin ligase FBW7. Where BVES fits into this coordination is not clear. We determined in Chapter 4 that BVES immunoprecipitates with PP2Ac, PR61α, and c-Myc, but to understand fully the role of BVES in promoting c-Myc degradation, we need to test whether BVES can associate with Axin1, Pin1, or GSK3β. These studies should be conducted in epithelial cell lines because c-Myc dysregulation is common in most cancer cell lines, and the components of this post-translational degradation complex are often mutated. Importantly, these studies should also be complemented with proximity ligation assays to identify *where* the complexes form.

What is the biological context in which BVES associates with PR61α to promote c-Myc degradation? This is a key question that should be addressed moving forward. BVES localization is dynamic, as BVES shifts from the cytoplasm to the plasma membrane when cells reach confluence[86] (**Figure 1.6**). My work in Chapter 4 does not discern a specific biological context in which BVES interacts with PR61α to promote c-Myc degradation. This is primarily due to relying on epitope-tagged BVES expression constructs due to low quality antibodies for BVES. As the Williams lab is currently developing BVES antibodies, proximity ligation assays should be used to determine if

endogenous BVES-PR61α and BVES-c-Myc interactions change depending on confluence. It is also important to determine whether POPDC2 or POPDC3 are involved in the c-Myc degradation complex. As the Popeye family members have been shown to heterodimerize, this question can be addressed by simply overexpressing or knocking down POPDC2 or POPDC3 and measuring c-Myc protein.

The BVES:PR61α complex

In Chapter 4, we identified that BVES and the PP2A regulatory subunit, PR61α, interact, and this interaction is required for BVES to mediate c-Myc degradation. We mapped the interaction onto the amino acids 330-345 on BVES. That BVES interacts with PR61α, a regulatory subunit linked to localizing the PP2A complex to several key substrates, is exciting and opens a new door of BVES function. Indeed, previous reports have linked PR61α to directing the PP2A complex to dephosphorylate and negatively regulate β-catenin and Bcl2[157]. β-catenin and Bcl2 regulate critical proliferation and apoptosis programs that can drive tumorigenesis. Whether BVES aids the PR61α-PP2A containing complex in negatively regulating β-catenin and Bcl2 should be examined. This can be performed by overexpressing BVES or knocking it down and measuring total and phosphorylated forms of β-catenin and Bcl2. If manipulation of BVES expression does have an effect on β-catenin or Bcl2, then testing whether BVES requires PR61α can be accomplished easily using the BVES mutant that uncouples its interaction with PR61a. This BVES mutant has already been generated (Chapter 4).

Similar to the BVES:c-Myc interaction, the fundamental biologic context of the BVES:PR61α interaction is unknown. What is the subcellular localization of BVES:PR61α? During what cellular context do the proteins interact with each other?

These questions can be answered effectively using PLA when good antibodies to endogenous BVES are developed. Another point of interest is that throughout Chapter 4, we assumed that BVES directed PR61α, but we have not tested if the PP2A-PR61α complex was directly acting on BVES itself. Perhaps the PP2A complex is dephosphorylating BVES? In early, preliminary experiments, I attempted to determine whether BVES itself is phosphorylated. I immunoprecipated HA-tagged BVES from the Lim2405 cell line and subsequently treated the precipitated complex with lambda phosphatase. My results showed no change in BVES molecular weight upon treatment of lambda phosphatase, suggesting BVES is not phosphorylated. There were important caveats to that experiment, however. If BVES is phosphorylated, it is possible that kinase is disrupted in the Lim2405 cell line. Moreover, it is possible that BVES is transiently phosphorylated or in specific biologic contexts. Thus, this line of inquiry should be tested in epithelial cell lines to definitively determine whether BVES itself is phosphorylated. Moreover, to increase the sensitivity of the assay, BVES could be immunoprecipitated after fixation in order to capture transient phosphorylation events.

Concluding remarks

The major findings of my thesis work are that MTGR1 and BVES regulate key intestinal biologic programs and that loss of MTGR1 or BVES dysregulates the intestinal epithelium, resulting in increased cancer risk. Placing these collective findings into a single cellular model, one can envision that as Notch and Wnt signaling continually drive intestinal stem cell renewal, MTGR1 maintains appropriate Notch and Wnt tone by recruiting transcriptional corepressors to Notch and Wnt target genes. Meanwhile, outside of the nucleus, BVES ensures that the protein levels of c-Myc, a potent oncogene and

Wnt target, are kept in check by directing the PP2A-PR61α complex to destabilize excess c-Myc. Thus, both MTGR1 and BVES serve to maintain appropriate levels of pro-proliferative programs in a tissue that is constantly undergoing self-renewal in response to injuries and environmental challenges. And when MTGR1 or BVES is lost, the intestinal epithelium loses an important guard against unchecked cellular division.

The clinical relevance of these findings is evident by the observation that loss of MTGR1 or BVES is observed in colorectal malignancies. Where loss of MTGR1 or BVES fits into the Vogelgram is not clear, but my thesis work has shown that MTGR1 and BVES are important negative regulators of colorectal cancer. Future studies have the potential to uncover the utility of MTGR1 and BVES as prognostic indicators or therapeutic targets.

References

1. Schuijers, J. & Clevers, H. Adult mammalian stem cells: the role of Wnt, Lgr5 and R-spondins. *EMBO J.* **31,** 3031–3032 (2012).

2. MacDonald, B. T., Tamai, K. & He, X. Wnt/b-Catenin signaling: components, mechanisms, and diseases. *Dev. Cell* **17,** 9–26 (2009).

3. Van der Flier, L. G. *et al.* The intestinal Wnt/TCF signature. *Gastroenterology* **132,** 628–632 (2007).

4. Tetsu, O. & McCormick, F. Beta-catenin regulates expression of cyclin D1 in colon carcinoma cells. *Nature* **398,** 422–426 (1999).

5. Mann, B. *et al.* Target genes of beta-catenin-T cell-factor/lymphoid-enhancer-factor signaling in human colorectal carcinomas. *Proc. Natl. Acad. Sci. U. S. A.* **96,** 1603–1608 (1999).

6. Korinek, V. *et al.* Constitutive transcriptional activation by a beta-catenin-Tcf complex in APC-/- colon carcinoma. *Science* **275,** 1784–1787 (1997).

7. Groden, J. *et al.* Identification and characterization of the familial adenomatous polyposis coli gene. *Cell* **66,** 589–600 (1991).

8. Su, L. K. *et al.* Multiple intestinal neoplasia caused by a mutation in the murine homolog of the APC gene. *Science* **256,** 668–670 (1992).

9. Harada, N. *et al.* Intestinal polyposis in mice with a dominant stable mutation of the β-catenin gene. *EMBO J.* **18,** 5931–5942 (1999).

10. Korinek, V. *et al.* Depletion of epithelial stem-cell compartments in the small intestine of mice lacking Tcf-4. *Nat. Genet.* **19,** 379–383 (1998).

11. Kuhnert, F. *et al.* Essential requirement for Wnt signaling in proliferation of adult small intestine and colon revealed by adenoviral expression of Dickkopf-1. *Proc. Natl. Acad. Sci. U. S. A.* **101,** 266–271 (2004).

12. Cheng, H. Origin, differentiation and renewal of the four main epithelial cell types in the mouse small intestine. IV. Paneth cells. *Am. J. Anat.* **141,** 521–535 (1974).

13. Barker, N. *et al.* Identification of stem cells in small intestine and colon by marker gene Lgr5. *Nature* **449,** 1003–1007 (2007).

14. Sato, T. *et al.* Single Lgr5 stem cells build crypt-villus structures in vitro without a mesenchymal niche. *Nature* **459,** 262–265 (2009).

15. Kumar, K. K., Burgess, A. W. & Gulbis, J. M. Structure and function of LGR5: Aan enigmatic G-protein coupled receptor marking stem cells. *Protein Sci.* **23,** 551–565 (2014).

16. Noah, T. K., Donahue, B. & Shroyer, N. F. Intestinal development and differentiation. *Exp. Cell Res.* **317,** 2702–2710 (2011).

17. Fre, S. *et al.* Notch signals control the fate of immature progenitor cells in the intestine. *Nature* **435,** 964–968 (2005).

18. Stanger, B. Z., Datar, R., Murtaugh, L. C. & Melton, D. A. Direct regulation of intestinal fate by Notch. *Proc. Natl. Acad. Sci. U. S. A.* **102,** 12443–12448 (2005).

19. Van Es, J. H. *et al.* Notch/gamma-secretase inhibition turns proliferative cells in intestinal crypts and adenomas into goblet cells. *Nature* **435,** 959–963 (2005).

20. Riccio, O. *et al.* Loss of intestinal crypt progenitor cells owing to inactivation of both Notch1 and Notch2 is accompanied by derepression of CDK inhibitors p27Kip1 and p57Kip2. *EMBO Rep.* **9,** 377–383 (2008).

21. Jensen, J. *et al.* Control of endodermal endocrine development by Hes-1. *Nat. Genet.* **24,** 36–44 (2000).

22. Shroyer, N. F. *et al.* Intestine-Specific Ablation of Mouse atonal homolog 1 (Math1) Reveals a Role in Cellular Homeostasis. *Gastroenterology* **132,** 2478–2488 (2007).

23. VanDussen, K. L. & Samuelson, L. C. Mouse atonal homolog 1 directs intestinal progenitors to secretory cell rather than absorptive cell fate. *Dev. Biol.* **346,** 215–223 (2010).

24. Kazanjian, A., Noah, T., Brown, D., Burkart, J. & Shroyer, N. F. Atonal homolog 1 is required for growth and differentiation effects of Notch/gamma-secretase inhibitors on normal and cancerous intestinal epithelial cells. *Gastroenterology* **139,** 918–28, 928.e1–6 (2010).

25. Kim, T. H. & Shivdasani, R. A. Genetic evidence that intestinal Notch functions vary regionally and operate through a common mechanism of math1 repression. *J. Biol. Chem.* **286,** 11427–11433 (2011).

26. Bjerknes, M. & Cheng, H. Cell Lineage metastability in Gfi1-deficient mouse intestinal epithelium. *Dev. Biol.* **345,** 49–63 (2010).

27. Shroyer, N. F., Wallis, D., Venken, K. J. T., Bellen, H. J. & Zoghbi, H. Y. Gfi1 functions downstream of Math1 to control intestinal secretory cell subtype allocation and differentiation. *Genes Dev.* **19,** 2412–2417 (2005).

28. López-Díaz, L. *et al.* Intestinal Neurogenin 3 directs differentiation of a bipotential secretory progenitor to endocrine cell rather than goblet cell fate. *Dev. Biol.* **309,** 298–305 (2007).

29. Bastide, P. *et al.* Sox9 regulates cell proliferation and is required for Paneth cell differentiation in the intestinal epithelium. *J. Cell Biol.* **178,** 635–648 (2007).

30. Gregorieff, A. *et al.* The Ets-domain transcription factor spdef promotes maturation of goblet and Paneth cells in the intestinal epithelium. *Gastroenterology* **137,** (2009).

31. Sato, T. *et al.* Paneth cells constitute the niche for Lgr5 stem cells in intestinal crypts. *Nature* **469,** 415–418 (2011).

32. Kim, T.-H., Escudero, S. & Shivdasani, R. A. Intact function of Lgr5 receptor-expressing intestinal stem cells in the absence of Paneth cells. *Proc. Natl. Acad. Sci.* **109,** 3932–3937 (2012).

33. Facts, C. Cancer Facts & Figures. *Health Policy (New. York).* (2010). doi:10.3322/caac.20121

34. Fearon, E. R. & Vogelstein, B. A genetic model for colorectal tumorigenesis. *Cell* **61,** 759–767 (1990).

35. Sansom, O. J. *et al.* Loss of Apc in vivo immediately perturbs Wnt signaling, differentiation, and migration. *Genes Dev.* **18,** 1385–1390 (2004).

36. Nishisho, I. *et al.* Mutations of chromosome 5q21 genes in FAP and colorectal cancer patients. *Science* **253,** 665–669 (1991).

37. Moser, A. R., Pitot, H. C. & Dove, W. F. A dominant mutation that predisposes to multiple intestinal neoplasia in the mouse. *Science* **247,** 322–324 (1990).

38. Batlle, E. *et al.* β-catenin and TCF mediate cell positioning in the intestinal epithelium by controlling the expression of EphB/EphrinB. *Cell* **111,** 251–263 (2002).

39. Uchida, H. *et al.* Overexpression of leucine-rich repeat-containing G protein-coupled receptor 5 in colorectal cancer. *Cancer Sci.* **101,** 1731–1737 (2010).

40. Rodilla, V. *et al.* Jagged1 is the pathological link between Wnt and Notch pathways in colorectal cancer. *Proc. Natl. Acad. Sci. U. S. A.* **106,** 6315–6320 (2009).

41. Fre, S. *et al.* Notch and Wnt signals cooperatively control cell proliferation and tumorigenesis in the intestine. *Proc. Natl. Acad. Sci. U. S. A.* **106,** 6309–6314 (2009).

42. Baumgart, D. C., Baumgart, D. C., Sandborn, W. J. & Sandborn, W. J. Inflammatory bowel disease: clinical aspects and established and evolving therapies. *Lancet* **369,** 1641–1657 (2007).

43. Mees, S. T. *et al.* Expression of tight and adherens junction proteins in ulcerative colitis associated colorectal carcinoma: Upregulation of claudin-1, claudin-3, claudin-4, and ??-catenin. *Int. J. Colorectal Dis.* **24,** 361–368 (2009).

44. Weber, C. R., Nalle, S. C., Tretiakova, M., Rubin, D. T. & Turner, J. R. Claudin-1 and claudin-2 expression is elevated in inflammatory bowel disease and may contribute to early neoplastic transformation. *Lab. Invest.* **88,** 1110–1120 (2008).

45. Gassler, N. *et al.* Inflammatory bowel disease is associated with changes of enterocytic junctions. *Am. J. Physiol. Gastrointest. Liver Physiol.* **281,** G216–G228 (2001).

46. Su, L. *et al.* Targeted epithelial tight junction dysfunction causes immune activation and contributes to development of experimental colitis. *Gastroenterology* **136,** 551–563 (2009).

47. Hermiston, M. L. & Gordon, J. I. Inflammatory bowel disease and adenomas in mice expressing a dominant negative N-cadherin. *Science* **270,** 1203–1207 (1995).

48. Vetrano, S. *et al.* Unique role of junctional adhesion molecule-A in maintaining mucosal homeostasis in inflammatory bowel disease. *Gastroenterology* **135,** 173–184 (2008).

49. Van der Sluis, M. *et al.* Muc2-deficient mice spontaneously develop colitis, indicating that MUC2 is critical for colonic protection. *Gastroenterology* **131,** 117–129 (2006).

50. Bergstrom, K. S. B. *et al.* Muc2 protects against lethal infectious colitis by disassociating pathogenic and commensal bacteria from the colonic mucosa. *PLoS Pathog.* **6,** (2010).

51. Obata, Y. *et al.* Epithelial cell-intrinsic Notch signaling plays an essential role in the maintenance of gut immune homeostasis. *J. Immunol.* **188,** 2427–36 (2012).

52. Hanby, A. M., Chinery, R., Poulsom, R., Playford, R. J. & Pignatelli, M. Downregulation of E-cadherin in the reparative epithelium of the human gastrointestinal tract. *Am. J. Pathol.* **148,** 723–729 (1996).

53. Sturm, A. & Dignass, A. U. Epithelial restitution and wound healing in inflammatory bowel disease. *World J. Gastroenterol.* **14,** 348–353 (2008).

54. McGuckin, M. A., Eri, R., Simms, L. A., Florin, T. H. J. & Radford-Smith, G. Intestinal barrier dysfunction in inflammatory bowel diseases. *Inflamm. Bowel Dis.* **15,** 100–113 (2009).

55. Kalluri, R. & Weinberg, R. A. Review series: The basics of epithelial-mesenchymal transition. *J. Clin. Invest.* **119,** 1420–1428 (2009).

56. Botaille, F. *et al.* Evidence for a role of epithelial mesenchymal transition during pathogenesis of fistulae in Crohn's disease. *Inflamm. Bowel Dis.* **14,** 1514–1527 (2008).

57. Danese, S. & Mantovani, A. Inflammatory bowel disease and intestinal cancer: a paradigm of the Yin-Yang interplay between inflammation and cancer. *Oncogene* **29,** 3313–3323 (2010).

58. Terzić, J., Grivennikov, S., Karin, E. & Karin, M. Inflammation and colon cancer. *Gastroenterology* **138,** 2101–2114.e5 (2010).

59. Eaden, J. A., Abrams, K. R. & Mayberry, J. F. The risk of colorectal cancer in ulcerative colitis: a meta-analysis. *Gut* **48,** 526–535 (2001).

60. Rennick, D. M., Fort, M. M. & Davidson, N. J. Studies with IL-10-/- mice: an overview. *J. Leukoc. Biol.* **61,** 389–396 (1997).

61. Kühn, R., Löhler, J., Rennick, D., Rajewsky, K. & Müller, W. Interleukin-10-deficient mice develop chronic enterocolitis. *Cell* **75,** 263–274 (1993).

62. Grivennikov, S. *et al.* IL-6 and Stat3 are required for survival of intestinal epithelial cells and development of colitis-associated cancer. *Cancer Cell* **15,** 103–113 (2009).

63. Katoh, H. *et al.* CXCR2-expressing myeloid-derived suppressor cells are essential to promote colitis-associated tumorigenesis. *Cancer Cell* **24,** 631–644 (2013).

64. Arthur, J. *et al.* Intestinal inflammation targets cancer-inducing actvity of the microbiota. *Science (80-.).* **338,** 120–123 (2012).

65. Miyoshi, H. *et al.* The t(8;21) translocation in acute myeloid leukemia results in production of an AML1-MTG8 fusion transcript. *EMBO J.* **12,** 2715–2721 (1993).

66. Wang, Q. *et al.* Disruption of the Cbfa2 gene causes necrosis and hemorrhaging in the central nervous system and blocks definitive hematopoiesis. *Proc. Natl. Acad. Sci. U. S. A.* **93,** 3444–3449 (1996).

67. Calabi, F. & Cilli, V. CBFA2T1, a gene rearranged in human leukemia, is a member of a multigene family. *Genomics* **52,** 332–341 (1998).

68. Lutterbach, B. *et al.* ETO, a target of t(8;21) in acute leukemia, interacts with the N-CoR and mSin3 corepressors. *Mol. Cell. Biol.* (1998).

69. Amann, J. M. *et al.* ETO, a target of t(8;21) in acute leukemia, makes distinct contacts with multiple histone deacetylases and binds mSin3A through its oligomerization domain. *Mol. Cell. Biol.* (2001). doi:10.1128/MCB.21.19.6470-6483.2001

70. Amann, J. M. *et al.* Mtgr1 is a transcriptional corepressor that is required for maintenance of the secretory cell lineage in the small intestine. **25,** 9576–9585 (2005).

71. Calabi, F., Pannell, R. & Pavloska, G. Gene targeting reveals a crucial role for MTG8 in the gut. *Mol. Cell. Biol.* **21,** 5658–5666 (2001).

72. Poindexter, S. V *et al.* Transcriptional co-repressor MTG16 regulates small intestinal crypt proliferation and crypt regeneration after radiation-induced injury. *Am. J. Physiol. - Gastrointest. Liver Physiol.* **0654,** ajpgi.00253.2014 (2015).

73. Martinez, J. A. *et al.* Deletion of Mtgr1 sensitizes the colonic epithelium to dextran sodium sulfate-induced colitis. *Gastroenterology* **131,** 579–588 (2006).

74. Williams, C. S. *et al.* MTG16 contributes to colonic epithelial integrity in experimental colitis. *Gut* **62,** 1446–1455 (2013).

75. Moore, A. C. *et al.* Myeloid translocation gene family members associate with T-cell factors (TCFs) and influence TCF-dependent transcription. *Mol. Cell. Biol.* **28,** 977–987 (2008).

76. Davis, J. N., McGhee, L. & Meyers, S. The ETO (MTG8) gene family. *Gene* **303,** 1–10 (2003).

77. Zhang, J., Kalkum, M., Yamamura, S., Chait, B. T. & Roeder, R. G. E protein silencing by the leukemogenic AML1-ETO fusion protein. *Science* **305,** 1286–1289 (2004).

78. Zhang, J. *et al.* Oligomerization of ETO is obligatory for corepressor interaction. *Mol. Cell. Biol.* **21,** 156–163 (2001).

79. Hildebrand, D., Tiefenbach, J., Heinzel, T., Grez, M. & Maurer, A. B. Multiple regions of ETO cooperate in transcriptional repression. *J. Biol. Chem.* **276,** 9889–9895 (2001).

80. Aaker, J. D. *et al.* Interaction of MTG family proteins with NEUROG2 and ASCL1 in the developing nervous system. *Neurosci. Lett.* **474,** 46–51 (2010).

81. Reese, D. E., Zavaljevski, M., Streiff, N. L. & Bader, D. bves: A novel gene expressed during coronary blood vessel development. *Dev. Biol.* **209,** 159–171 (1999).

82. Andrée, B. *et al.* Isolation and characterization of the novel popeye gene family expressed in skeletal muscle and heart. *Dev. Biol.* **223,** 371–382 (2000).

83. Osler, M. E., Chang, M. S. & Bader, D. M. Bves modulates epithelial integrity through an interaction at the tight junction. *J. Cell Sci.* **118,** 4667–4678 (2005).

84. Brand, T. The Popeye domain-containing gene family. *Cell Biochem. Biophys.* **43,** 95–103 (2005).

85. Osler, M. E., Smith, T. K. & Bader, D. M. Bves, a member of the Popeye domain-containing gene family. *Dev. Dyn.* **235,** 586–593 (2006).

86. Kawaguchi, M. *et al.* Identification of a novel intracellular interaction domain essential for Bves function. *PLoS One* **3,** e2261 (2008).

87. Andrée, B., Fleige, A., Arnold, H.-H. & Brand, T. Mouse Pop1 is required for muscle regeneration in adult skeletal muscle. *Mol. Cell. Biol.* **22,** 1504–1512 (2002).

88. Wu, Y. C. *et al.* Blood vessel epicardial substance (Bves) regulates epidermal tight junction integrity through atypical protein kinase C. *J. Biol. Chem.* **287,** 39887–39897 (2012).

89. Williams, C. S. *et al.* BVES regulates EMT in human corneal and colon cancer cells and is silenced via promoter methylation in human colorectal carcinoma. *J. Clin. Invest.* **121,** 4056–4069 (2011).

90. Kim, M. *et al.* Frequent silencing of popeye domain-containing genes, BVES and POPDC3, is associated with promoter hypermethylation in gastric cancer. *Carcinogenesis* **31,** 1685–1693 (2010).

91. Feng, Q. *et al.* DNA methylation in tumor and matched normal tissues from non-small cell lung cancer patients. *Cancer Epidemiol. Biomarkers Prev.* **17,** 645–654 (2008).

92. Russ, P. K. *et al.* Bves modulates tight junction associated signaling. *PLoS One* **6,** e14563 (2011).

93. Smith, T. K. *et al.* Bves directly interacts with GEFT, and controls cell shape and movement through regulation of Rac1/Cdc42 activity. *Proc. Natl. Acad. Sci. U. S. A.* **105,** 8298–8303 (2008).

94. Hager, H. a, Roberts, R. J., Cross, E. E., Proux-Gillardeaux, V. & Bader, D. M. Identification of a novel Bves function: regulation of vesicular transport. *EMBO J.* **29,** 532–545 (2010).

95. Froese, A. *et al.* Popeye domain containin proteins are essential for stress-mediated modulation of cardiac pacemaking in mice. *J. Clin. Invest.* **122,** (2012).

96. Bray, S. J. Notch signalling: a simple pathway becomes complex. *Nat. Rev. Mol. Cell Biol.* **7,** 678–689 (2006).

97. Katoh, M. & Katoh, M. Notch signaling in gastrointestinal tract (Review). *Int. J. Oncol.* **30,** 247–251 (2007).

98. Zecchini, V., Domaschenz, R., Winton, D. & Jones, P. Notch signaling regulates the differentiation of post-mitotic intestinal epithelial cells. *Genes Dev.* **15,** 1686–1691 (2005).

99. Jensen, J. *et al.* Control of endodermal endocrine development by Hes-1. *Nat. Genet.* **24,** 36–44 (2000).

100. Chyla, B. J. *et al.* Deletion of Mtg16, a target of t(16;21), alters hematopoietic progenitor cell proliferation and lineage allocation. *Mol. Cell. Biol.* **28,** 6234–6247 (2008).

101. Van Es, J. H., de Geest, N., van de Born, M., Clevers, H. & Hassan, B. a. Intestinal stem cells lacking the Math1 tumour suppressor are refractory to Notch inhibitors. *Nat. Commun.* **1,** 18 (2010).

102. Whitehead, R. H. & Robinson, P. S. Establishment of conditionally immortalized epithelial cell lines from the intestinal tissue of adult normal and transgenic mice. *Am. J. Physiol. Gastrointest. Liver Physiol.* **296,** G455–G460 (2009).

103. Barrett, C. W. *et al.* MTGR1 is required for tumorigenesis in the murine AOM/DSS colitis-associated carcinoma model. *Cancer Res.* **71,** 1302–1312 (2011).

104. Engel, M. E., Nguyen, H. N., Mariotti, J., Hunt, A. & Hiebert, S. W. Myeloid translocation gene 16 (MTG16) interacts with Notch transcription complex components to integrate Notch signaling in hematopoietic cell fate specification. *Mol. Cell. Biol.* **30,** 1852–1863 (2010).

105. Jarriault, S. *et al.* Signaling downstream of activated mammalian Notch. *Nature* **377,** 355–358 (1995).

106. Hunt, A., Fischer, M., Engel, M. E. & Hiebert, S. W. Mtg16/Eto2 contributes to murine T-cell development. *Mol. Cell. Biol.* **31,** 2544–2551 (2011).

107. Durand, a. *et al.* Functional intestinal stem cells after Paneth cell ablation induced by the loss of transcription factor Math1 (Atoh1). *Proc. Natl. Acad. Sci.* **109,** 8965–8970 (2012).

108. Barker, N., Van Oudenaarden, A. & Clevers, H. Identifying the stem cell of the intestinal crypt: Strategies and pitfalls. *Cell Stem Cell* **11,** 452–460 (2012).

109. Kopan, R. & Ilagan, M. X. G. The Canonical Notch Signaling Pathway: Unfolding the Activation Mechanism. *Cell* **137,** 216–233 (2009).

110. Peignon, G. *et al.* Complex interplay between β-catenin signalling and Notch effectors in intestinal tumorigenesis. *Gut* **60,** 166–176 (2011).

111. Fre, S. *et al.* Notch and Wnt signals cooperatively control cell proliferation and tumorigenesis in the intestine. *Proc. Natl. Acad. Sci. U. S. A.* **106,** 6309–6314 (2009).

112. Sjoblom, T. *et al.* The consensus coding sequences of human breast and colorectal cancers. *Harv. Bus. Rev.* **84,** 268–74 (2006).

113. Gao, J. *et al.* Integrative analysis of complex cancer genomics and clinical profiles using the cBioPortal. *Sci. Signal.* **6,** pl1 (2013).

114. Cerami, E. *et al.* The cBio Cancer Genomics Portal: An open platform for exploring multidimensional cancer genomics data. *Cancer Discov.* **2,** 401–404 (2012).

115. Parang, B. *et al.* The transcriptional corepressor MTGR1 regulates intestinal secretory lineage allocation. *FASEB J.* **29,** 786–795 (2014).

116. Soler, E. *et al.* The genome-wide dynamics of the binding of Ldb1 complexes during erythroid differentiation. *Genes Dev.* **24,** 277–289 (2010).

117. Trapnell, C., Pachter, L. & Salzberg, S. L. TopHat: Discovering splice junctions with RNA-Seq. *Bioinformatics* **25,** 1105–1111 (2009).

118. Anders, S. & Huber, W. Differential expression analysis for sequence count data. *Genome Biol.* **11,** R106 (2010).

119. Benjamini, Y., Drai, D., Elmer, G., Kafkafi, N. & Golani, I. Controlling the false discovery rate in behavior genetics research. *Behav. Brain Res.* **125,** 279–284 (2001).

120. Smith, J. J. *et al.* Experimentally Derived Metastasis Gene Expression Profile Predicts Recurrence and Death in Patients With Colon Cancer. *Gastroenterology* **138,** 958–968 (2010).

121. Kochetkova, M. *et al.* CBFA2T3 (MTG16) Is a Putative Breast Tumor Suppressor Gene from the Breast Cancer Loss of Heterozygosity Region at CBFA2T3 (MTG16) Is a Putative Breast Tumor Suppressor Gene from the Breast. **3,** 4599–4604 (2002).

122. Reva, B., Antipin, Y. & Sander, C. Predicting the functional impact of protein mutations: Application to cancer genomics. *Nucleic Acids Res.* **39,** (2011).

123. Mi, H., Muruganujan, A. & Thomas, P. D. PANTHER in 2013: Modeling the evolution of gene function, and other gene attributes, in the context of phylogenetic trees. *Nucleic Acids Res.* **41,** D377–86 (2013).

124. Krämer, A., Green, J., Pollard, J. & Tugendreich, S. Causal analysis approaches in Ingenuity Pathway Analysis. *Bioinformatics* (2014).

125. Yang, K. *et al.* Interaction of Muc2 and Apc on Wnt signaling and in intestinal tumorigenesis: Potential role of chronic inflammation. *Cancer Res.* **68,** 7313–7322 (2008).

126. Silverman, K. A., Koratkar, R., Siracusa, L. D. & Buchberg, A. M. Identification of the modifier of Min 2 (Mom2) locus, a new mutation that influences Apc-induced intestinal neoplasia. *Genome Res.* **12,** 88–97 (2002).

127. Weyden, L. Van Der, Arends, M. J., Dovey, O. M., Harrison, H. L. & Lefebvre, G. Loss of Rassf1a co-operates with Apc Min to accelerate intestinal tumourigenesis. **27,** 4503–4508 (2013).

128. Mantovani, A. *et al.* Cancer-related inflammation. *Nature* **454,** 436–44 (2008).

129. Jess, T. *et al.* Decreasing risk of colorectal cancer in patients with inflammatory bowel disease over 30 years. *Gastroenterology* **143,** 375–81.e1; quiz e13–4 (2012).

130. Schmitz, H. *et al.* Altered tight junction structure contributes to the impaired epithelial barrier function in ulcerative colitis. *Gastroenterology* **116,** 301–309 (1999).

131. Gibson, P., Rosella, O., Nov, R. & Young, G. Colonic epithelium is diffusely abnormal in ulcerative colitis and colorectal cancer. *Gut* **36,** 857–863 (1995).

132. Karayiannakis, A. J. *et al.* Expression of catenins and E-cadherin during epithelial restitution in inflammatory bowel disease. *J. Pathol.* **185,** 413–418 (1998).

133. Severson, E. a. & Parkos, C. a. Mechanisms of outside-in signaling at the tight junction by junctional adhesion molecule a. *Ann. N. Y. Acad. Sci.* **1165,** 10–18 (2009).

134. Orsulic, S., Huber, O., Aberle, H., Arnold, S. & Kemler, R. E-cadherin binding prevents β-catenin nuclear localization and β-catenin / LEF- 1-mediated transactivation. *J. Cell Sci.* **1245,** 1237–1245 (1999).

135. Toon, C. W. *et al.* Immunohistochemistry for Myc predicts survival in colorectal cancer. *PLoS One* **9,** e87456 (2014).

136. Koo, S. H. *et al.* Genetic alterations of gastric cancer: comparative genomic hybridization and fluorescence In situ hybridization studies. *Cancer Genet. Cytogenet.* **117,** 97–103 (2000).

137. Cowling, V. H. & Cole, M. D. E-cadherin repression contributes to c-Myc-induced epithelial cell transformation. *Oncogene* **26,** 3582–3586 (2007).

138. Yekkala, K. & Baudino, T. A. Inhibition of intestinal polyposis with reduced angiogenesis in ApcMin/+ mice due to decreases in c-Myc expression. *Mol. Cancer Res.* **5,** 1296–1303 (2007).

139. Ciclitira, P. J., Macartney, J. C. & Evan, G. Expression of c-myc in non-malignant and pre-malignant gastrointestinal disorders. *J. Pathol.* **151,** 293–296 (1987).

140. Brentnall, T. a. *et al.* Proteins that underlie neoplastic progression of ulcerative colitis. *Proteomics - Clin. Appl.* **3,** 1326–1337 (2009).

141. Suzuki, R., Miyamoto, S., Yasui, Y., Sugie, S. & Tanaka, T. Global gene expression analysis of the mouse colonic mucosa treated with azoxymethane and dextran sodium sulfate. *BMC Cancer* **7,** 84 (2007).

142. Arnold, H. K. *et al.* The Axin1 scaffold protein promotes formation of a degradation complex for c-Myc. *EMBO J.* **28,** 500–512 (2009).

143. Salghetti, S. E., Kim, S. Y. & Tansey, W. P. Destruction of Myc by ubiquitin-mediated proteolysis: Cancer-associated and transforming mutations stabilize Myc. *EMBO J.* **18,** 717–726 (1999).

144. Wang, F. *et al.* RNAscope: A novel in situ RNA analysis platform for formalin-fixed, paraffin-embedded tissues. *J. Mol. Diagnostics* **14,** 22–29 (2012).

145. Kohno, H., Suzuki, R., Sugie, S. & Tanaka, T. B-Catenin mutations in a mouse model of inflammation-related colon carcinogenesis induced by 1,2-dimethylhydrazine and dextran sodium sulfate. *Cancer Sci.* **96,** 69–76 (2005).

146. Arnold, H. K. & Sears, R. C. Protein Phosphatase 2A regulatory subunit B56α associates with c-Myc and negatively regulates c-Myc accumulation protein. *Mol. Cell. Biol.* **26,** 2832–2844 (2006).

147. Yeh, E. *et al.* A signalling pathway controlling c-Myc degradation that impacts oncogenic transformation of human cells. *Nat. Cell Biol.* **6,** 308–318 (2004).

148. Issa, J. J., Ahuja, N. & Toyota, M. Accelerated Aage-related CpG island methylation in ulcerative colitis. *Cancer Res.* 3573–3577 (2001).

149. Fukata, M. *et al.* Toll-Like Receptor-4 Promotes the Development of Colitis-Associated Colorectal Tumors. *Gastroenterology* **133,** 1869–81 (2007).

150. Alcalay, Y. *et al.* Popeye Domain Containing 1 (Popdc1/Bves) Is a Caveolae-Associated Protein Involved in Ischemia Tolerance. *PLoS One* **8,** (2013).

151. Dunagan, M., Chaudhry, K., Samak, G. & Rao, R. K. Acetaldehyde Disrupts Tight Junctions in Caco-2 Cell Monolayers by a Protein Phosphatase 2A-Dependent Mechanism. *AJP Gastrointest. Liver Physiol.* **303,** G1356–64 (2012).

152. Kim, J. *et al.* A Myc Network Accounts for Similarities between Embryonic Stem and Cancer Cell Transcription Programs. *Cell* **143,** 313–324 (2010).

153. Finch, A. J., Soucek, L., Junttila, M. R., Swigart, L. B. & Evan, G. I. Acute overexpression of Myc in intestinal epithelium recapitulates some but not all the changes elicited by Wnt/beta-catenin pathway activation. *Mol. Cell. Biol.* **29,** 5306–5315 (2009).

154. Ashizuka, S. *et al.* Adrenomedullin treatment reduces intestinal inflammation and maintains epithelial barrier function in mice administered dextran sulphate sodium. *Microbiol. Immunol.* **53,** 573–581 (2009).

155. Li, Y. *et al.* STAT1, STAT6 and adenosine 3',5'-cyclic monophosphate (cAMP) signaling drive SOCS3 expression in inactive ulcerative colitis. *Mol. Med.* **18,** 1412–9 (2012).

156. Zimmerman, N. P., Kumar, S. N., Turner, J. R. & Dwinell, M. B. Cyclic AMP dysregulates intestinal epithelial cell restitution through PKA and RhoA. *Inflamm. Bowel Dis.* **18,** 1081–1091 (2012).

157. Arnold, H. K. & Sears, R. C. A tumor suppressor role for PP2A-B56a through negative regulation of c-Myc and other key oncoproteins. *Cancer Metastasis Rev.* **27,** 147–158 (2008).

158. Blank, U., Karlsson, G. & Karlsson, S. Signaling pathways governing stem-cell fate. *Blood* **111,** 492–503 (2008).

159. Davies, R. J., Miller, R. & Coleman, N. Colorectal cancer screening: prospects for molecular stool analysis. *Nat. Rev. Cancer* **5,** 199–209 (2005).